CHALMERS
UNIVERSITY OF TECHNOLOGY

Contamination Study for Heavy Duty Vehicles using Smoothed Particle Hydrodynamics

Master's thesis in Applied Mechanics

AKHILESH ARJUN
ANAND JOSEPH MICHAEL

DEPARTMENT OF MECHANICS AND MARITIME SCIENCES

CHALMERS UNIVERSITY OF TECHNOLOGY
Gothenburg, Sweden 2022
www.chalmers.se

MASTER'S THESIS IN APPLIED MECHANICS

Contamination Study for Heavy Duty Vehicles using Smoothed Particle Hydrodynamics

AKHILESH ARJUN
ANAND JOSEPH MICHAEL

Department of Mechanics and Maritime Sciences
Division of Fluid Mechanics
CHALMERS UNIVERSITY OF TECHNOLOGY
Göteborg, Sweden 2022

Contamination Study for Heavy Duty Vehicles using Smoothed Particle Hydrodynamics
AKHILESH ARJUN
ANAND JOSEPH MICHAEL

Master's thesis 2022:01
Department of Mechanics and Maritime Sciences
Division of Fluid Mechanics
Chalmers University of Technology
SE-412 96 Göteborg
Sweden
Telephone: +46 (0)31-772 1000

Chalmers Reproservice
Göteborg, Sweden 2022

Contamination Study for Heavy Duty Vehicles using Smoothed Particle Hydrodynamics
AKHILESH ARJUN
ANAND JOSEPH MICHAEL
Department of Mechanics and Maritime Sciences
Division of Fluid Mechanics
Chalmers University of Technology

Abstract

Advancement in automobile technology has lead to increasingly complex driver assistance technology. Many of these involve the placement of sensors on the external surface(s) of vehicles. In the case of heavy duty vehicles, these sensors could be exposed to harsh driving conditions which could lead to contamination or soiling of their surfaces. Sensors must perform reliably and safely in such extreme conditions and must be kept clean for optimal performance. Additionally, contamination can also adversely affect the visibility of the driver as well as other road users. The durability and lifetime of components are also affected by contamination. Thus, studying contamination is vital. Contamination study for heavy duty vehicle development includes a combination of physical testing and numerical simulations. Traditional numerical simulations use a computational mesh, which makes the inclusion of multiphysics and replication of vehicle kinematics a formidable task.

An alternative to the current method, broadly known as purely particle based methods, removes the need for a computational mesh and allows various topological changes to be captured more easily. The purpose of this thesis was to evaluate particle based methods for studying contamination, in particular Smoothed Particle Hydrodynamics (SPH). Three software developed on SPH were used to simulate splashing phenomena of a simplified as well as a detailed truck model driving through a pool of water. These simulations were used to study the capabilities of the software in terms of accuracy of the modelled physics, computational demand and ease of usage. The three SPH-based software studied were LS-Dyna, Preonlab and Simcenter SPH.

SPH being of Lagrangian framework allowed inclusion of kinematics needed for replicating the motion of a truck moving through a pool. The methodology included an initial parameter study to understand the behaviour of certain tuning parameters in each software needed to setup realistic simulations. The comparisons of the results from the parameter study was achieved by capturing the splash height and wetting area on the surface(s) of the vehicle. Further, a detailed truck model was used to replicate a splashing scenario in the three software whose results were then compared against a similar physical test.

The study has shown that SPH is a reliable method to capture the large scale phenomena such as waves seen while driving heavy duty vehicles through water pools. Splash and spray phenomena in some of the tools evaluated might require a smaller SPH particle sizing to capture the required droplet density seen in the same phenomena in reality. It was also noted that the resolution of mesh used in importing the geometry has an influence when evaluating the surface area wetted after the simulations due to the interpolation techniques used to display the results. Further, the cost of computation of the three software were compared as part of the parameter study.

Keywords: Computational Fluid Dynamics, Smoothed Particle Hydrodynamics, Contamination, Multiphase Flows

Preface

The following report covers the masters thesis carried out in the field of fluid dynamics. The thesis is worth 30 ECTS, from 17th January to 30th June 2022 and was carried out as an obligatory part of the Masters programme at Chalmers University of Technology, Gothenburg, Sweden. The thesis has been conducted within Cab Analysis department at Volvo Technology AB, Volvo Group Trucks Technology with a purpose to evaluate particle based fluid simulation methods to study contamination. CFD Analysis Engineer Johan Forsgren was supervising the project on behalf of Volvo GTT. The project was examined by Professor Srdjan Sasic, belonging to the Division of Fluid Mechanics at the Department of Mechanics and Maritime Sciences at Chalmers University of Technology.

Acknowledgements

We would like to thank our supervisor Johan Forsgren, for his valuable mentorship and guidance during the course of this thesis work. His regular feedback has helped keep us focused on the objectives at hand. We would also like to acknowledge our examiner Srdjan Sasic for his valuable insights that provided us with a clearer vision for the project results.

We would like to thank all the software support teams at Preonlab, Simcenter SPH and LS-DYNA for providing us with assistance all through the course of this project. We would like to make a special mention of Rasmus Schützer from DYNAmore Nordic and Kevin Seidler from Simcenter SPH for providing their assistance at a moments notice and helping us out of tight spots with the simulation work.

We would like to express our gratitude to Peter Rundberget and the cab analysis team at Volvo GTT for welcoming us and making us feel as part of the team at every occasion especially at the Friday fikas which were always a highlight of our week. We would also like to extend a special thanks Björn Cognell for his help with setting up our LS-DYNA simulations. We also appreciate the support provided by David Eyre for helping us carry out the experimental tests.

We would like to thank God for this opportunity. Finally, we would like to thank our family and friends for their constant support throughout the duration of this project.

Anand Joseph Michael and Akhilesh Arjun, Gothenburg, June 2022

Nomenclature

Symbols and Constants

$\mathbf{u}$,$\mathbf{v}$	$[m/s]$	Velocity Vector
t	$[s]$	Time
ρ	$[kg/m^3]$	Density
p	$[Pa]$	Pressure
$\mathbf{g}$	$[m/s^2]$	Acceleration due to gravity
$\mathbf{F}_s$	$[N/m^3]$	Surface tension as force per unit volume
$\mathbf{F}_{ext}$	$[N]$	External forces
μ	$[kg/(m \cdot s)]$	Dynamic viscosity
F_D	$[N]$	Drag froce acting on particle
F_p	$[N]$	Pressure gradient force acting on particle
ν	$[m^2/s]$	Kinematic viscosity
σ	$[N/m^2]$	Cauchy stress tensor
ψ	$[J/m^3]$	Elasto-potential energy density
F	$[-]$	Deformation Gradient
F_E	$[-]$	Elastic part of Deformation Gradient
m_i	$[kg]$	Mass of particle i
W	$[-]$	Weighting (Kernel) function
W_{ij}	$[-]$	Weighting (Kernel) function acting on particle i due to neighboring particles j
v_i	$[m/s]$	Velocity of particle i
$\mathbf{r}_e$	$[m]$	Radius of influence of weighting function
$\mathbf{r}_i$	$[m]$	Position of particle i from origin
$\mathbf{r}_{ij}$	$[m]$	Distance between i and j
n_i	$[-]$	Particle Number Density of particle i
λ	$[-]$	Correction Coefficient
n^0	$[-]$	Standard particle number density
D	$[-]$	Number of dimensions
δ	$[-]$	Dirac delta function
A_s	$[-]$	Summation approximation
h	$[m]$	Smoothing length / support radius
ϕ	$[-]$	Color function
$\mathbf{n}$	$[-]$	Normal to surface
κ	$[-]$	Curvature of interface
σ	$[-]$	Coefficient of surface tension
δ	$[-]$	Surface delta function
s_{ij}	$[-]$	Strength of interaction between particles i and j
$\prod_{ij}$	$[-]$	Viscosity term
μ_{ij}	$[kg/(m \cdot s)]$	Dynamics viscosity between particles i and j
$\mathbf{F}_{ij}$	$[-]$	Interaction force acting between particles i and j
c_0	$[m/s]$	Artificial Speed of Sound
ρ_0	$[kg/m^3]$	Rest Density
U_{max}	$[m/s]$	Maximum velocity of fluid
γ	$[-]$	Polytropic constant
$\mathbf{v}^*$	$[m/s]$	Intermediate velocity
$\mathbf{F}_i$	$[N]$	Non-pressure forces
$\mathbf{F}_{pi}$	$[N]$	Pressure forces
Φ_i	$[N]$	Interaction force acting on particle i
γ	$[-]$	Surface tension coefficient
A	$[-]$	Spline function for adhesion force
C	$[-]$	Spline function for cohesion force
$\mathbf{F}_{ij}^{curvature}$	$[N]$	Curvature forces
$\mathbf{F}_{ij}^{cohesion}$	$[N]$	Cohesion forces
$\mathbf{F}_{ij}^{adhesion}$	$[N]$	Adhesion forces
K_{ij}	$[-]$	Symmetrized correction factor

V_{b_i}	$[-]$	Reciprocal of number density
ψ_{b_i}	$[kg]$	Mass of boundary particle
l	$[m]$	Characteristic length
l_0	$[m]$	Distance between particles
n_0^{st}	$[-]$	Particle number density of flat surface
n_i^{st}	$[-]$	Particle number density of convex surface

Abbreviations and Acronyms

CFD	Computational Fluid Dynamics
SPH	Smoothed Particle Hydrodynamics
EWM	Exterior Water Management
VOF	Volume of Fluid
FVM	Finite Volume Method
FSI	Fluid Solid Interaction
OED	Ocean Energy Devices
DEM	Discrete Element Method
MPM	Material Point Method
PDE	Partial Differential Equation
MPS	Moving Particle Semi-Implicit
RANS	Reynolds-Averaged Navier Stokes
DNS	Direct Numerical Simulation
LES	Large Eddy Simulation
PIC	Particle-in-Cell
PPE	Pressure Poisson Equation
CSF	Continuum Surface Force
PF	Pairwise Force
WCSPH	Weakly Compressible SPH
IISPH	Implicit Incompressible SPH

Contents

List of Figures

List of Tables

1 Introduction

Automotive industry plays a vital role in the transport of goods and services for smooth functioning of everyday life. Engineers across the globe are finding ways to adopt the latest technology into road vehicles to reduce the burden of the driver and increase the safety of passengers and other road users. This is facilitated by various sensors and camera(s) mounted on the external surfaces of the vehicles. The Volvo Active Driver Assist technology is an example where cameras and radar technology has been used to reduce risk of on road collisions. It provides features such as detection of on-road objects, distance alerts, lane departure warning, blind spot detection etc[1]. Vehicles are subjected to various scenarios and extreme conditions leading to deposition of foreign material such as water, dirt, snow etc. on the surface of such devices adversely affecting their performance[2][3]. Figure 1.1 is an example of contamination that occurs in harsh operating conditions[4].The visibility of the driver could also be hindered as a result of contamination of the windows or mirrors[2][5]. Additionally, the contamination of the vehicle side body and underbody could reduce the aesthetic appeal of the vehicle while also negatively impacting the lifetime of various components used in the vehicle[2][6]. Hence, it becomes vital to study and minimize contamination on vehicles.

Figure 1.1: *Volvo Truck in operation highlighting surface contamination[4]*

Numerical simulations are often used to study contamination as they alleviate the need for physical testing which are time consuming, expensive and limited in terms of what can be measured[2]. Fluid simulation methods can provide valuable feedback that can be used to reduce effects of contamination during early stages of vehicle development. Contamination usually involves the presence of multiples phases such as air, water, snow, soil etc, and these simulations try to predict their deposition on the vehicle by using multiphase flow modelling approaches[2]. However, simulation techniques to study contamination still face many challenges in terms of capturing deformation of the phase interface as well as the kinematics of the vehicle body. The following chapter will describe the thesis background, some previous work, the thesis objectives along with the limitations and a thesis outline.

1.1 Background

Aerodynamics pertaining to automobiles extends beyond the forces and moments experienced when a vehicle is moving through the atmosphere. Phenomena such as rain, snow etc. or deposition of road soil hinder safe operation of vehicles. Contamination has been considered part of aerodynamics for a long time. It produces undesirable effects, studying and mitigating its effects has been a subject of interest for the automotive industry[2].

By the end of the 1960s surface contamination was seriously considered during the development of cars. These included: preventing overflow over of surface water from the windscreen on to the front side windows or from the roof on to the rear windshield etc., since it limited driver visibility[2][5]. Modern vehicles have various devices mounted on its surface(s) such a cameras to improve vision when reversing, detect blind spots, lane-departure warnings etc.[1]. Surfaces of these devices must be kept clean to ensure optimal performance[2][3]. Deposition of solid contaminants such a road soil, snow etc. hinder smooth operations of various mechanical

components exposed underneath the vehicle. In the long run components such as drive axles, differentials are subjected to phenomena such as corrosion which reduces the lifetime of the vehicles. Investigation of surface contamination and fluid flow along the surface of the vehicle, known as Exterior Water Management (EWM), has been facilitated by a range of tools including test tracks, wind tunnels and numerical simulations[2].

Test tracks were the earliest form of investigating contamination. A controlled environment such as a wetted test track or drive-through troughs of water, often referred to as wading channels, allowed the control of height of water while carrying out contamination studies. However, the difficulties involved in setting up and maintaining such facilities prove to be a limitation to such testing methods [2]. There are other disadvantages to this method: a real driveable vehicle is required; environmental conditions cannot be controlled; measurement of contaminant deposition and surface water flow is difficult; confidential vehicle designs are at risk of exposure.

Wind tunnels provide control of more parameters compared to test tracks such as air flow rate, water flow rate and ambient temperature to artificially simulate a driving scenario [2]. It also allows for testing of vehicles that are not fully operational since the tests are performed under stationary conditions. Apart from this, it allows for testing of confidential prototypes since the tests are performed indoors. It facilitates for easier measurements to be made since the vehicle is stationary but usually large quantities of water is required to simulate contamination [2]. Gaylard et al. noted that replication of tyre spray scenarios cannot be replicated in aerodynamic wind tunnels since these use moving belts and floor boundary layer suction devices which are not compatible to water. Instead, climatic wind tunnels are an alternative since they are more robust to handle water and have been used for simulating contamination. As a consequence, some of the aerodynamic forces influencing surface contamination are neglected. Visual measurements are facilitated by water mixed with a special dye to enable flow visualization. Further, quantitative measurements are a limitation of experimental methods for validating numerical simulations since it is often hard to quantify or capture the amount of contamination on a particular surface from these tests[2].

With the improvement in computational performance, simulation tools now aid in solving complex and practical problems in engineering and science. It acts as a platform for validation of theories, a method to visualize complex physics and sometimes the discovery of new physics [7]. Various techniques used to simulate fluid flows are classified under computational fluid dynamics (CFD). Numerical simulations have the potential to provide insight into physical processes during early developmental stages. Prior to the development of prototype(s), much insight about various design changes can be obtained and the cost of development can be reduced while increasing product quality. Contamination involves the presences of multiples phases such as air and water. It also involves complex fluid phenomena such as splashing and spray. Apart from this, it involves the movement of the vehicle body such as wheel rotation or translation of the vehicle body. Over the years, CFD codes have expanded to include multiphase flows and multiphysics models which combined with the advancement in computational power, make it a viable tool to capture the complex physics involved in contamination. It provides better control over the events as long as the modelling assumptions and boundary conditions are carefully considered. Investigation of EWM and surface soiling has commonly used conventional CFD for simulation of aerodynamic flow field combined with Lagrangian particle modelling for representing airborne particles. Here, conventional CFD refers to the modelling of the fluid as a continua using meshes to capture the region under study (Eulerian modelling), while Lagrangian particle modelling refers to discretizing the fluid into particles and then following the particles around to understand how the fluid behaviour changes. A relatively simple scheme initially used was where particles are modelled to be of point sized volume and particles are influenced by the fluid flow and not vice versa (i.e, a one-way coupling approach). Later, two-way momentum coupling was introduced for this method to be valid over a wider range of particle Reynolds numbers. This technique gained popularity due relative computational economy [2]. Since Eulerian methods require a computational mesh, the inclusion and implementation of multi-physics models to capture moving interface, droplet breakup as well as vehicle kinematics has proved to be a laborious task and computationally heavy [8].

Particle based methods are an alternate way of studying contamination. Since such methods belong to the purely Lagrangian framework, the need for computational mesh is overcome [7]. Hence, particle based models are often regarded as mesh-free methods. The potential of one such model for studying contamination, namely Smoothed Particle Hydrodynamics will be discussed in the coming chapters. A moving vehicle setup is included in the computational model, using reasonable resources to study a truck wading through a pool of water. Smoothed Particle Hydrodynamics is a particle based method originally developed to study astrophysics

and compressible flows, later extended to study multiphase flows.

1.2 Previous Work

Previous work within the field of contamination has attempted to study vehicle wading using alternate CFD methods suitable for multiphase flows. In his Masters thesis, Idoffsson investigated the capabilities of SPH as a viable substitute for Volume of Fluid (VOF) to carry out wading simulations [8]. VOF simulations were carried out in Star-CCM+ while Preonlab was used for SPH simulations. Different SPH particle sizes were simulated to study the effects of computational demand, propagation of the free surface and the forces experienced at different surfaces of the vehicle body. These results were then compared with VOF and experimental results. Here, SPH particle represents a certain volume of fluid that the simulation considers to be moving together as a single parcel. Reduction in SPH particle sizing noted a significant increase in computational time with structures at the finer scales being better captured. However, the time taken for VOF simulations were noted to be far greater than any of the SPH simulations. VOF tended to smooth out the finer structures in areas where the mesh was not fine enough like the wake downstream of the vehicle. At different particle sizing, the structures at different water levels showed a similar trend although the structures were smoothed out at larger particle sizing. Upstream propagation has been well captured in VOF closely followed by the smaller particle sizing SPH simulation. Different particle sizing produced solutions without much differences and similar solution accuracy. Further, conclusions drawn in Idoffson were that the stationary vehicle model used for Finite Volume Method (FVM) cannot be replicated in real life and a fair measurement regarding whether SPH or VOF predict the forces experienced on the exterior parts of the vehicle could not be made [8]. Additionally, the replication of motion in the FVM framework with reasonable resources turns out to be a formidable task.

SPH has proved to be a viable tool for tackling problems in ocean engineering, free surface flows, fluid-structure interaction (FSI) and various industrial applications. Meshfree methods have been pursued and developed owing to its ability to easily model moving boundaries and capture free surface fragmentation compared to mesh based methods. Lyu et al. were dedicated towards providing a review about SPH techniques used for simulating ocean energy devices (OEDs)[9]. The SPH techniques were particularly evaluated for multi-physics models needed for simulating OEDs, computational efficiency and computational capacity. The review discussed the challenges of incorporation of multibody dynamics for replication of kinematics in OEDs into SPH framework. Open source codes, DualSPHysics and SPHinXsys were coupled with FSI solvers to handle complex multi-joint systems used in ocean engineering. Combining muliphysics solvers with SPH continues to be a challenge but these models are often evaluated using simple benchmarks like a dam-breaking flows impacting on an elastic plate. Many engineering problems involve multiphase flows with mixtures of high density difference between the phases, such as air-water, which is hard for basic SPH frameworks to handle. Pioneering work was carried out by Colagrossi and Landrini to create a modified SPH framework for simulating air-water system at realistic density ratios. But, it was also noted that the expensive computational cost of SPH for modelling of multiphase problems prevents it from being used in industrial applications. The reason for a high cost of computation is due to high density ratios which governs the size of time step that can be used. Vehicle wading involves free surface flow and fragmentation as well as fluid-structure interaction(FSI) which have been modelled through these prior mentioned studies using SPH, making it a potential model to be evaluated for predicting contamination.

1.3 Purpose

The purpose of this Master's thesis is to acquire knowledge from literature surveys about different particle based methods. Three software based on SPH, a particle based method has been evaluated to replicate splashing of a truck through a pool of water and capture the splashing phenomena. To achieve this, a parameter study with a simplified truck has been carried out initially. It was followed up with simulations of a detailed truck model which was compared with experimental test runs to understand accuracy of physics, computational cost and ease of usage of each of these software.

1.4 Aim and Objective

The problem will here be divided into a number of questions which will be evaluated in different phases during the project. In this manner, a simplified overview of the project will be achieved.

Literature Survey

- What is the theoretical background behind each of the particle based fluid simulation methods,i.e SPH,

MPM and DEM?

- What are the assumptions made for each method? How are the equations being solved?
- Compared to traditional finite volume methods, what are the merits and demerits of using particle based solvers?
- Evaluate different papers that used these software to study the modelling of liquid (water) behaviour. Are there any recommended settings?
- Evaluate different papers that study how well the software capture surface tension, contact angles, droplet breakup, cohesion etc.

Phase 1

- Study the three different software involved in this project, with focus on the following-
  - What is the algorithm followed in each software?
  - What modelling approach is considered in each software to model water in the best way possible?
  - How are the forces modelled in each software?

Phase 2

- Develop a computational model of a truck wading through water and evaluate the behavior of each software.
- Using the simulations, try to predict contamination on the surface of the vehicle during wading by varying different parameters like vehicle speed, depth of water etc.
- Evaluation criteria of each software for the wading simulation
  - Robustness and accuracy of the solvers.
  - Ease of simulation setup and post processing required to get results
  - Computational cost

1.5 Delimitations

In order to be able to perform the project within the time frame given, a few limitations have to be made. The limitations of the project are given below-

- A simplified geometry of the truck was used to evaluate the different parameters of the SPH based fluid simulation software so that the computational demand on the programs was reduced.
- Only sprays(small droplets) and splashes(large droplets/sheets of liquid) created by the truck's own wheels will be studied during the project. Contamination caused by weather phenomena such as rain and snow is not modelled. Neither is contamination caused by splashes or sprays generated by other vehicles considered in the study.
- Water(H_2O) will be the material use in the simulation setup. No other contaminants will be included (for eg. dirt).
- LS-DYNA, Simcenter SPH Flow and PreonLab will be the only SPH based software used in our investigations.

1.6 Thesis Outline

Chapter 2 - Theory: This chapter aims to provide knowledge regarding contamination in general as well as various types of particle based simulation (SPH, DEM, MPM etc.) techniques used for multiphase flow simulation. Since SPH was used to carry out the splashing simulations in this study, theoretical aspects on this technique are presented in more detail.

Chapter 3 - Method: The method used for studying the three software including the workflow of each software used to setup a splashing simulation are discussed in this chapter. Further, details of a parameter study and the detailed truck simulation setup are also discussed in this chapter.

Chapter 4 - Results and Discussion: This chapter contains the results of the parameter study using the simplified truck as well as a comparison of detailed truck simulations with an experimental test. The results are followed by relevant discussions regarding each software in terms of accuracy of modelled physics, computational costs involved and ease of software usage.

Chapter 5 - Conclusion: This chapter contains the summary of the project along with some important deductions made from the results and discussions. Some proposals for future work related this study are also presented at the end.

2 Theory

In this chapter the theory about contamination and different multiphase modelling methods are presented. At the beginning, an introduction of the relevant terminology and phenomena pertaining to contamination in vehicles is presented. The section after that is devoted to an introduction to different types of multiphase modelling approaches developed for simulating various engineering problems. It includes the popular methods traditionally used in the automotive industry to evaluate contamination. Further, an overview about the theoretical aspects of different particle-based simulation methods are presented to acquire an understanding about potential usage and challenges of each one. Then, one such particle based method, SPH is presented in detail since the tools being evaluated in this thesis are based on it. Important features of this method and some common challenges are reported, as well. The relevant terms in the governing equations in SPH framework are introduced. Some theoretical aspects about the different approaches and models used in the software are described.

2.1 Surface Contamination

Any substance that is not part of the vehicle body can be considered to be a contaminant [2]. Gaylard et al. (2017) stated that these contaminants could cause degradation of driver visibility, vehicle surface sensor performance or vehicle aesthetics[2][5][3]. The most common source of liquid vehicle contamination is water from various environmental phenomena. Solid vehicle contaminants, both natural and man made, can be found on road surfaces. Natural contaminants include soil, desert sand, ocean salt, biogenic materials etc. Man made contaminants come mainly from fuel combustion in vehicle engines but could also include contaminants formed by the wear of brakes, tyres or even the road surfaces. All these solid contaminants often mix with rain water and get thrown up on to vehicle surfaces by vehicle tyres. Contamination can be classified into three main types based on its source [2]:

- *Direct soiling* refers to contamination of vehicles surfaces caused by weather phenomonen such as rain where the contaminant directly lands on the vehicle surface without any man made influences.
- *Self soiling* refers to contamination of vehicle surfaces caused by the sprays generated by its own tyres. They can usually be found on surfaces downstream of the vehicle tyres.
- *Third party soiling* refers to contamination caused by the sprays generated by the tyres of other vehicles. This type of contamination usually occurs on the forward facing surfaces of vehicles as they drive through the tyre sprays of neighbouring vehicles.

In both third-party soiling and self soiling scenarios, it is the interaction of the wheel with the fluid on the roads that creates droplets of contaminants which travel downstream and hit the vehicle surface. The fluid lifted from the road can be classified broadly into splashes and sprays based on the size of the fluid drops[2]. Splashes usually have larger drop sizes because of which the fluid particles follow more of a projectile motion. In contrast, sprays have smaller drop sizes which allow their motion to be influenced by the airflow around the vehicle. If the direction of the fluid drop and the mechanism of its release from tyre surfaces is added to the classification, it can be further divided into the following categories[10]:

- bow wave
- side splashing wave
- tread pickup
- capillary adhesion

When a tyre passes through a shallow pool of water, some volume of water passes through the tyre grooves while the remaining water is splashed forward(bow wave) or to the sides (side splash waves) as seen in figure 2.2 [10]. The water that is picked up by the tyre treads on the other hand is released immediately behind. The droplets from the tread pickup are smaller than the bow and side splashes drops. Many of the large droplets generated by the first three phenomenon often hit other surfaces and break into smaller drops. Some of the water manages to reach higher up on the tyre surfaces due to capillary adhesion where it is stripped off the tyre surface by incoming air stream creating a cloud of very fine droplets [10].

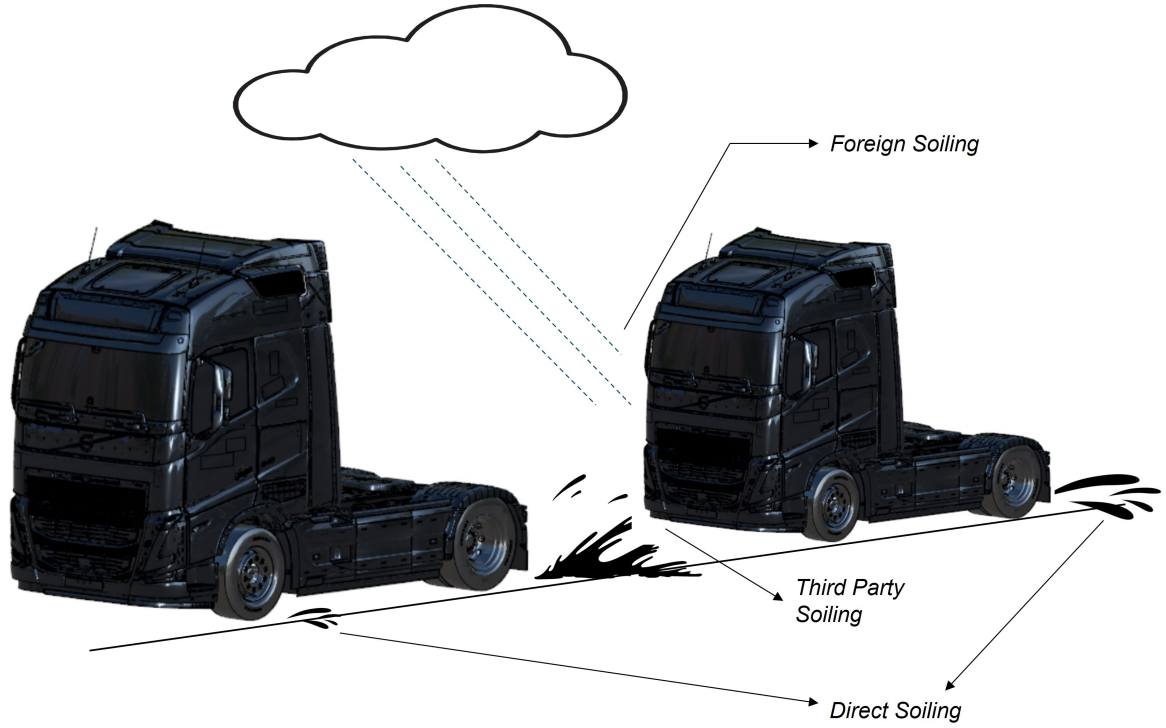

Figure 2.1: *Classification of contamination based on source*

2.2 Computational Fluid Dynamics

CFD is a branch of fluid dynamics that uses computational resources governed by the laws of mass, momentum and energy to analyze practical engineering problems. In recent years, CFD rapidly developed as numerical tool to validate theories, visualize flow behavior and study new phenomena. In the automotive industry CFD is applied to improve vehicle performance, fuel consumption, thermal systems amongst many others. Majority of the CFD models can be classified as: Eulerian or Lagrangian. In Eulerian approaches, the unknown state variables are attached to the stationary observer while in Lagrangian approaches, the unknown state variables are attached to the moving observer [11]. Eulerian methods use a grid or mesh to solve partial differential equations (PDEs) that govern the occurring physical phenomena [7]. The process of meshing or discretization involves dividing the continuum domain into small discrete sub-domains. The individual grid points (nodes) are connected in a pre-defined manner to form a mesh or grid. In FVM, the subdomains are referred to as cells. The mesh must be pre-defined to establish the relationship between nodes, so that the PDEs can be converted to a set of algebraic equations which can be solved to obtain nodal values of the field variables [7]. Many practical problems in engineering and science are currently being solved using grid based numerical models. Liu et al. mentioned that a large portion of the engineering problems pertain to multiphase flows and various techniques for simulating such problems continue to be developed [7].

2.2.1 Multiphase Modelling Approaches

The development of various computational models allows for extending the applications of CFD to complex systems comprising of multiple phases. Numerical tools alleviate cost of development and increase the product quality provided the simulations are based on feasible assumptions. In CFD, methods for handling multiphase systems are broadly classified into three main groups [12]. First, a fully Eulerian approach, such as VOF where all phases are considered to be of a continuum nature. Such methods are characterized by a mesh that is stationary or adaptive to capture the motion of the phase interface(s). These simulations are based on treating the Navier-Stokes equation in the Eulerian frame of reference. Second, a hybrid Eulerian-Lagrangian approach, where the field variables of one phase are computed using a static mesh and Navier-Stokes equation in the Eulerian framework while the particles are tracked using equation(s) of motion [13]. Finally, a fully Lagrangian approach such as SPH or Moving Particle Semi-Implicit (MPS) method where all phases present in the system are dis-

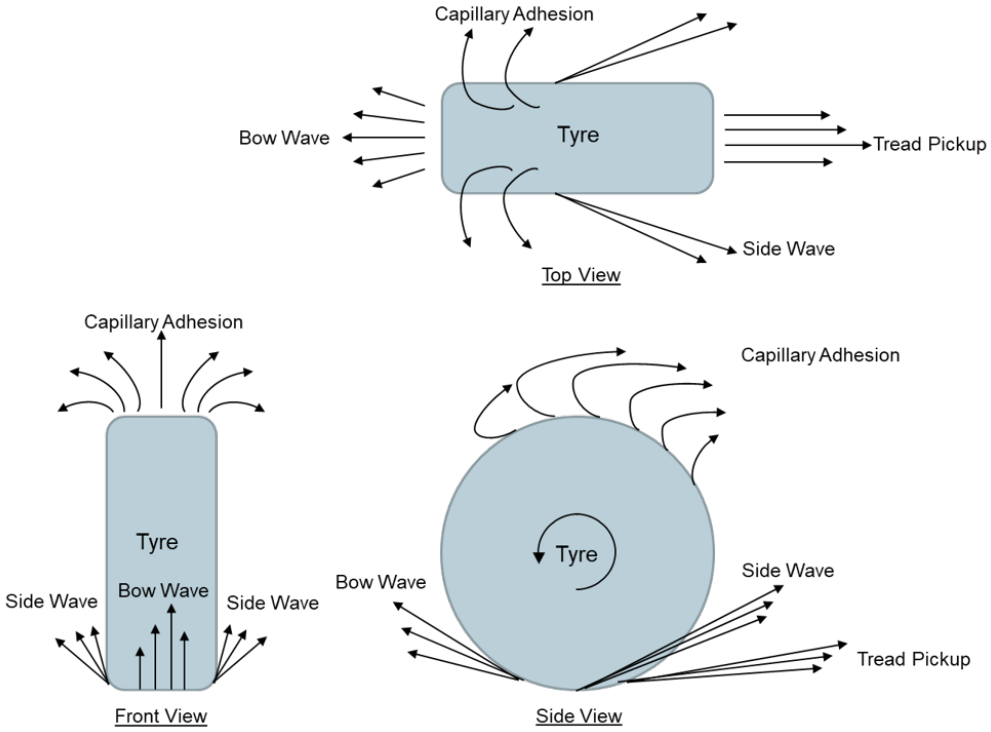

Figure 2.2: *Different types of way that a wheel throws up water from a surface[10]*

cretized as particles of finite size and governing Navier Stokes equations are in the Lagrangian frame of reference.

Although many engineering applications have been successfully addressed with the purely Eulerian framework, simulation of free surface flows, multiphase flows and FSI has proven to be computationally demanding. The most challenging issues with such methods are the inclusion of multibody dynamics to simulate real world conditions and the inclusion of methods for accurately replicating topological changes like fluid jets and droplet breakup [9]. Simulation of multibody dynamics using mesh based methods requires techniques such as an overset mesh. An overlapping mesh that moves with the body of interest needs to be coupled with the static background mesh which is both a challenge to setup as well as simulate with reasonable resources. The other issue with purely Eulerian methods is that the interfaces of multiphase flows or free surface flows are smeared out due numerical diffusion [14]. Natsui et al. (2014) listed some of the popular techniques used to prevent numerical diffusion include level set method, donor-acceptor method etc. These methods have advantages and disadvantages related to volume conservation and interface reconstruction methods [14]. So, based on the calculation conditions, a suitable method must be chosen [14]. Eulerian-Lagrangian approaches tend to have difficulties with mesh-particle coupling since the particle properties need to be interpolated on to the mesh accurately making it challenging as well as expensive. Further, modelling of interparticle collisions and boundary-particle collisions as well as numerical accuracy during the coupling process are issues that could come up[13].

Fully Lagrangian approaches are mesh-free methods where the fluid volume is discretized as rigid spherical particles. In this method the particles themselves are advected based on their mass and volume. The algorithm is simple and each particle maintains a sharp interface [14]. Shakibaenia and Jin (2012) mentioned that the behaviour of the phases originates from the interaction between the simulation particles and its location with respect to interface is irrelevant. Such methods have shown potential to simulate free-surface flow. However, simulation of large densities and viscosity ratios near the interface, such a gas-liquid flows cause severe stability issues and numerical oscillations have been observed [12]. So, the instability of the free-surface has been relieved by tracking only the liquid phase as a single-phase flow [15]. The effect of air is often added using a drag model[16][17]. Further, surface tension models have been introduced in order to alleviate the numerical fluctuations at the interface.

2.3 Governing Equations In Lagrangian Formulation

Since this thesis aims to evaluate particle based methods, introducing the governing equations in Lagrangian framework at this point would be appropriate. The incompressible continuity and Navier-Stokes equations are expressed as [14]:

$$\frac{D\mathbf{u}}{Dt} + \rho(\nabla \cdot \mathbf{u}) = 0 \tag{2.1}$$

$$\frac{D\mathbf{u}}{Dt} = -\frac{1}{\rho}\nabla p + \nu\nabla^2\mathbf{u} + \mathbf{g} + \frac{1}{\rho}\mathbf{F}_s + \frac{1}{\rho}\mathbf{F}_{ext} \tag{2.2}$$

where $\mathbf{u}$ denotes velocity, t is time, ρ is density, p is pressure, $\mathbf{g}$ is gravity, ν is kinematic viscosity, $\mathbf{F}_s$ is surface tension expressed as force per unit fluid volume and $\mathbf{F}_{ext}$ denotes external forces acting on the fluid volume.

2.4 Discrete Element Method (DEM)

DEM is a Lagrangian approach of simulating multiphase flows, particularly for solid particle transport, spray behaviour and behaviour of small bubbles [13]. Such flows consist of a continuous phase and dispersed phase. DEM is used to compute the motion of the dispersed phase. Using this technique various multiphase problems associated with atmospheric pollutants, sand, wind driven rain, spray of pesticides etc. has been studied [18]. This technique handles polydispersity, heat and mass transfer, chemical reactions well and provides detailed information about individual simulation particles [13].

The continuum phase is commonly calculated using a FVM, i.e, a Eulerian method. The coupling of the Eulerian and Lagrangian frameworks is facilitated by the fact that the material property (*Lagrangian*) of a fluid particle is the same as the spatial property (*Eulerian*) of the fluid particle at the same point [13]. Fundamental principles of DEM include a state vector which is used to compute position and velocity of each particle while interactions between particles are treated on a particle-particle pair basis [13]. The general outline for DEM involves:

- Carry out fluid flow calculation in Eulerian framework like RANS, LES, DNS etc.
- Compute trajectory and velocity of each particle of the dispersed phase using equation of motion by taking into consideration the relevant forces
- If needed introduce models for turbulent dispersion, particle-wall and particle-particle interactions

The equation of motion used for calculation of the dispersed phase is a balance of the inertial forces acting on the particle and the forces due to aerodynamic drag, pressure gradient and gravity effects as in the following equation[19]:

$$m_i\frac{d\mathbf{v}}{dt} = F_D + F_p + F_{ext} \tag{2.3}$$

where m_i denotes mass of particle(s), $\mathbf{v}$ is the velocity of the particle, F_D, F_p and F_{ext} are forces due to drag, pressure gradient and other effects acting on the particle respectively.

In this approach, the particles are assumed to be point sources i.e, have no physical volume. The most basic form assumes that particles are only advected by the flow and do not alter the flow field, known as a one-way coupling [13]. Subsequent models developed were able to handle a wide range of particle Reynolds numbers and particle-flow interactions using a two way momentum coupling where the influence of the dispersed phase on the continua is also considered in the simulation[2],[20]. Two way coupling is achieved by tracking the volume fraction and interphase momentum exchange term in the momentum equation [21]. The computational demand can be reduced by tracking groups of particles (parcels) instead of tracking individual particles [2]. Particles within the parcels are assumed to move with the same velocity and the density of the parcel is equal to the material density of an individual particle [13].

Hagemeier et al. (2011) noted that numerical approach to automotive soiling was derived from the aerospace industry [22]. DEM was used to represent the airborne particles used in jet engines which was extended to cylinder fuel spray simulations of the engine in the automotive industry. Subsequently formulations for

wall impingement, splash and droplet breakup were introduced and these models form the foundation of the main approaches used for surface contamination in automobiles [2]. In Exterior Water Management (EWM) simulations of flow around the A-pillar of passenger vehicle, DEM has been used to model the airborne water droplets and thin film model to represent the accumulating surface water [22]. Although, multiple research demonstrated some important phenomena are well highlighted for EWM using DEM, this method is limited since surface tension, capillary forces etc. are not taken into account [2]. Gaylard et al. (2017) went on to say that these simple models along with suitable extensions and complemented by wind tunnel testing have provided useful surface flow behavior.

2.5 Material Point Method (MPM)

MPM is a hybrid method and uses both Eulerian meshes and Lagrangian (material) points to represent a material. The mathematical foundation for this method was provided by Sulsky et al. (1995). It is a version of particle-in-cell (PIC) method. PIC was proposed to model high deformations in fluid flows while MPM was developed to model solids [23]. MPM has been applied to study geomechanics [24], manufacturing [25] and sea ice dynamics [26]. Many researchers have experimented with hybrid grid and particle methods. Most PIC solvers like MPM have shown the potential to implicitly handle self-collision and fracture with the use of background fixed grid [27]. This feature allows to capture topological changes such as droplet breakup [27].

The basic equations used in MPM are the conservation of mass, conservation of momentum and the elasto-plastic constitutive relations as shown in equation 2.4[27]. Here, ρ, refers to density, t to time, $\mathbf{v}$ to velocity, σ to Cauchy stress tensor, $\mathbf{g}$ is gravity, ψ is the elasto-plastic potential energy density, F_E is the elastic part of deformation gradient F and $J = det(F)$.

MPM uses Lagrangian points to capture the location and deformation of the phases involved, i.e. track the position, velocity, and mass of the phase. The Eulerian mesh in the background is used to compute the gradients of the stresses required for force calculations in the solution process. Interpolating functions are used to exchange information regarding velocity, denstiy etc. between the Lagrangian points and the Eulerian mesh. The Eulerian mesh solves for the forces acting at each node of the mesh using the weak form as used in Finite Element Methods(FEM). Stress is then computed from this and used to deform the mesh temporarily and obtain velocity at the mesh nodes. These velocities are then interpolated back to the Lagrangian points using weighting functions. The points are then moved forward and the Eulerian mesh is reset to its original position to begin the next timestep in the solution process.

$$\frac{D\rho}{Dt} = 0 \tag{2.4}$$

$$\rho\frac{D\mathbf{v}}{Dt} = \nabla \cdot \sigma + \rho g \tag{2.5}$$

$$\sigma = \frac{1}{J}\frac{\partial \psi}{\partial F_E}F_E^T \tag{2.6}$$

MPM has been shown to have an advantage over purely Lagrangian or Eulerian methods of numerical simulation of problems involving materials with large deformations [28]. It avoids mesh distortion and tangling issues associated with Lagrangian methods by resetting of the mesh that occurs at the end of every time step [23] and advection errors with Eulerian methods [28]. Hence, its application is well suited for simulating multiphase flow problems. Lagrangian points avoid the need to advect state variables through a fixed mesh and avoid issues due to numerical diffusion. However, the high cost of computation is a disadvantage of this method. This is because the motion of the Lagrangian points needs to be tracked and updated on to the Eulerian mesh nodes simultaneously[28].

2.6 Moving Particle Semi-Implicit (MPS) Method

MPS is a purely Lagrangian method for fluid simulations developed by Koshizuka and Oka. Field variables and trajectory of the fluid particles are determined using the interaction the neighboring particles and a kernel function [29]. Separate kernel functions are used to define gradient, divergence and Laplacian operations. Fluid pressure is computed implicitly using a Pressure Poisson equation (PPE) while all other terms are computed explicitly. Hence it is known as semi-implicit method.

MPS approximations

Particle based solvers represent a volume of fluid discretized as identical particles of finite size and the fluid behavior is replicated by the motion of these particles. Particle interaction with its neighbors is established using a weighting function taking into the account the distance between the particles, $\mathbf{r}_{ij} = |\mathbf{r}_j - \mathbf{r}_i|$, for particles i and j. Koshizuka and Oka defined the weighting function as follows:

$$W_{ij} = \begin{cases} \frac{\mathbf{r}_e}{\mathbf{r}_{ij}} - 1 & (\mathbf{r}_{ij} \leq \mathbf{r}_e) \\ 0 & (\mathbf{r}_{ij} > \mathbf{r}_e) \end{cases} \tag{2.7}$$

where r_e is the influence of the weighting function, Natsui et al. assumed it to be $\mathbf{r}_e = 2.1d_p$, d_p is particle diameter [14].

The particle number density is expressed as the sum of the weighting functions of the neighboring particles, as follows:

$$\langle n_i \rangle = \sum_{j \neq i} W_{ij} \tag{2.8}$$

where $\langle\rangle$ represents kernel approximation. Thus, density for the real fluid particle is defined as [14]:

$$\langle \rho \rangle_i = \sum_{j \neq i} m_j W_{ij} / \int_V W_{ij} dV \tag{2.9}$$

where m_j is the mass of particle j and V is the volume of fluid.

The pressure gradient term, smoothed divergence of velocity vector,$\mathbf{u}$ and Laplacian in the diffusion term are discretized as [30],[29]:

$$\langle \nabla p \rangle_i = \frac{D}{n^0} \sum_{j \neq i} [\frac{p_j + p_i}{\mathbf{r}_{ij}^2} \mathbf{r}_{ij} W_{ij}] \tag{2.10}$$

$$\langle \nabla \cdot \mathbf{u} \rangle_i = \frac{D}{n^0} \sum_{j \neq i} [\frac{\mathbf{u}_j - \mathbf{u}_i}{\mathbf{r}_{ij}^2} \mathbf{r}_{ij} W_{ij}] \tag{2.11}$$

$$\langle \nabla^2 \mathbf{u} \rangle_i = \frac{2D}{n^0 \lambda} \sum_{j \neq i} [(\mathbf{u}_j - \mathbf{u}_i) W_{ij}] \tag{2.12}$$

$$\text{where, } \lambda = \langle \mathbf{r}_{ij}^2 \rangle_i = \frac{\sum_{j \neq i} \mathbf{r}_{ij}^2 W_{ij}}{\sum_{j \neq i W_{ij}}} \tag{2.13}$$

where D is the number of dimensions, n^0 is a standard particle number density and λ is a correction coefficient obtained from analytical solution.

2.7 Smoothed Particle Hydrodynamics (SPH)

SPH was originally developed for astrophysical applications due to its ease of usage while allowing for reasonable accuracy [31]. It was used to simulate compressible flows but, was later extended to a wide range of problems like single or multiphase flows, free surface flows with extension to three dimensional application [8]. Since it is a purely Lagrangian approach, the fluid volume is treated as a set of particles. It does not need a mesh to compute spatial derivatives. All scalars and vector field properties are expressed using kernels and averaged across the domain. The kernels serve as interpolating functions. Since it was derived from compressible flow applications, much research has been conducted to formulate modified methods to simulate low Reynolds number ($Re \leq 1$) incompressible flows using SPH.

2.7.1 SPH Approximations

SPH like other particle based methods, represents a fluid volume as particles of fixed volume which follow fluid motion[31]. Fundamental concept of SPH method is to express all field properties using an integral interpolant defined over the entire domain as shown below:

$$A(r_j) = \int A(r) W(\mathbf{r} - \mathbf{r}_j, h) dr \tag{2.14}$$

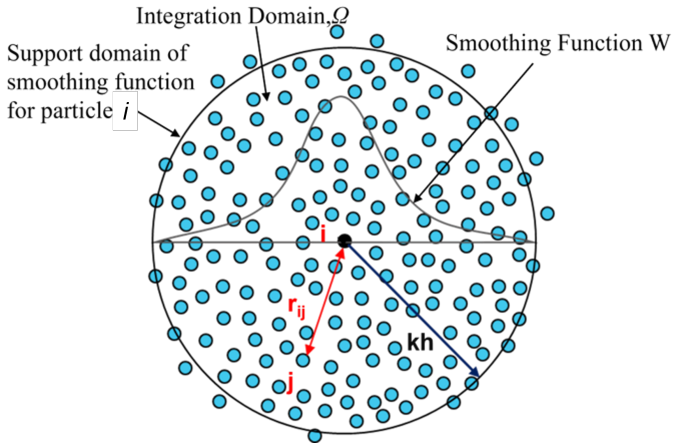

Figure 2.3: *Particle approximation using smoothing function (kernel), W for particle i. Solid, black line denotes the support radius h over which the interpolation is performed.*

where W is the smoothing function, a function of Euclidean norm $||\mathbf{r} - \mathbf{r}_j||$.

W, the smoothing function, is interchangeably referred to as kernel, smoothing kernel or weight function. But, kernel used in SPH must satisfy some basic requirements, as follows [7]:

- The kernel must be normalized.

$$\int W(\mathbf{r} - \mathbf{r}_j, h)\, dr = 1 \tag{2.15}$$

- The smoothing function must satisfy the Dirac delta function.

$$\lim_{h \to 0} W(\mathbf{r} - \mathbf{r}_j, h) = \delta(\mathbf{r} - \mathbf{r}_j) \tag{2.16}$$

  the smoothing function,W tends to the Dirac delta function as $h \to 0$. When h, the smoothing length is non-zero, interpolation is performed by smoothing function, W.

- It must have sufficient compact support.

$$W(\mathbf{r} - \mathbf{r}_j) = 0, |\mathbf{r} - \mathbf{r}_j| > \kappa h \tag{2.17}$$

  The physical interpretation of compact support is that the interaction with particles at distances larger than κh reduce to zero.

For numerical computation, the integrals are approximated by a summation interpolant, a powerful feature which SPH allows:

$$A_s(r) = \sum_j m_j \frac{A_j}{\rho_j} W(\mathbf{r} - \mathbf{r}_j, h) \tag{2.18}$$

where A_s, m_j, ρ_j are the summation approximation, mass and density of adjacent particle(s) j, respectively. The summation is done over the entire supporting range h. Such an approximation results in an error usually $O(h^2)$ or better.

In SPH, spatial gradients can be computed using the kernel function, without the need for a grid. Since the kernel is defined by functions, it must be easily differentiable. The gradient of A is computed by rewriting equation 2.14 with gradient operator acting on the kernel.

$$\nabla A_s(r) = \sum_j m_j \frac{A_j}{\rho_j} \nabla W(\mathbf{r} - \mathbf{r}_j, h) \tag{2.19}$$

It would be beneficial to attain higher order accuracy using a symmetrized form, as shown later with formulation of the terms used in the governing equations.

Monaghan stated that usage of kernels based on splines have proven to be computationally efficient. A golden rule of SPH is to assume that the kernel used is a Gaussian in order to find the physical interpretation of an SPH equation. The usage of kernels in SPH is the equivalent to different discretization schemes used in finite difference methods. The advantage of using kernels in SPH is that it can be calculated in a subroutine or pre-computed using a table[31].

Important to note that formally the smoothing is carried out over the entire domain. But only, a small number of particles actually contribute to the chosen smoothing function. Hence the equations governing the evolution of the fluid properties are expressed as summation interpolants using the kernel function, W over a neighbourhood of particles in the smoothing length h [8].

Advantages of SPH over traditional grid based computational methods [7]:

- SPH being a Lagrangian approach is Galilean invariant i.e, time history of particles can be obtained. Thus, transport quantities can be calculated.
- Tracking of free surface, interface deformation and topological changes are easily handled during the simulation which is challenging in Eulerian methods.
- It is a mesh-free method. Thus, it is straightforward to handle large deformations since the inter-particle connections are governed as part of the computation and allowed to change with time.
- SPH represents a particle of finite volume at the continuum scale. Similar to molecular dynamics which represents a molecule at a nano-scale or dissipative particle dynamics which represents a cluster of molecules at the meso-scale. So, SPH can be extended to the smaller scales or be coupled with such methods for applications in bio-physics or bio-chemistry.
- Numerical implementation of SPH is easier and can be extended to 3D models much more easily than grid based methods.

During the development of SPH method, a wide range of problems were reported and corresponding modifications proposed leading to the advancement of its formulation. Original SPH algorithm did not conserve linear and angular momentum, so Gingold and Monaghan suggested a new algorithm that conserved both linear and angular momentum [32]. Hu and Adams formulated an angular momentum conservative SPH algorithm particularly for incompressible viscous flows [33]. Fang et al. proposed formulations for simulating free surface flows using incompressible viscous fluids. Many reseachers have conducted studies to investigate the numerical accuracy, stability, convergence and efficiency of this method. Swegle et al. was the first to address the tensile instability issue for solid mechanics applications [34]. Multiphase flows with large density differences like liquid-air or fluid- solid interactions often witnessed this numerical issue. It occurred due to density underestimation, where the densities of the particles were lower than the rest (reference) density when the density summation approach was used. This led to erroneous computation of pressure since an equation of state related pressure to density, causing negative pressures to arise and result in particle clustering. One approach to overcome this issue taken by Monaghan as well as Macklin and Mueller was to use artificial pressure forces which resulted in spurious surface tensions[35], [36]. Some of the other common practices to avoid tensile instability were to either use a density correction technique or simply prevent negative pressures. However, particle clustering still persisted since the pressure field was not reconstructed in a physically sensible way. So, Akinici et al. proposed pre-computing a single layer of boundary layer particles for solid boundaries and Schechter and Bridson used ghost SPH particles that were dynamically generated at the liquid-air or solid-liquid interfaces[37], [38].

2.7.2 Evolution of Density

Density is computed as [31]:

$$\rho_i = \sum_j m_j W_{ij} \tag{2.20}$$

where $W_{ij} = W(\mathbf{r}_{ij}, h)$ and $\mathbf{r}_{ij} = \mathbf{r}_i - \mathbf{r}_j$, denotes the distance between particle i and particle j in the support radius h.

However, Monaghan noted for free surface flows, the density is smoothed at the fluid edge. This causes spurious pressure gradients to be induced at the surface resulting in poor estimation of terms like turbulent viscosity. Monaghan avoided this problem by setting an initial reference density and allowed particle density to evolve using the continuity equation in SPH formalism as:

$$\frac{d\rho_i}{dt} = \sum_j m_j v_{ij} \nabla W_{ij} \tag{2.21}$$

Equation 2.21 allowed density to evolve with particle velocities and other field properties. The advantage of this formulation was that the rate of change required less computational effort. However, equation 2.21 does not ensure that mass is conserved, where as equation 2.20 does, when the total number and mass of particles are constant[31].

2.7.3 Pressure Gradient Term

The pressure gradient term can be formulated in a similar manner:

$$\rho_i \nabla p_i = \sum_j m_j (p_j - p_i) \nabla W_{ij} \tag{2.22}$$

The disadvantage with equation 2.22 was that linear and angular momentum were not exactly conserved and a pair of particles could bootstrap themselves to infinity, according to Monaghan. Hence, the pressure gradient term was symmetrized by rewriting it in $\nabla P/\rho$ form. However, it does not ensure that when two adjacent particles have the same pressure, pressure gradient would be 0. Many symmetric forms of SPH momentum equation can be obtained at the particles by summation involving the kernel and its derivatives[31].

Morris et al. used a symmetric formulation of the pressure gradient to conserve linear and angular momentum exactly as follows [39]:

$$-\frac{\nabla p_i}{\rho_i} = -\sum_j m_j (\frac{p_i}{\rho_i^2} + \frac{p_j}{\rho_j^2}) \nabla_i W_{ij} \tag{2.23}$$

2.7.4 Viscosity Term

The viscosity term($\prod_{ij}$) in the momentum equation in Monaghan is introduced to compute artificial viscosity for high Re, compressible flows, where viscosity is modelled as a repulsive force which increases in magnitude as the distance between the particles decreases. If the interparticle distance increases then the repulsive forces are 0. This formulation has the key advantage of guaranteeing conservation of linear and angular momentum[31].

$$\prod_{ij} = \begin{cases} \frac{-\alpha c \overline{\mu}_{ij} + \beta \overline{\mu}_{ij}^2}{\overline{\rho}_{ij}} & \mathbf{v}_{ij} \cdot \mathbf{r}_{ij} < 0 \\ 0 & \text{otherwise} \end{cases} \tag{2.24}$$

$$\mu_{ij} = \frac{h \mathbf{v}_{ij} \cdot \mathbf{r}_{ij}}{\mathbf{r}_{ij}^2 + 0.01h^2} \tag{2.25}$$

The term $0.01h^2$ ensures the denominator is non-zero. But, equation 2.24 is useful only in applications where the flow velocities are high or there exists an unbounded fluid edge. So for applications with low fluid velocities and the SPH particles fill up the entire space, a more realistic formulation of viscosity was provided by Morris:

$$\{(\frac{1}{\rho} \nabla \cdot \mu \nabla) \mathbf{v}\}_i = \sum_j \frac{m_j (\mu_i + \mu_j) \mathbf{r}_{ij} \cdot \nabla W_{ij}}{\rho_i \rho_j (\mathbf{r}_{ij}^2 + 0.01h^2)} \mathbf{v}_{ij} \tag{2.26}$$

where $\mu = \rho\nu$, denotes dynamic viscosity. This expression guarantees conservation of linear momentum while angular momentum is approximately conserved. Morris simplified the viscosity term to the following[39]:

$$\{(\frac{1}{\rho} \nabla \cdot \mu \nabla) \mathbf{v}\}_i = \sum_j \frac{m_j (\mu_i + \mu_j) \mathbf{v_{ij}}}{\rho_i \rho_j} (\frac{1}{\mathbf{r}_{ij}} \frac{\partial W_{ij}}{\partial r_i}) \tag{2.27}$$

2.7.5 Surface Tension Term

Surface tension is an effect that occurs due to the interplay between the cohesive and adhesive forces, at the molecular level. Essentially, at the interface of two different materials, the difference in molecular binding energy results in surface energy density which seeks to minimize itself [40]. For example, the force that keeps the water molecules together when being poured in to a glass is surface tension. Inside the fluid each molecule is equally attracted by its neighbors but at the edge of free surface, due to the lack of neighbors on all sides, this cohesive force tends to minimize surface area[41]. While, adhesion is phenomena that occurs during interaction of fluid with dissimilar materials.

The details about which specific model(s) are adopted in each software will be discussed later.The current section is intended to give a brief overview of the previous work from which the models used in the three software were derived. Two common but fundamentally different approaches to modelling surface tension, the continuum surface tension (CSF) approach proposed by Brackbill and the pairwise force method of Tartakovsky and Pachenko are compared here[42].

Continuum Surface Force (CSF) Model

Brackbill et al. proposed the CSF model, but Morris later adapted it for SPH [43]. The CSF model reinterprets surface tension from a boundary condition to a volume force model that can be imposed within close proximity of the interface. Within the CSF framework there are two approaches, one to compute surface tension as function of local curvature of the interface and the other is to compute the surface tension force using the surface tension tensor (CSF-SST). The first approach is considered sufficient for basic understanding. Since surface tension is converted to volume force, it is expressed as:

$$\mathbf{F}_s = \sigma\kappa\hat{\mathbf{n}}\delta_s \tag{2.28}$$

where σ is the coefficient of surface tension, κ is the curvature of the interface, $\hat{\mathbf{n}}$ is the unit surface normal and δ is the surface delta function. A color function is used to distinguish between the different fluids present, which assigns a constant integer to the different fluid particles.

$$\phi(\mathbf{r}) = \begin{cases} 1 & \text{if particle a belong to phase 1} \\ 0 & \text{if particle a belong to phase 2} \end{cases} \tag{2.29}$$

The gradient of the color function is then used to compute the surface normals:

$$\mathbf{n} = \frac{\nabla\phi}{|\nabla\phi|} \tag{2.30}$$

Curvature is computed as the divergence of the unit surface normals, $\hat{\mathbf{n}}$:

$$\kappa = \nabla \cdot \hat{\mathbf{n}} \tag{2.31}$$

and δ_s in equation 2.28 is computed as $|\mathbf{n}|$.

In SPH formalism, Morris expressed the gradient of the color function using the density weighted formulation:

$$\nabla\phi_i = \sum_j \frac{m_j}{\rho_j}(\overline{\phi}_j - \overline{\phi}_i)\nabla W_{ij} \tag{2.32}$$

where the smoothed color function, $\overline{\phi}_i = \sum_j \frac{m_j}{\rho_j}\phi_j W_{ij}$ Then, curvature is computed as the divergence of the surface normal:

$$\kappa_i = \sum_j \frac{m_j}{\rho_j}(\mathbf{n}_i - \mathbf{n}_j) \cdot \nabla W_{ij} \tag{2.33}$$

A commonly reported problem with CSF model is the reliance on the computation of the local surface normals [42]. This issue was well observed in the droplet-droplet collision simulations. Accurate modelling of droplet-droplet collisions can be achieved when the van der Waals force are also included in the model. But the CSF model is based on the continuum framework and inter-molecular force(s) such as van der Waals is lost when the resolution is reduced to observe the system. The literature considered the CSF model that does not conserve momentum exactly, even though there are formulations using the CSF method where momentum is exactly conserved.

Pairwise force (PF) Model

This method was first proposed by Nugent and Posh and subsequently developed by Tartakovsky and Meakin and Tartakovsky and Panchenko [42]. It is more coherent with molecular dynamics. Surface tension is generated at an interface as pairwise forces between the fluid particles. In multiphase flows, the wetting and non-wetting nature at the fluid-fluid and fluid-solid interface is a consequence of the interplay of the forces acting between molecules of different fluid and solid phases. Further, with a PF model, the need to accurately capture surface curvature was overcome.

The model being studied has been developed by Tartakovsky and Meakin [44]. The particle interaction force is used to take into account the interactions between other fluid particles as well solid particles specific to handling of immiscible fluid mixtures. The interaction force acting on particle i, $\mathbf{F}_{ij}$ due to particle j is defined as:

$$\mathbf{F}_{ij} = \begin{cases} s_{ij}\cos(\frac{1.5\pi}{3h}|\mathbf{r}_j - \mathbf{r}_i|)\frac{\mathbf{r}_j - \mathbf{r}_i}{|\mathbf{r}_j - \mathbf{r}_i|} & |\mathbf{r}_j - \mathbf{r}_i| \leq h \\ 0 & |\mathbf{r}_j - \mathbf{r}_i| > h \end{cases} \tag{2.34}$$

where s_{ij} is the strength of particle interaction. The total force due to particle interactions acting on particle i is given by:

$$\mathbf{F}_i^{interaction} = \sum_j \mathbf{F}_{ij} \tag{2.35}$$

which can be included instead of $\mathbf{F}_\sigma$ in equation 2.1.

Since $\mathbf{F}_{ij} = -\mathbf{F}_{ji}$, the particle interaction ensures momentum is conserved [44]. The interaction force is modelled to be repulsive for distance lesser than $h/3$, attractive between $h/3$ and h but beyond h it is zero. The interaction force on fluid particles is non-zero at fluid-fluid and fluid-solid interfaces. Also within the bulk of the fluid where a local density gradient exists the interparticle interaction force is non-zero.

The strength of wetting (denoted by subscript w) and non-wetting (denoted by subscript n) nature between similar fluid particles is set using s_{ww} and s_{nn} respectively [44]. This interaction strength is set to be larger than the interaction strength between particles of different fluids, s_{nw}. With respect to wetting nature with solid boundaries (denoted by subscript b), the interaction strength is controlled by s_{wb} and s_{nb} where subscript w denotes wetting and subscript n denotes non-wetting. The strength of wetting is determined by the interplay between the strength of interaction between the fluid-boundary particles and that between the fluid-fluid particles. In other words, the nature of wetting is controlled by the interplay between adhesive and cohesive forces between the SPH particles.

2.8 Governing Equations: Weakly Compressible and Truly Incompressible Hypotheses

Since SPH was derived from astrophysics to simulate compressible flows[31], much research has been conducted towards enforcing the incompressibility condition in the SPH framework to simulate various practical engineering problems. Two popular hypotheses for enforcing incompressibility are presented in this section.

2.8.1 Weakly Compressible Hypotheses (WCSPH)

A stiff equation of state (EOS) is used to explicitly compute pressure from particle density. The governing equations including the EOS are:

$$\begin{cases} \frac{D\mathbf{u}}{Dt} & +\rho(\nabla\cdot\mathbf{u}) = 0 \\ \frac{D\mathbf{u}}{Dt} & = -\frac{1}{\rho}\nabla p + \nu\nabla^2\mathbf{u} + \mathbf{g} + \frac{1}{\rho}\mathbf{F}_s + \frac{1}{\rho}\mathbf{F}_{ext} \\ p & = \frac{c_0^2\rho_0}{\gamma}\left(\left(\frac{\rho}{\rho_0}\right)^\gamma - 1\right) \end{cases} \tag{2.36}$$

where equation 2.36 is the equation of state with ρ_0, c_0 denoting rest density of the fluid and artificial speed of sound. In his review work, Monaghan states that the artificial speed of sound was assumed to be 10 times higher than the expected maximum velocity of the fluid, U_{max}, so that the density variations are less than 1%,

i.e $c_0 \geq 10U_{max}$ [45]. γ is the polytropic constant, $\gamma = 1.4$ for air and $\gamma = 7$ for water. Morris et al. found that this EOS was rather stiff and the slight variations in density would result in strong changes in pressures. So, for $\gamma = 1$, Morris proposed a simplified EOS: $p = c^2(\rho - \rho_0)$. Such a formulation exhibited more stability within the WCSPH framework [9].

The key advantage of WCSPH is its fully explicit property in time. Velocity, density and position of the particle can be computed easily using:

$$\mathbf{v}^{n+1} = \mathbf{v}^n + \Big(-\frac{1}{\rho}\nabla p + \nu\nabla^2\mathbf{v} + \mathbf{g}\Big)^n \Delta t \tag{2.37}$$

$$\mathbf{r}^{n+1} = \mathbf{r}^n + \mathbf{v}^n\Delta t \tag{2.38}$$

$$\rho^{n+1} = \rho^n - \rho^n(\nabla\cdot\mathbf{v})^n\Delta t \tag{2.39}$$

The pressure can be computed using the updated density in the EOS. In practice, to ensure numerical stability either a predictor-corrector or Runge-Kutta method of time integration are often adopted.

Two popular WCSPH models are δ-SPH and Riemann SPH, which have been widely used to solve engineering problems.

2.8.2 Truly Incompressible Hypotheses

The governing equations used for a truly incompressible framework consist of:

$$\begin{cases} \nabla\cdot\mathbf{u} & = 0 \\ \frac{D\mathbf{u}}{Dt} & = -\frac{1}{\rho}\nabla p + \nu\nabla^2\mathbf{u} + \mathbf{g} + \frac{1}{\rho}\mathbf{F}_s + \frac{1}{\rho}\mathbf{F}_{ext} \end{cases} \tag{2.40}$$

Incompressibilty is enforced by solving the Pressure Poison Equation(PPE). The method comprises of two steps: a prediction and correction step. In the prediction step, an intermediate velocity(v^*) is calculated using the non-pressure forces:

$$\frac{\mathbf{v}^* - \mathbf{v}^n}{\Delta t} = \nu\nabla^2\mathbf{u} + \mathbf{g} + \frac{1}{\rho}\mathbf{F}_s + \frac{1}{\rho}\mathbf{F}_{ext} \tag{2.41}$$

Subsequently, velocity is corrected using the pressure forces:

$$\frac{\mathbf{v}^{n+1} - \mathbf{v}^*}{\Delta t} = -\frac{1}{\rho}\nabla p^{n+1} \tag{2.42}$$

The intermediate velocity is then projected on to a divergence free space by taking the divergence of equation 2.42 which yields the following PPE,

$$\nabla^2 p^{n+1} = \frac{\rho}{\Delta t}\nabla\cdot v^* \tag{2.43}$$

From the PPE, the pressure is derived and the velocity and pressure at $n+1^{th}$ step are computed by:

$$\mathbf{v}^{n+1} = \mathbf{v}^* - \Big(\frac{1}{\rho}\nabla p^{n+1}\Big)\Delta t \tag{2.44}$$

$$\mathbf{r}^{n+1} = \mathbf{r}^n + \mathbf{v}^{n+1}\Delta t \tag{2.45}$$

2.8.3 Weakly Compressible or Truly Imcompressible for Simulating Multiphase flows

Conventionally, SPH practitioners have favored truly incompressible SPH over WCSPH for simulating free-surface and fluid-solid interactions for applications such as ocean engineering, since it provides a noise-free solution. Lee et al. compared the two approaches and concluded that ISPH provides smoother velocity and pressure fields than WCSPH for every case they had implemented[46]. However, many researchers have proposed various methods to reduce the spurious numerical noise of WCSPH. Monaghan and Gingold proposed an artificial viscosity term to alleviate the oscillations induced by the shock waves for simulating compressible flows [47]. Antunono et al. proposed $\delta-$ SPH which was noted to produce accurate density and pressure fields[48].

Consequently, this model was later extended to violent free-surface flows by Marrone et al [49]. Simulation of large scale problems required sufficiently refined particles to capture the spatio-temporal free-surface evolution, implying that significant computational resources would be required to accommodate the total particle number. For such simulations, WCSPH could be a more feasible than ISPH considering the balance between numerical accuracy and computational capacity [9].

2.9 Comparison of Models In Each Software

The following section is aimed at explaining the different methods of implementation of SPH used in each of the software. In particular, the method by which the incompressibility has been imposed and different surface tension models adopted by each of the software.

2.9.1 Discrete Governing Equations In Each Software

Simcenter SPH

Riemann-SPH, a WCSPH model has been used in Simcenter SPH. Riemann SPH solver includes a Riemann solver with the governing equation to stabilize and reduce the non-physical pressure noise. The governing equations of the Riemann-SPH model are listed below [9]:

$$\begin{cases} \frac{D\rho}{Dt} = 2\rho \sum_j (\mathbf{v}_i - U^*) \cdot \nabla W_{ij} V_j \\ \\ \frac{D\mathbf{v}_i}{Dt} = -\frac{2}{\rho_i} \sum_j P^* \nabla W_{ij} V_j + \mathbf{g} \\ \\ p_i = c_0^2(\rho_i - \rho_0), \qquad c_0 \geq 10\text{max}\Big(||\mathbf{U}_{max}||, \sqrt{\frac{P_{max}}{\rho}}\Big) \end{cases} \tag{2.46}$$

where U^* and P^* are the results from an inter-particle Riemann problem along with a vector pointing from particle i to particle j.

Popular time integration schemes used are 4th order Runge-Kutta scheme (RK4), the predictor-corrector scheme etc. But, the primary criteria that any scheme used must fulfill is the Courant-Friedrich-Levy (CFL) condition. Simcenter SPH uses a RK4 for time stepping and has a CFL first order accuracy. The computational cost would not increase, though more inner loops are required per time step, due to the relatively larger value of CFL with this scheme [9].

LS-DYNA and Preonlab

An implicit incompressible SPH formulation has been implemented in LS-DYNA and Preonlab [16], [50], [51]. It was formulated using a semi-implicit Euler time integration. The velocities v_i^{n+1} and displacements x_i^{n+1}, for all particles i:

$$\begin{cases} \mathbf{v}_i^{n+1} & = \mathbf{v}_i^n + \Delta t \frac{\mathbf{F}_i^n}{m_i} \\ \mathbf{r}_i^{n+1} & = \mathbf{r}_i^n + \Delta t \mathbf{v}_i^{n+1} \end{cases} \tag{2.47}$$

The total force $\mathbf{F}_i^n$ has been decomposed into all forces acting on the particle excluding pressure forces, $\tilde{\mathbf{F}}_i^n$ and pressure forces that are unknown, $\mathbf{F}_{pi}^n$:

$$\mathbf{F}_i^n = \tilde{\mathbf{F}}_i^n + \mathbf{F}_{pi}^n \tag{2.48}$$

From this the intermediate velocities have been predicted using only the non-pressure based forces:

$$\tilde{\mathbf{v}}_i^{n+1} = \mathbf{v}_i^n + \Delta t \frac{\tilde{\mathbf{F}}_i^n}{m_i} \tag{2.49}$$

The density according to equation 2.20:

$$\rho_i = \sum_j m_j W_{ij} \tag{2.50}$$

Equation 2.1 has been discretized by forward differencing and applied to the SPH formulation of the continuity equation, described in equation 2.21:

$$\frac{\rho_i^{n+1} - \rho_i^n}{\Delta t} = \sum_j m_j \mathbf{v}_{ij}^{n+1} \nabla W_{ij} \tag{2.51}$$

where $\mathbf{v}_{ij}^{n+1} = \mathbf{v}_i^{n+1} - \mathbf{v}_j^{n+1}$. The predicted density at t_{n+1} is:

$$\tilde{\rho}^{n+1} = \rho_i^n + \Delta t \sum_j m_j \tilde{\mathbf{v}}_{ij}^{n+1} \nabla W_{ij} \tag{2.52}$$

The pressure forces $\mathbf{F}_{pi}^n$ have been computed such that $\rho_i^{n+1} = \rho_0$ where ρ_0 is the rest density of the fluid and in this manner the incompressibilty condition has been enforced:

$$\rho_0 - \tilde{\rho}_i^{n+1} = \Delta t^2 \sum_j m_j \Big(\frac{\mathbf{F}_{pi}^n}{m_i} - \frac{\mathbf{F}_{pj}^n}{m_j} \Big) \nabla W_{ij} \tag{2.53}$$

Using the expression for pressure forces from equation 2.23 yields:

$$\mathbf{F}_{pi}^n = -m_i \sum_j m_j \Big(\frac{p_i^n}{(\rho_i^n)^2} + \frac{p_j^n}{(\rho_j^n)^2} \Big) \nabla W_{ij}^n \tag{2.54}$$

Combining equations 2.53 and 2.54, a linear system of equation of the form $\mathbf{A}^n \mathbf{p}^n = \mathbf{r}^n$, where $\mathbf{p}_i^n$ is the pressure of particle i can be obtained at time t_n and $\mathbf{r}_i^n = \rho_0 - \tilde{\rho}_i^n$. With the help of a linear solver the system of equation are solved to obtain the resulting pressure forces, $\mathbf{F}_{pi}^n$. This pressure force can be used to solve equation 2.47 at time t_{n+1}.

2.9.2 Surface Tension Model Used In Each Software

Preonlab

The default surface tension model used in Preonlab is a Potential Force model based on the PF model proposed by Tartakovsky and Meakin[44]. A cohesion and adhesion coefficient has been defined to control the degree of wetting effect [16]. The interaction force has been defined as :

$$\nabla \Phi_i = -\sum_j \sigma_j^c w^c (\frac{\mathbf{r}_{ij}}{h}) \frac{\mathbf{r}_{ij}}{h^3} \tag{2.55}$$

where σ_j^c is the cohesion or adhesion coefficient of neighboring fluid particle or solid particle j respectively. w^c is the weighting kernel similar to the one proposed by Tartakovsky and Meakin.

In Preonlab, the user can adjust the cohesion coefficient for the liquid and the adhesion coefficient for the solid object, resulting in surface tension and wetting effect(s). If the adhesion value is increased while cohesion is held constant, the hydrophilic behavior of the object is increased. A value of zero indicated no adhesion or cohesion[16].

LS-DYNA and Simcenter SPH

The method implemented in these two software has been aimed to provide realistic handling of surface tension in SPH such that it can handle very large cohesive forces, avoid particle clustering near the free surface edge of the fluid, minimize surface area in all scales and ensure momentum is exactly conserved[41]. To avoid particle clustering at the free surface edge of the fluid, repulsive forces at close distances are introduced. The adhesion force model proposed aimed to provide realistic way of handling fluid-solid interaction to simulate different wetting effects.

The PF method was aimed to avoid normal computation and curvature estimation while ensuring momentum is conserved. The usage of cohesive forces between particles do not ensure that the surface area is minimized. The work conducted by Akinici et al. highlighted that large cohesive forces often resulted in cobweb-like structures, that reinforced intermolecular attraction [41].

The surface tension model in these software comprises of two terms: cohesion term and the surface minimization term. The cohesion term was derived using the PF framework but addressed the particle clustering by adding a repulsion term at close particle distances. The proposed cohesion force was formulated as:

$$\mathbf{F}_{ij}^{cohesion} = -\gamma m_i m_j C(|\mathbf{r}_i - \mathbf{r}_j|)\frac{\mathbf{r}_i - \mathbf{r}_j}{|\mathbf{r}_i - \mathbf{r}_j|} \tag{2.56}$$

where i, j are the neighboring SPH particles and m denotes mass and $\mathbf{r}$ denotes the position of the corresponding particle, γ is surface tension coefficient and C is the spline function.

$$C(r) = \frac{32}{\pi h^9}\begin{cases}(h-r)^3 r^3 & 2r > h \leq h \\ 2(h-r)^3 r^3 - \frac{h^6}{64} & r > 0 \wedge 2r \leq h \\ 0 & \text{otherwise}\end{cases} \tag{2.57}$$

Akinici et al. added the normalization factor h^9, to ensure that the force resulted in the same acceleration for different smoothing lengths [41]. The constant term was used to shift the practical value of γ close to 1. The spline function has a positive and negative part resulting in attractive and repulsion respectively. The attraction term has a maximum at particle distance $h/2$, beyond which the attractive force gradually decreases to 0 at full support radius, h. The force gradually decreases to a negative repulsive value when the distance between particles is lower than the rest distance. The spline function chosen behaves similar to the Gaussian to avoid particle clustering.

Another term was introduced to minimize surface area. The normal was computed by using SPH approximation on the gradient of the smoothed color field.

$$\mathbf{n}_i = h\sum_j \frac{m_j}{\rho_j}\nabla W_{ij} \tag{2.58}$$

h, smoothing length has been used to make the computed normal scale independent. Instead of computing the curvature by taking the divergence of the normal as in equation 2.31, the magnitude of the normal, $\mathbf{n}_i$ has been considered to be proportional to the curvature. Thus for flat regions, $\mathbf{n}_i - \mathbf{n}_j = 0$ and inside the fluid, $\mathbf{n}_i \approx 0$ and $\mathbf{n}_j \approx 0$. But for large curvature, it increases proportionally.

$$\mathbf{F}_{ij}^{curvature} = -\gamma m_i(\mathbf{n}_i - \mathbf{n}_j) \tag{2.59}$$

Combination of the cohesion and curvature term defined the surface tension model as [41]:

$$\mathbf{F}_{ij}^{\sigma} = K_{ij}(\mathbf{F}_{ij}^{cohesion} + \mathbf{F}_{ij}^{curvature}) \tag{2.60}$$

where $K_{ij} = \frac{2\rho_0}{\rho_i + \rho_j}$ is the symmetrized correction factor. This factor is used to explicitly ensure that spurious surface tension forces are not generated. All terms in the equation are symmetrized and hence conserve momentum.

A separate adhesion model has been used to model the interaction between the solid boundaries and the fluid particles. Boundary handling, where the solid boundaries are sampled as SPH particles, is employed to ensure that fluid particles do not tend to stick to the surface of the rigid body. Two way coupling of fluids particles and rigid bodies ensured that different slip conditions can be modelled while hydrodynamic forces and momentum exchange were taken in to account [41].

The volume of the boundary particle has been approximated by taking the reciprocal of the number density, $V_{b_i} = \frac{1}{\delta_{b_i}}$. The number density has been computed using the fluid particles neighboring the boundary. Mass of the boundary particle has been estimated by $\psi_{b_i} = \rho_0 V_{b_i}$, to allow two way interaction between the fluid particles and solid surface. [41].

The adhesion forces have been computed using fluid and boundary particles, as per the following:

$$F_{ij}^{adhesion} = -\beta m_i \psi_{b_k} A(|\mathbf{r}_i - \mathbf{r}_k|)\frac{\mathbf{r}_i - \mathbf{r}_k}{|\mathbf{r}_i - \mathbf{r}_k|} \tag{2.61}$$

where k denotes the boundary particles, $\mathbf{r}$ denotes position of the respective particle, β is the adhesion coefficient and A is the spline used to scale the magnitude of attraction based on distance between the two particles.

$$A(r) = \frac{0.007}{h^{3.25}} \begin{cases} \sqrt[4]{-\frac{4r^2}{h} + 6r - 2h} & 2r > h \wedge r \leq h \\ 0 & \text{otherwise} \end{cases} \tag{2.62}$$

The term $h^{3.25}$ has been used as a normalization factor to ensure that force results in the same acceleration for different radii, similar to the cohesive force term. The constant term has been used to scale the value β so that it is in the same range as γ, such that when $\beta \approx \gamma$, moderate hydrophilic behavior is exhibited. This force model has been modelled to attract particles between distances $h/2$ and h. Instead of a Gaussian like function, a steep parabolic function was used to prevent unrealistic detachment of the fluid from the solid and generate strong attractive forces with most of the neighboring fluid particles, in the test cases simulated by Akinici et al[41]. Like the cohesion term, the adhesive force has been modelled to be symmetric and conserve momentum [41].

3 Methodology

The aim of the project was to evaluate a scenario where a truck splashes through a pool of water using simulations set up in three different software - Preonlab, Simcenter SPH and LS-DYNA. The initial period of the project was spent on literature review to understand how the SPH method works in general while also learning how the three software worked. Once the general workflow of the software was understood, a simplified truck geometry was used to conduct a parameter study of the software. An experimental run using an real truck (FH 2021) was also performed at the Hällered Proving Grounds (HPG) to get some videos that the simulation results could be compared against. After the parameter study was run, a set of simulations were run with the detailed truck model. The default settings used for the parameter study were used in each software to run the detailed truck model down the same wading channel. The settings used for the simulations were similar to the ones used for the experimental run at HPG.

The simulation results were used to analyze each software with respect to the accuracy of the physics it modelled, the computational cost involved and its ease of usage. To understand the accuracy of the modelled physics a qualitative comparison of the results were done with the experimental results obtained from the HPG test runs. Apart from this, the simulations were also tracked to capture the splash height as well as the wetting pattern on the surface. In the case of computational cost, the number of nodes used along with the time taken to run the simulations were tracked in each simulation. The results section has more detailed description of each type of results and how it has been used. When it comes to ease of usage, the method used to setup each simulation has been recorded and a subjective analysis of its ease of usage is provided as a discussion in the subsequent section.

3.1 Parameter Study

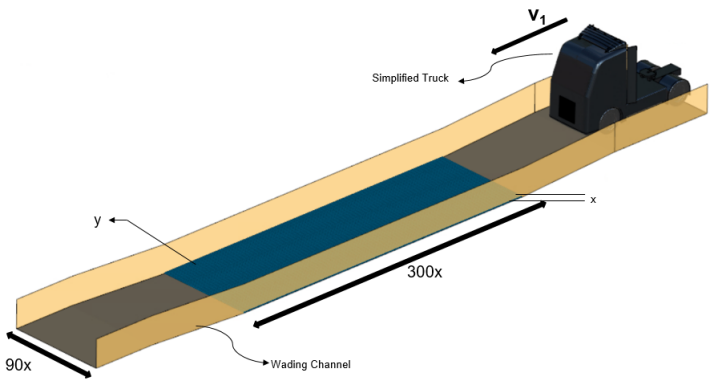

Figure 3.1: *Simulation Setup*

The purpose of the initial parameter study was to understand how certain critical parameters would alter the results of the simulations. A simplified truck geometry was used for the parameter study to reduce the computation time and resources required per simulation. The parameters selected and their corresponding values are summarized against each software as listed in Table 3.1. The default values for these parameters are highlighted in bold. The actual values have been hidden and have been replaced with symbols for confidentiality reasons. The changes in each parameter have been shown as fractions of the default settings. The particle sizing was chosen as it could affect the accuracy of physics captured by the simulation especially while capturing phenomena involving small length scales. It could also affect the simulation run time. The surface tension related parameters listed could affect the surface wetting patterns while the drag model could affect the way that the water particles splash through the air around the truck. All other parameters were maintained at a constant default value while these parameters were individually changed to analyze their effect on simulation results. As seen in figure 3.1, the simulation setup involved the truck driving along a wading channel at a speed of v_1. The wading channel had water up to a depth of x. The simulation was run until the front wheels of the truck reached the end of the wading pool. The simulation was stopped at this point as it was deemed unnecessary to simulate the exit of the truck from the pool. The contamination of the surface of the truck as it drives through the pool is expected to have been captured to a satisfactory detail by this point. The details of

the truck and wading channel are described in upcoming sections.

Software	Parameter	Values
Preonlab	SPH Particle Sizing	y/2, y, 3y/2
Simcenter SPH		
LS-Dyna		
Preonlab	Solid-liquid Adhesion factor	$\alpha/10$, α, 10α
Simcenter SPH	Surface Contact angle	2a/3,a,4a/3
LS-Dyna	Beta values	$\beta/10$, β, 10β
Preonlab	Drag Model	Active/ Inactive
Simcenter SPH		
LS-Dyna		

Table 3.1: Parameters Values used for Simulations

3.2 Comparison study of simulations with experimental tests

An experimental run was performed using the FH2021 truck model at Volvo's Hällered Proving Grounds to obtain videos and photographs for the comparison with the simulation results. The truck was driven through the wading channel at speeds v_1 and v_2, with v_2 being greater than v_1. The wading channel used had water to a depth of approximately x.

The splash generated by the truck was captured using 4 different views as shown in figures 3.2 and 3.3. The first three views depicted in figure 3.2 are obtained using cameras placed on the body of the truck. They were used to capture the shape of the splash and wave generated by the tyres of the truck as seen from the truck. On the other hand, the center view depicted in figure 3.3, was obtained using a camera placed on the ground in front of the truck. It captured the movement of the truck along with the splashes and waves generated by it.

(a) *Top View*

(b) *Back View*

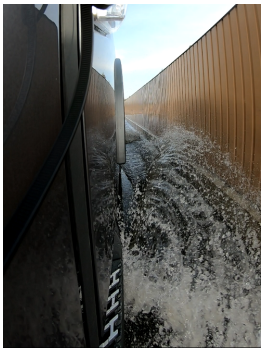

(c) *Front View*

Figure 3.2: *Views obtained from cameras placed on the truck*

Figure 3.3: *Center View*

After the HPG test had been completed, two simulations were run on each software to replicate the test runs done at HPG. The same speeds of v_1 and v_2 were used for these simulations. The default settings for particle sizing and surface tension parameters along with an active drag model was used to run these detailed truck model simulations. An asymmetry in the truck design was used to generate different splash patterns on each side of the truck. An exact replica of this geometry was used in the detailed truck simulations to check if these differences in splash pattern could be generated by the simulations as well.

3.3 Pre-Processing of Geometry files

The geometry files required for all the simulations were pre-processed in ANSA and exported out into formats that were suitable for being imported into each software. The general process involved generating a surface mesh for all the geometries used in the simulations namely the trucks and the wading channel. After surface meshing these geometries, their positions were modified such that the truck was at the beginning of the wading channel and its wheels were in contact with the wading channel surface. In the case of Preonlab and Simcenter SPH, the geometry was exported as .stl files but in the case of LS-DYNA the geometry was converted into a .k file format. The following sub-sections describe the pre-processing carried out in the case of each geometry.

3.3.1 Truck Geometries

The truck geometry used for all the simulations was provided by Volvo GTT. For the initial parameter study a simplified truck geometry was used as the lower amount of detail in the geometry allowed for faster simulations. For ease of post processing operations, the truck geometry was subdivided into 4 parts namely - upper body, underbody, front wheels and rear wheels, as indicated in figure 3.4. The truck geometry was surface meshed to produce triangular cells. The triangular cells were selected since LS-DYNA required triangular elements to generate SPH particles on the solid surfaces involved in the simulations.

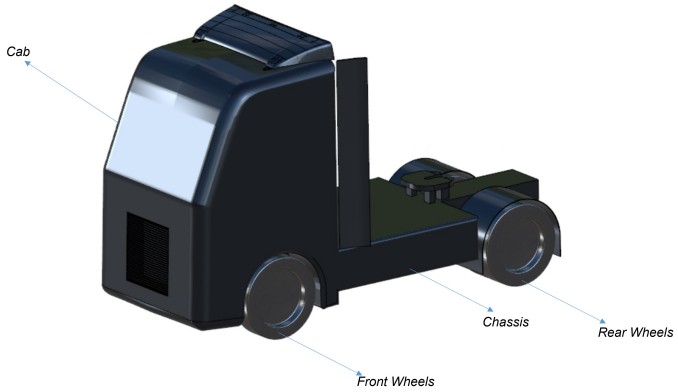

Figure 3.4: *Simplified Truck*

The parameter study was only intended as a means to understand the effect of simulation settings on the simulations results. Hence it was not essential to use an accurate truck model, as these would not be the simulations used to predict actual surface wetting or for comparison with the test videos. For actual surface wetting prediction, a detailed truck geometry of the FH 2021 was used to run a final set of simulations. The detailed truck model is shown in figure 3.5. The initial geometry provided in this case was also provided by Volvo GTT but the model was modified to reduce the mesh cell count and reduce the file size to allow for import in to Simcenter SPH.

Figure 3.5: *Detailed Truck Model - FH2021*

3.3.2 Wading Channel Geometry

A wading channel geometry based on the HPG wading channel was drawn using ANSA for the purpose of the simulations. The width of the channel was maintained the same as the original wading channel at HPG. The splashing phenomenon observed with the wading simulation becomes a repeating pattern after the initial few meters of the truck entering the wading channel. It was only essential to simulate the initial few meters of the truck wading in the channel and the same pattern could then be assumed to repeat till the end of the actual wading channel. Hence, the length of the base channel was reduced in length to reduce the run time of each simulation. The wading channel geometry was split into two parts namely the base and the walls in order to use them to later capture the splashing pattern on the wading channel walls. The wading channel geometry is depicted in figure 3.1.

3.4 Software setup

The steps involved in the setup procedure for each software has been listed out under the subsection for each software. The general setup procedure in all three involved conversion of the truck and wading geometry into a format suitable for import into the software. The subsequent steps were used to setup the motion of the truck and the SPH model required to simulate the motion of the water at the base of the wading channel. The sensors required to capture the required outputs were added to the setup as required in each software before the simulation file was ready to run. Finally, a script file was written to run the simulation on the cluster maintained by Volvo GTT.

3.4.1 Preonlab

All the setup procedure for the simulation using Preonlab was carried out on the Graphical User Interface(GUI) available for the software. There were no major differences in the steps required to setup a simplified truck geometry and a detailed truck geometry. The steps required to setup a simulation are described below. They are based on the vehicle wading simulation tutorial provided by Preonlab[52] as well as the Preonlab manual[16].

1. **Geometry and Kinematics Setup** - The wading channel and truck geometry were imported into the Preonlab Graphical User Interface (GUI) from ANSA as .stl files. The imported files could be seen under the solids tab in GUI. Then transform groups were created for the front wheels, rear wheels, cabin and chassis of the truck respectively. The transform groups were used to group different parts of the truck and prescribe a common motion. A python script provided by Preonlab was used to prescribe the forward motion of the truck with the transform group acting as the link between the imported geometry and the Python script. The connections between each of these parts and Python script were set using the Connection Editor tab, as seen in figure 3.6. The rotation and velocity of the front and rear wheels were prescribed using the *rotation_wheels_front* and *rotation_wheels_rear* transform groups respectively while the *transform_sprung_mass* transform group was used to translate the cabin and chassis in the positive x-direction across the wading channel. The Python script used in Preonlab also ensured the constant contact of the wheels of the truck to the wading channel. In the script the following parameters were user defined: time at which truck started moving, time at which truck stopped moving, time between two generated key frames, maximum distance moved per time step, velocity of the truck, front wheel radius and rear wheel radius. The script controls the motion of the truck using the geometry of the wading channel and the transform groups named *transform_script*,*rotations_wheels_front* and *rotations_wheels_rear*.

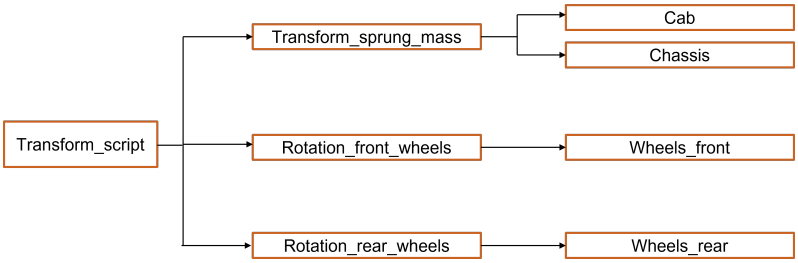

Figure 3.6: *Transform group connections with the geometries and with each other*

2. **Setting up water and boundary conditions** - A volume source was used to generate a body of water at the base of the wading channel. The size and position of the volume source was modified such that it covered the base of the wading channel and extended above the required height. A seedpoint was added within the volume source which was used to ensure that the SPH particles were generated above the wading channel. Further, a bounding domain surrounding the entire wading channel and truck was included. This bounding region was used to delete all SPH particle that spilled out of the computational domain for efficient use of the computational resources. The *Preon Solver*, which is Preonlab's SPH solver was then included to carry out the SPH computations needed for the simulation. In the solver settings *spacing* is used to set the particle sizing used in the simulation. A particle sizing of y is the default setting used in most of the simulations, if particle sizing has not been explicitly mentioned.

3. **Setting up sensors** - A wetting sensor was added to all the solid objects in the simulation so that it could capture the average and instantaneous wetting pattern on each surface. Apart from this volume sensors were placed at periodic height intervals to capture the volume of fluid rising to different heights in the channel. This data was output as .csv files which was later used to generate the splash height distribution graphs.

4. **Altering parameters for Parameter Study** - As mentioned in table[3.1], multiple parameters of the Preonlab simulations were modified to understand how they influence the simulations results. The ways in which these parameters were modified are explained below:

   (a) **Particle Sizing** - The particle size was varied between y/2, y and 3y/2. The *spacing* parameters under the *Preon Solver* settings was used to vary and control the particle sizing.

   (b) **Surface Tension** - The surface tension or contact forces that act between the solid and liquid phases influence how the fluid behaves once it comes into contact with the surface. The option to control the solid-liquid adhesion factor under every solid part was used to vary the surface tension force during the parameter study. This factor is multiplied with the cohesion of the fluid in order to obtain the effective adhesive forces between the solid and fluid SPH particles[16]. The default value used for the adhesion factor was varied between $\alpha/10$, α and 10α.

   (c) **Drag Model** - The drag model used affects the way in which the fluid behaves as it is splashing through the air surrounding the truck. The drag model was kept active or inactive to see how much influence it had on the splash generated by the truck. The drag model was added as an additional external force apart from gravity in the *Force Fields* tab of the software.

3.4.2 Simcenter SPH

All the setup procedure for the simulation using Simcenter SPH (previously known as Nextflow) was carried out on the Graphical User Interface(GUI) available for the software. There were some differences in the steps required to setup a simplified truck geometry and a detailed truck geometry which will be pointed out while describing the geometry and kinematics setup. The steps required to setup a simulation are described below. They are based on the instructions provided in the wading tutorial provided by Simcenter SPH [53]

1. **Geometry and Kinematics setup** - The geometry was split into separate sections based on the post processing requirements and exported as .stl files from ANSA. The truck was split into front wheels, rear wheels, chassis and cabin. The wading channel was divided into its base region and its walls. These are then imported into the Simcenter SPH GUI individually. The way that Simcenter SPH had been installed

in the Volvo GTT systems prevented the import of files beyond a certain size. Due to this, the geometry used for the detailed truck had to be split into even smaller parts than that required for the outputs. Once the geometry had been imported, the truck geometry was shifted to ensure that there was minimal gap between the wading channel base and the truck tyres. In the case of the simplified truck since both the wheels had the same diameter this was quite straight forward. But in the case of the detailed truck model, the front and rear wheels had different diameters and it could only be ensured that the front wheels were in contact with the channel base with the rear wheels were marginally below the channel. The motion for each part of the truck geometry was specified using ASCII files composed of 7 columns. The first column specified the time in seconds. The next three columns specified the translational velocity (in m/s) in the x, y and z direction at that particular time instant while the final three columns specified the angular velocity (in rad/s) of the geometry about the x, y and z axis at that time instant. The translational and angular velocities between two specified time instances was obtained by the software using linear interpolation. An excel file provided by Simcenter SPH was used to generate 7 columns required for the ASCII text files. The excel file generated velocities for the front wheels, the rear wheels and the remaining truck body. It required the x and z coordinates of the centers of the front and rear wheel as inputs . Apart from these, the x and z coordinates of certain positions of the wading channel as shown in figure 3.7 were required as inputs.

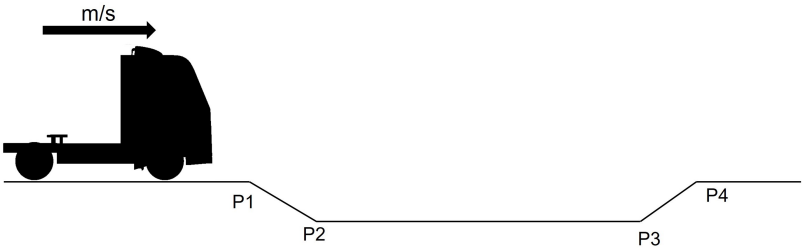

Figure 3.7: *The x and z coordinates of the points P1, P2, P3 and P4 on the wading channel base are entered as inputs into the excel sheet used to generate the motion files needed for prescribing the kinematics in Simcenter SPH*

2. **Setting up water and boundary conditions** - The wading channel geometry was used to split a cuboid and generate a geometry that would represent the initial volume of wading pool. This geometry was assigned as a fluid domain specifying the SPH particle sizing. Along with viscosity, the advanced surface tension model is activated to allow for variation of the surface tension parameters in the simulation. Water was selected as the fluid model so that the default values corresponding to viscosity and density of water could be used for the simulation. The wall boundary condition was set to no-slip conditions. Apart from this a domain boundary was included in this simulation which would also delete any SPH particle that splashed out of the wading channel. Finally, the range allowed for fluctuations in density (0.95-1.05 times rest density) and the maximum Mach number (0.3) was set to ensure that the weakly compressible (explicit in pressure) solver used by Simcenter SPH did not diverge. Any particle with corresponding properties outside this bounding range would be deleted to stabilize the simulation.

3. **Setting up Sensors** - The average wetting and instantaneous wetting of all the solid surfaces was captured by default in Simcenter SPH and no addition sensors were required for these outputs. Fluid flow rate sensors were placed at periodic height intervals in the wading channel to capture the volume of fluid rising to various heights as the truck passes through the channel. The data recorded by this sensor was output as .csv file like in Preonlab and was run through a python script to generate the splash height distribution graphs.

4. **Altering the variables for the Parameter Study** - In this case as well, the SPH particle sizing, surface tension parameters and the drag model presence were altered to understand their effect on simulation results. The way in which each parameter was varied has been explained below.

   (a) **Particle Sizing** - The particle sizing was varied between y/2, y and 3y/2. The discretization option in the initial domain section was used to control the SPH particle sizing.

(b) **Solid-Liquid contact angle** - The solid-liquid contact angle parameter that becomes available when the advanced surface tension model was turned on and was used to control the surface tension displayed at the solid-liquid interface. The contact angle was varied between 2a/3, a and 4a/3. The lower the contact angle value the more strongly the liquid was expected to stick to the surface of the solid.

(c) **Drag Model** - The drag model in the *Environment* tab can be ticked or unticked to add or remove the drag model in the simulation setup. No velocity was added to the air to mimic quiescent air conditions.

3.4.3 LS-DYNA

The pre-processing for LS-DYNA simulation setup was carried out using two tools: ANSA followed by LS-Prepost. ANSA has the provision for a LS-DYNA workbench built into it. The functions required for establishing contact of the truck with the wading channel, the motion of the truck and material properties of the solid objects were included using ANSA[54]. However, the SPH related functions were included into the model using LS-Prepost since some of the functions are unavailable in ANSA. Further, for calculations to be carried efficiently on the cluster, some Message Parallel Passing (MPP) functions were also included into the model using LS-Prepost, based on the recommendations of Dynamore Nordic. A similar procedure was used for the detailed truck as well, with values of certain functions needing to be altered based on the size of the mesh used by the geometry. The steps required to setup a simulation are listed below:

1. **Geometry and Kinematics Setup** - Like in the other two software for post-processing requirements, the geometry was divided into sections and a unique property ID (PID) was set to each geometric part prior to being exported as .k files. In the case of the wading channel, it was split into road and the walls. The two were assigned to a rigid material definition. In the material cards for the road and the walls, the center of mass was constrained along all 6 degrees of freedom (DOF) to ensure it stayed still in space. A rigid joint was included to keep the road and walls attached. For the truck, it was divided into the front wheels, rear wheels, the cabin and the chassis. Each of these sections are assigned to unique PID and each a unique rigid material. The center of mass was arrested in the necessary degrees of freedom for each part, for example, the wheels were allowed to rotate about the y-axis and translate in the x- and z- directions. Subsequently, rigid revolute joints were included to the front wheels and the chassis to replicate the front axle of the truck. A rear axle was created in a similar manner. A rigid body joint was created between the chassis and the cabin. Since, the provided geometry was made of shell elements, additional mass needed to be introduced as a point source at the center of gravity (CoG) of the truck, in order to replicate realistic mass conditions. The chassis and the cabin of the truck were prescribed a translational velocity in the positive x-direction. The truck and the wading channel geometry were each saved in the .k format. A Main.k file was created, in which the truck and wading channel geometry were included as modules. A contact card was included that established contact between the four wheels of the truck and the road of the wading channel with a high friction coefficient. When carrying the setup with detailed truck model, a similar procedure was carried out.

2. **Setting up the SPH part of the Simulation** - The implicit formulation of LS-DYNA allows for the fluid-structure interaction to be handled directly by the SPH solver. No contact definition is required between the SPH particles and the structure surfaces. In order to create the SPH particles to replicate the water at the base of channel,* *Define_SPH_Mesh_Box* was included to automatically generate a volume of water made of SPH particles. The length, width and height of the box were defined as well as the number of particles distributed along each direction. A set of **Define_SPH_Mesh_Surface* was used to sample the surface of the truck body, wheels and wading channel with SPH boundary particles to handle fluid structure interaction implicitly. All SPH particles outside a certain region were deactivated which was achieved by including **Define_SPH_Active_Region*, as seen in figure 3.8. The incompressible SPH formulation was achieved by setting $Form = 13$ in **Control_SPH* keycard.

3. **Additional essential functions** - The time step was controlled by defining a curve and passed as an argument in the *Control_Timestep* keyword. **Control_Termination* keyword was included to control the total simulation time. These additional essential functions were all included into the Main.k file. The MPP keywords were included here to ensure the computational domain was decomposed across the available processors and communication between processors was effectively carried out as the simulation evolved.

4. **Setting up Sensors** - **Database_Binary_ISPHFOR* was included to control the output interval of the SPH interfacial force file. This file was used to store the instantaneous wetness at each time step and the accumulated wetness data. The SPH particle position data was stored at all output time instances and were later used to generate the splash height distribution graph data in $META$, post-processing tool. It was redrawn using a python script to replicate the format obtained from the other two software.

5. **Altering the variables for the Parameter Study** - The variables of the parameter study were varied to study the effects of the particle sizing, surface tension and drag model on the computational time and flow physics. The means by which they were varied in LS-DYNA have been listed below:

   (a) **Particle Sizing**- The particle sizing was varied between y/2, y and 3y/2 by changing the particle distribution along each direction of box volume in the * *Define_SPH_Mesh_Box* keyword.

   (b) **Surface Adhesion Coefficient**- The surface adhesion coefficient, beta in the **Mat_SPH_Incompressible_Structure* was varied between $\beta/10$, β and 10β, with β being the default recommended value for water. This material was used for all structures that were sampled with the * *Define_SPH_Mesh_Surface* keyword. This coefficient is a purely numerical value and was normalized based on the formulation of surface tension mentioned in LS-DYNA manual [54].

   (c) **Drag Model** - The influence of the drag model on the flow physics and computational cost was evaluated by simply including the formulation into the computational model and excluding it. **Define_SPH_Ambient_Drag* was used to add drag force to the SPH particles in the model. However, note that no velocity was prescribed to mimic quiescent conditions. The density and viscosity values of the surrounding gas were set to those of air.

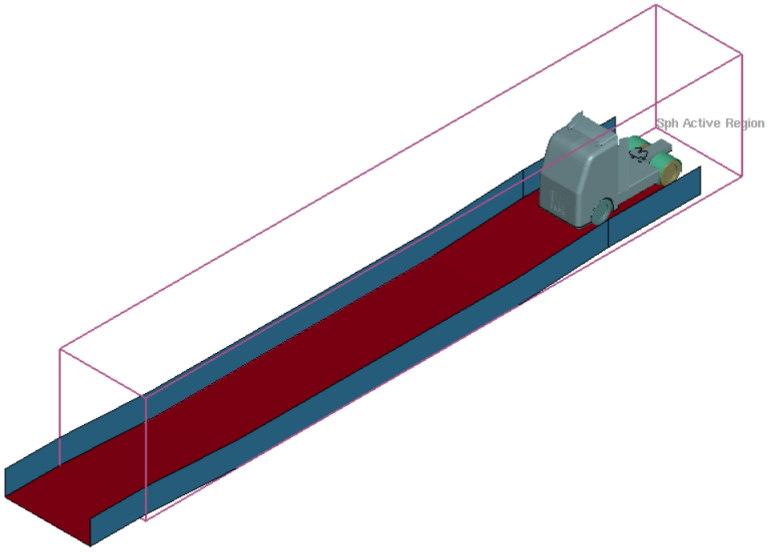

Figure 3.8: *A box volume defined by *Define_SPH_Active_Region outside which SPH particles are deactivated*

4 Results and Discussion

The results and discussions have been divided into two major sections. The first section deals with the results of the parameter study done using the simplified truck model while the second section deals with the results of the simulations run using the detailed truck model.

The results used to evaluate each software have been briefly described here. The average wetting, instantaneous wetting, splash height distribution and core hours have been used to analyze the parameter study as well as the final simulations using the detailed truck model. However in the case of the detailed truck some additional results such as various rendered views as well as height maps have also been generated to compare the results with the images obtained from the HPG tests.

1. **Average Wetting** - The average wetting pattern shows which areas of the truck surface has been wet and the duration of time for which these areas have been wet. The range for the wetting pattern was set from 0%-48% of the total simulation time for both the simplified and detailed truck. This was done to preserve confidentiality of the information, the data for all simulations have been normalized. The results were captured such that the truck was at the same position in the wading channel whether it was running at speed v_1 or v_2.

2. **Instantaneous Wetting** - The instantaneous wetting pattern of the wading channel walls shows the area of the wading channel walls that is in contact with the fluid in the time instant for which the image has been captured. It has been used to capture how high the splashes or waves generated by the truck reaches under different parameter settings.

3. **Splash Height Distribution** - The splash height distribution shows the volume of fluid that is rising to different heights in the wading channel as the truck passes through the wading channel. The volume of fluid rising to different heights in the channel has been captured for every time step in each software. These were then averaged over the same set of time steps such the effects of the initial entry into the pool as well as the influence of the exit ramp can be minimized. The splash height distribution thus gives a measure of how high the splash generated by the truck rises. The height up to which the fluid volume rises has been normalized with the height of water used in the wading channel.

4. **Core Hours** - The number of nodes used to run each simulation as well as the total time in hours taken for running the simulations were captured and multiplied together to get the core hours used to run the simulations. These have been used to provide a measure of how expensive the simulations are to run.

5. **Rendered images** - The rendered images of the detailed truck simulations have been captured from multiple views which we have named as - top view, front view, center view and back view. These views have been rendered such that they closely resemble the camera views used in the HPG test. These were then used to provide a qualitative analysis of whether the splashes and waves generated by the simulations resemble the test results.

6. **Height Map** - The height to which SPH particles rise from the base of the wading channel has been captured from the same views used to generate the rendered views. These images provided a qualitative idea about the amount of fluid particles at various heights and has been used to evaluate if the simulations are able to replicate the splashes and waves observed in the HPG test.

4.1 Parameter Study

The parameter study was carried out with the intent of understanding how to select parameters in each software that would affect the results of the simulation. The parameters varied influenced the particle sizing, the surface tension between the solid-liquid interface and the presence of an air drag model. The results are presented below divided by the software used such that the influence of each parameter can be analyzed within the software. A final set of results comparing the default simulation setup between the software has also been provided at the end of the section.

4.1.1 Preonlab

The results obtained from Preonlab for the parameter study have been displayed and discussed in this subsection. The default simulation was run using a particle size of y, solid-liquid adhesion factor of α and an active drag model. Each of these parameters were varied independently to understand their influence on the results.

Particle Sizing

The particle sizing was varied between y/2, y, and 3y/2. The average wetting pattern on the truck, the instantaneous wetting of the wading channel walls and the splash height distribution for the three simulations have been analyzed to understand the influence of the particle sizing on the simulation.

Average Wetting - The average surface wetting of the bottom surface of the truck has been displayed in the figure 4.1. As seen from the images, the surface close to the inner side of the front wheel has been wet in all three cases. There is also a small amount of wetting at the front edge of the wheel house indicating a bow wave splash that has hit the inner front surface of the wheel house. The wetting pattern is quite symmetric in all three cases. However, the area wet by the fluid is observed to increase as the SPH particle size used for the simulation decreases.

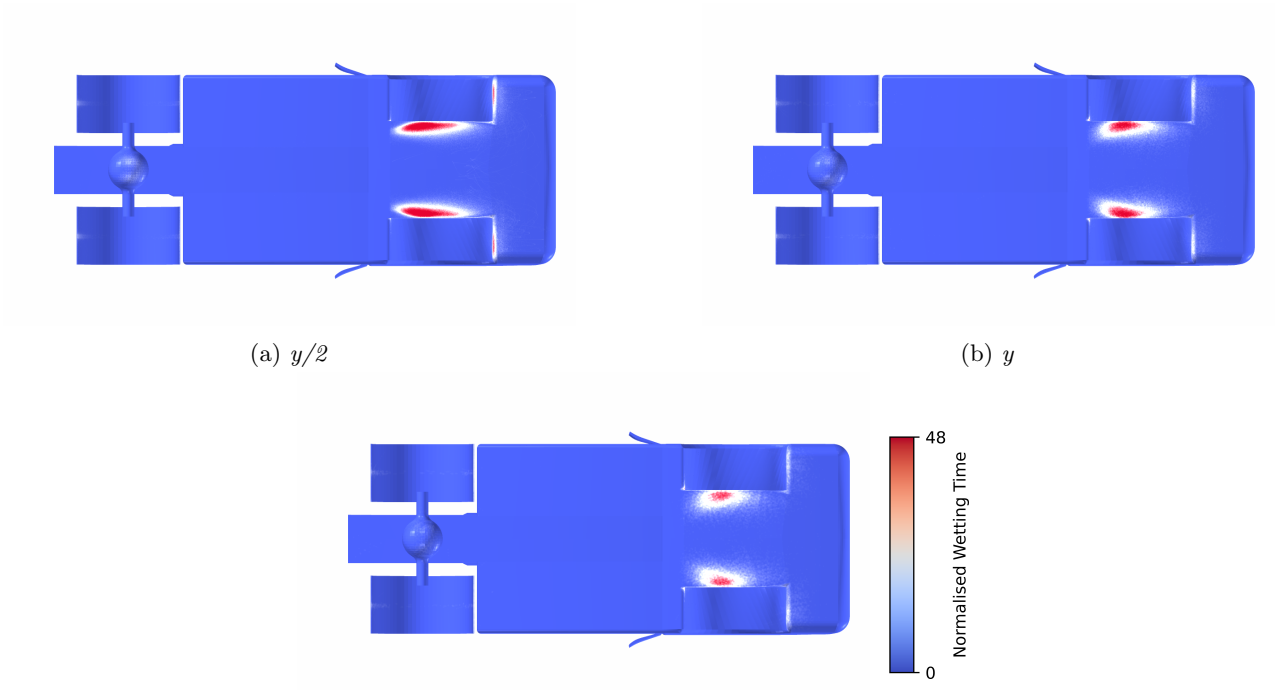

(a) *y/2* (b) *y*

(c) *3y/2*

Figure 4.1: *Average wetting of the bottom surface of the simplified truck as the SPH particle sizing used for Preonlab simulations was varied between y/2, y and 3y/2*

The average wetting pattern on the side surface of the truck is displayed in figure 4.2. The bottom region of the wheel housing shows wetting from the splash generated by the front wheel. The splash spread seems to be more concentrated to the front of the wheel house in the case of the y/2 simulation while the other two cases have more concentration towards the rear end. The spread of the wetting pattern is also more smoother in the case of the y/2 particles. In contrast, the 3y/2 particle sizing case has very coarse spreading pattern where the individual particle impact positions can be identified on the surface of the truck.

Instantaneous Wetting - The instantaneous wetting pattern on the walls of the wading channel are displayed in figure 4.3. The solid red curves rising above the base in all three images depict the waves generated by the front and rear wheels. The scattered spots on the other hand indicate the regions on the wall hit by the splash drops propelled through the air either directly from the wheels or from the waves striking the walls. The images corresponding to y/2 particle sizing seem to depict more spread of the splash particles while the splash pattern progressively decreases with increase in particle sizing. This is particularly observable in the case of the splash generated by the rear wheel that appears clearly between the two waves in the case of the y/2 particle size simulation. But this splash progressively disappears with increase in particle size and becomes negligible in the 3y/2 particle size simulation. The waves generated by the wheels also seem to be more damped reaching lower heights at their crest with the increase in particle size.

Splash Height Distribution - The splash height distribution as the particle sizing is varied is depicted

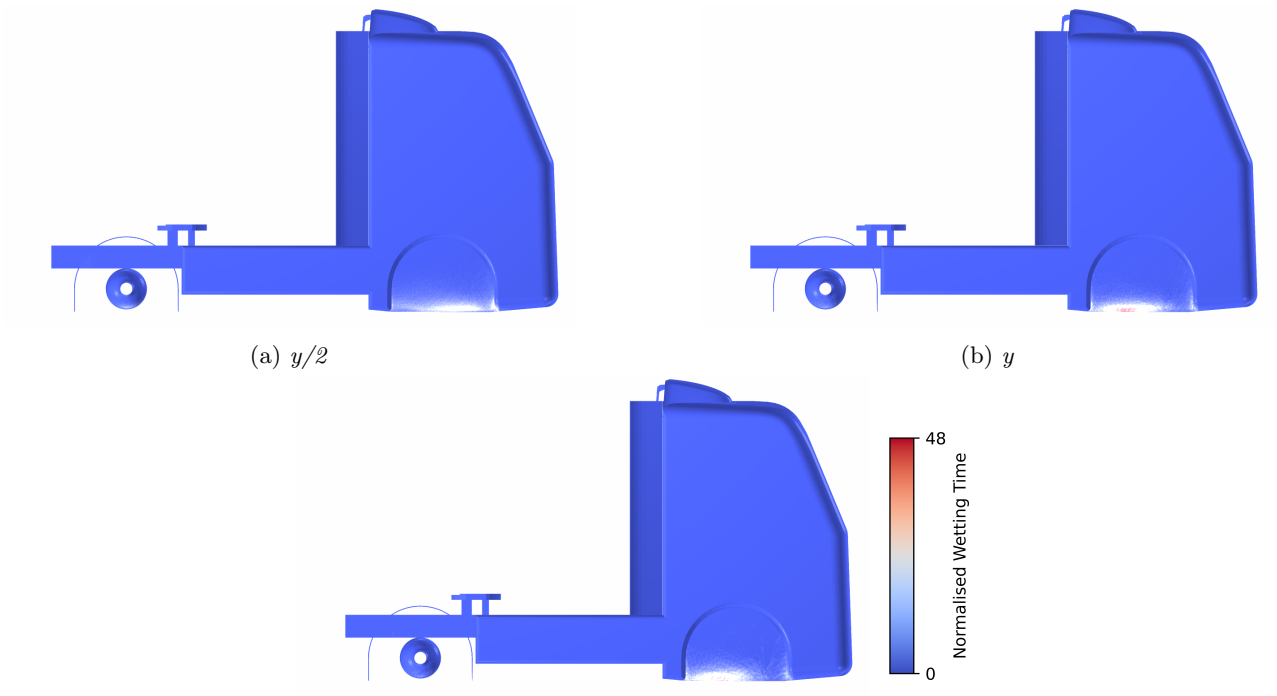

(a) *y/2* (b) *y*

(c) *3y/2*

Figure 4.2: *Average wetting of the side surface of the simplified truck as the SPH particle sizing used for Preonlab simulations was varied between y/2, y and 3y/2*

in figure 4.4. It can be seen that height to which water rises is higher in the case of the y/2 simulation with significant volume of fluid rising up to 9-10 times the wading channel height(x). The y curve is also a somewhat higher than the 3y/2 curve in the 4x-7x range however their maximum heights seem to coincide. The y/2 and y curves coincide for heights lower than 4x. All three curves coincide for heights below 2x. The pattern indicates that the y/2 simulation depicts fluid particles rising or splashing to higher heights while the increase in particle size prevents this rising up of particles leading to a lower splash size. This observation is also supported by the instantaneous wetting pattern on the wading channel walls discussed in the previous section.

Core hours - The normalized core hours along with the normalized number of particles in the simulation is shown in table 4.1 as the particle size is varied for the Preonlab simulations. The quantities have been normalized with the values from Preonlab since it had the least run time among the software at the default settings. The run time of the simulation exponentially scales up as the particle size is decreased. The increase in run time is proportional to the increase in particle size as the number of calculations that have to be performed goes up by the number of additional particles that are present in the simulation. The increase in particle number is close to $(oldparticlesize/newparticlesize)^3$ and hence the run time also increases by at least this quantity. The run time increases by almost 12 as the particle size is reduced from y to y/2.

Particle Sizing	Normalized no of particles	Normalized Core Hours
y/2	1	12
y	1	1
3y/2	1	0.3

Table 4.1: Normalized Core Hours for Preonlab simulations as the particle size is varied

Solid-Liquid Adhesion Factors

The solid-liquid adhesion factor is multiplied with the cohesion of the fluid particles to obtain the adhesion between the solid surface and the fluid particles. The cohesion of the fluid in this case is taken to be 0.072N/m which is the cohesive force or surface tension of water. The solid-liquid adhesion factor is varied between $\alpha/10$,

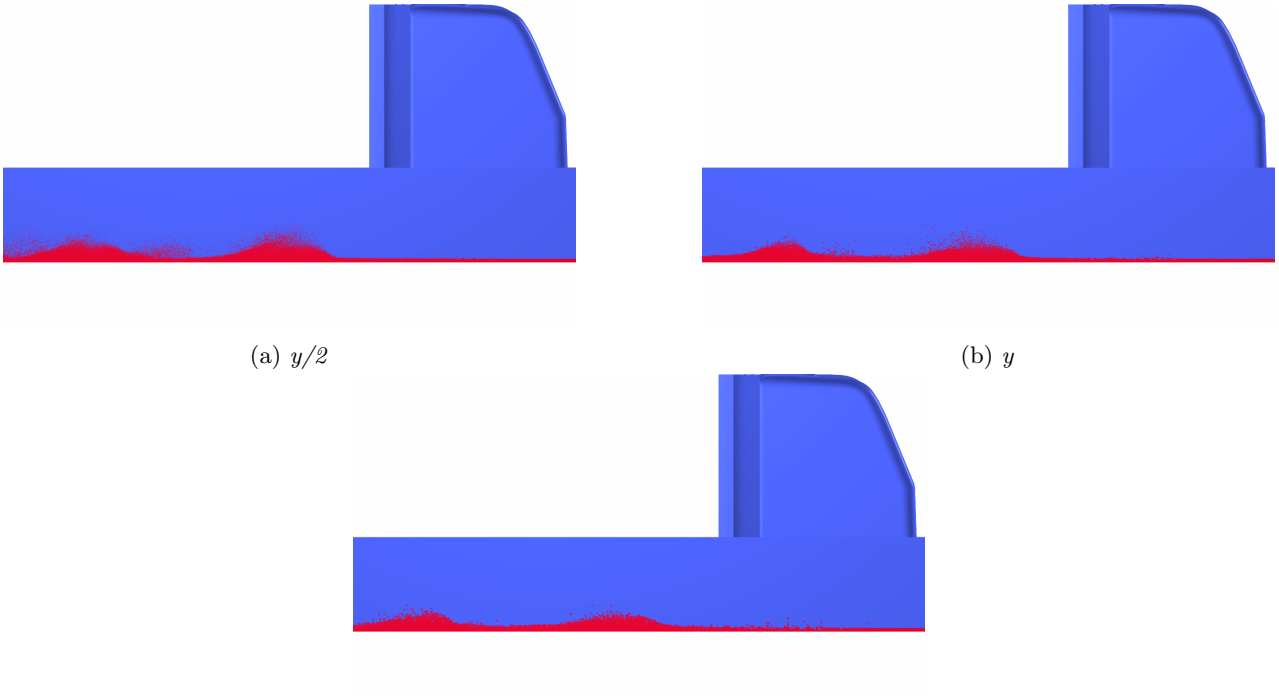

(a) *y/2*

(b) *y*

(c) *3y/2*

Figure 4.3: *Instantaneous wetting of the walls of the wading channel as the SPH particle sizing used for Preonlab simulations was varied between y/2, y and 3y/2*

α and 10α for the purpose of the parameter study. A solid-liquid adhesion factor greater than 1 implies that the force of attraction between the solid and liquid particles is greater than the force of attraction between the fluid particles themselves. There are very minor differences between the three different Solid-Liquid Adhesion factors used for the parameter study. There is a minor increase in the wetting duration between the three software with more area on the truck displaying a red patch.The wetting pattern however remains relatively the same. From the instantaneous wetting pattern it could be seen that more particles generated by the waves striking the walls stick to the wall surface at higher adhesion factors. The computational cost was quite similar in all three cases. Since the results did not show notable differences, the images corresponding to this parameter study has been displayed only in appendix A of the report.

Drag Model Usage

The drag model used for the simulation is turned from active in the default case to inactive in this particular parameter study. Since the air surrounding the truck is assumed to have no velocity, the drag model acts such that it slows the SPH particles irrespective of the direction in which they are moving. The average wetting pattern on the bottom surface of the truck does not show any significant differences. There is a minor decrease in the concentration of the wetting pattern at the bottom of the front wheel house implying that the drag inactive model allows water to rise to higher heights than the active case. In the case of the instantaneous wetting images of the wading channel, the top of the wave generated by the front and rear wheels are more rounded off when the drag model is active while the wave has a sharper crest when the drag model is inactive. This implies that the drag model is the one that opposes the forward motion of the wave producing the rounded off wave crest. There is a minor increase in splash height distribution at the higher heights as the drag model is turned inactive implying that the drag model does damp down the splash generated by the truck. The core hours for the drag active and the drag inactive case are quite close. Since the difference between the drag active and the drag inactive simulations are minor, their pictures have not been displayed here but they can be found in appendix A.

Discussion of Parameter Study in Preonlab

The parameter study carried out for Preonlab seems to imply that the particle size plays a big role in the results obtained especially in terms of the splashes generated by the truck. The smaller the particle size, the

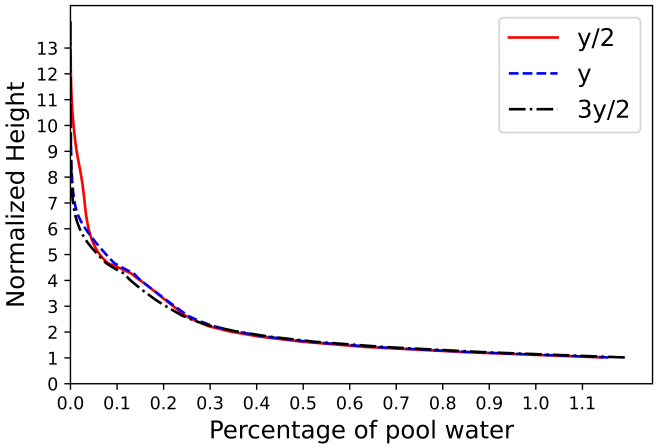

Figure 4.4: *Splash Height Distribution for different Particle Sizes in Preonlab simulations*

higher and finer the splash and spray generated by the particles. The smaller particles might be able to resolve the finer spray and splash phenomena such as droplet breakup and coalescence that the larger particle size might not be able to capture. The resolution of phenomena observed is restricted by the size of the particles used and any phenomenal that includes volumes of fluid smaller than the particle volume might not be captured properly. The wetting pattern also seems to be larger which could be because more particles rise to a higher height and hit the bottom surface of the truck. This could be because the smaller particle are imparted more moment which the gravitational forces along with drag forces take longer to counteract. The larger wetting pattern could also be because the adhesive force is able to overcome the gravitational force in the case of the smaller particles and cling to the solid surfaces for longer time. Although the smaller particle size allows for better resolution of the fluid phenomena it should be noted that this comes with an exponential increase in computational time.

The parameter study indicates that the drag model seems to have a very minor damping influence on the splashes and waves generated by the simulations. However, it must noted that the variation in drag model was done at y particle sizing and going lower or higher in particle sizing might produce a stronger or weaker influence on the simulation results from these parameters. Since the run time is not significantly affected by the drag model, it could be included to model the damping effect that air drag could have on the splashing and wave patterns.

4.1.2 Simcenter SPH

The results obtained from Simcenter SPH for the parameter study have been displayed and discussed in this subsection. The default simulation has been run using a particle size of y, solid-liquid contact angle of a and an active drag model. Each of these parameters have been varied independently to understand their influence on the results.

Particle Sizing

The particle sizing was varied between y/2, y, and 3y/2. The average wetting pattern on the truck, the instantaneous wetting of the wading channel walls and the splash height distribution for the three simulations have been analyzed to understand the influence of the particle sizing on the simulation.

Average Wetting - The average wetting pattern on the bottom surface of the truck is depicted in the figure 4.5. The images from the y and 3y/2 simulations show significant asymmetry in the wetting pattern with more wetting on the driver side of the truck than the passenger side. In contrast the y/2 simulation shows a more symmetric wetting pattern with marginal increase in wetting intensity on the passenger side. The general wetting pattern however consists of a wet patch on the inner surface of the bottom of the truck and a wet patch on the forward section of the front wheel house. This indicates that the wheel creates a side splash as well as a forward bow wave. The wetting pattern generated in the y/2 simulation is generally larger with a progressive decrease in the wet surface area as the particle size increases.

The average wetting pattern on the side surface of the truck is depicted in figure 4.6. In this case as well the wet surface area is maximum in the case of the y/2 simulation and it progressively decreases with increase in particle size. The major wetting as observed from the side view is on the front end of the wheel house. In

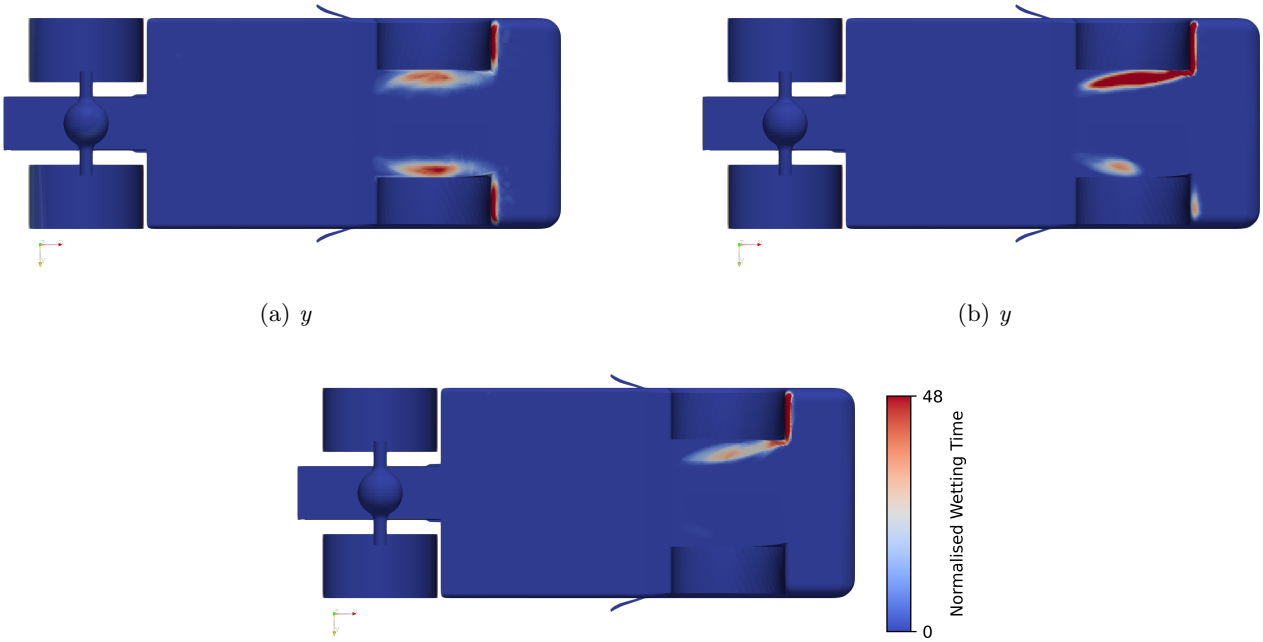

(a) *y* (b) *y*

(c) *3y/2*

Figure 4.5: *Average wetting of the bottom surface of the simplified truck as the SPH particle sizing used for Simcenter SPH simulations was varied between y/2, y and 3y/2*

the y/2 simulation wetting can also be observed on the inner surface of the wheel house as well.

Instantaneous Wetting - The instantaneous surface wetting on the wading channel walls is displayed in figure 4.7. The instantaneous wetting pattern has very sharp jagged edges and does not show exact particle strike positions. The sharp edged wetting patterns are able to differentiate the two prominent waves generated by the front and rear wheels however they are unable to identify the splashes or droplets that strike the surface of the wading channel walls. From the images it can be seen that the y/2 simulation gives a sharp crest to the front wave while the wave crest flattens out as the particle size increases. The rear wave seems be a flat long rise in the y/2 case while it rounds off in the y case. In the 3y/2 case the wave again becomes flat but it is shorter in length than the y/2 case.

Splash Height Distribution - The variation in the splash height distribution as the particle sizing is changed is depicted in figure 4.8. The volume of water splashing to a height of 6x and above is higher in the case of y/2 particle sizing. This progressively decreases with increase in particle size indicating that the high splashes are more higher with the smaller particle size of y/2. In contrast, the reverse trend is observed at lower heights below 3x, with the y/2 simulation producing the least rise from the base pool. The 3y/2 simulation produces the maximum volume of fluids at these heights.

Core hours - The normalized core hours along with the normalized number of particles in the simulation is shown in table 4.2 as the particle sizing is varied for the Simcenter SPH simulations. Similar to the Preonlab case, the simulation run time increase exponentially as the particle size decreases with the increase in time proportional to the increase in the number of particles in the simulation. The increase in particles is again approximately equivalent to $(oldparticlesize/newparticlesize)^3$, as mentioned in the Preonlab subsection.

Particle Sizing	Normalized no of particles	Normalized Core Hours
y/2	8	94
y	1	10
3y/2	0.3	4

Table 4.2: Core Hours for Simcenter SPH simulations as the particle size is varied

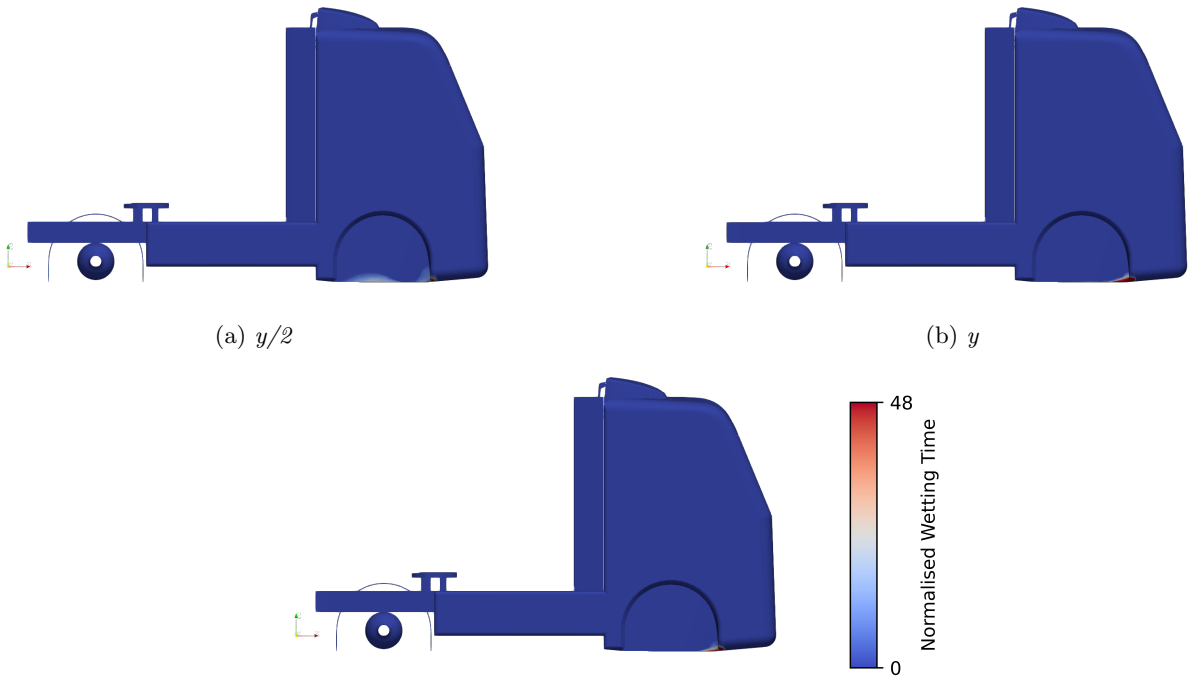

(a) *y/2* (b) *y*

(c) *3y/2*

Figure 4.6: *Average wetting of the side surface of the simplified truck as the SPH particle sizing used for Simcenter SPH simulations was varied between y/2, y and 3y/2*

The parameter study done with respect to particle sizing seems to indicate that a smaller particle size produces a wider spread in the wetted surface area. As seen in the Preonlab case, this could be because smaller particles are capable of rising to higher heights and replicating physical phenomena such as droplet breakup and coalescence to a smaller scale. The possible reasons for the higher rise and spread were discussed in the Preonlab section and similar reasoning can be considered here as well. However, in the Simcenter SPH results the exact spray pattern on the walls could not be identified as the location of strike of individual particles could not be pinpointed. The results are all averaged out over the mesh cells and hence a more accurate analysis requires a finer meshing of the solid surfaces. The finer particle sizes require a much larger simulation time in this case as well even though they might be able to capture certain phenomena better.

Solid-Liquid Contact Angle

The solid-liquid contact angle used in the simulations were varied between $2a/3$, a and $4a/3$. The contact angle in this case is used to quantify the wettability of the solid surface with a lower contact angle indicating more wettability with the liquid clinging more strongly to the surface. The wetted surface area decreases as the contact angle is increased as expected. With an increase in contact angle the solid surface wettability decreases and the fluid stays on the surface for shorter time. Hence, the area in red or wet for more than 48% of the simulation time goes down. The average wetting on the side surface of the truck however, does not change significantly with the change in the contact angle. When it comes to the instantaneous wetting images of the walls, the waves generated by the front and rear wheels seem to be more spread out in the case of the $2a/3$ simulation with the spread progressively decreasing with the increase in the contact angle. This implies that the wave sticks to more areas on the wall as it hits and spreads along the wall. There does not seem to be a significant difference in the splash height pattern between the three contact angles. At the higher heights there is a minute increase in the volume of fluid with the increase in contact angle. This indicates that the increase in contact angle cause the water to rise higher by a very small measure. There does not seem to be any significant difference in the core hours between the simulations indicating that the contact angle does not change the amount of calculations involved in the simulations. The results referred to in this section have not been displayed since the changes are minor between the three settings, however they can be can be found in appendix A

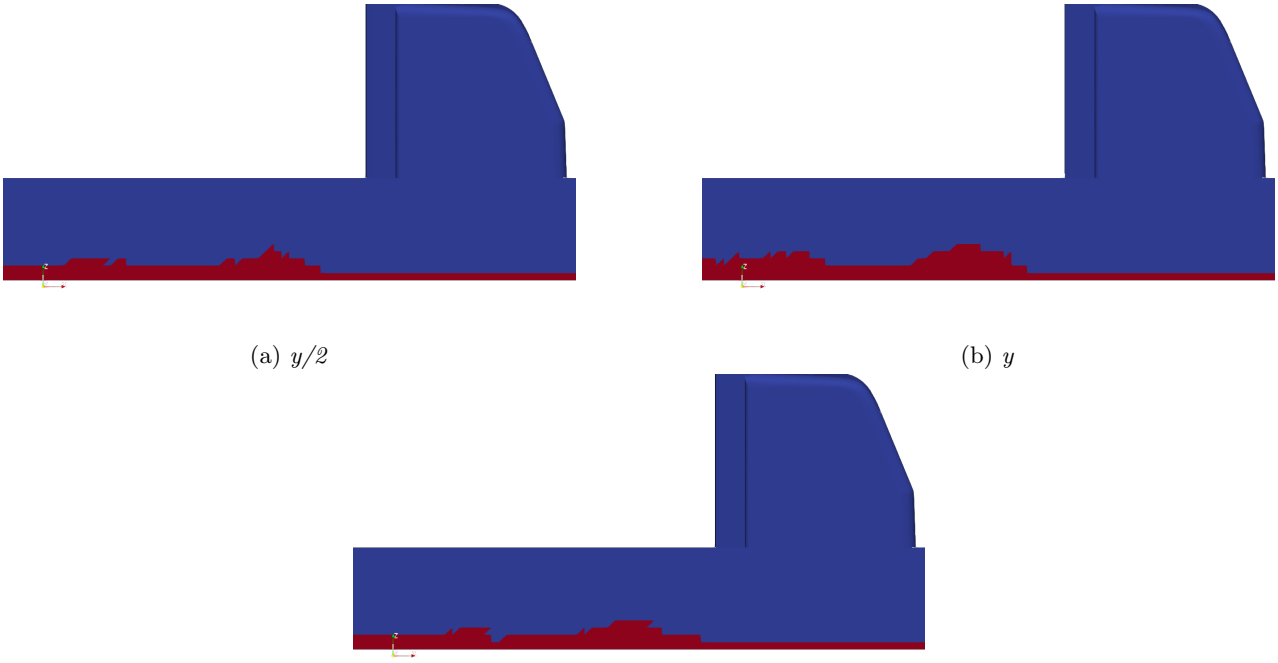

(a) *y/2*

(b) *y*

(c) *3y/2*

Figure 4.7: *Instantaneous wetting of the walls of the wading channel as the SPH particle sizing used for Simcenter SPH simulations was varied between y/2, y and 3y/2*

Drag Model Usage

The drag model was activated and inactivated to understand how it influences the simulations results. Similar to the Preonlab simulations, the air velocity was not specified and hence the modeled drag force decelerated particles moving in all directions. In the case of the average wetting pattern of the bottom surface, the spread of the wet patch increases as the drag model is deactivated. However, the intensity of wetting with the wet area is higher for the case when the drag model is active. The differences are however quite minor. When it comes to the instantaneous wetting of the walls, it could be seen that the wave generated by both the front and rear wheels have a sharp flat crest in the case of the drag inactive simulation. On the other hand, when the drag model is activated the wave crest is more rounded off implying that the drag model damps the movement of the particles to produce the round crest. The drag inactive simulation produces a splash height distribution that has marginally more volume at certain heights than the drag active simulation again indicating that the drag model damps the rise of fluid particles. There is a minor increase in core hours from the drag inactive to active simulation. In this cases as well, since the differences in results only marginally differ, they have not been displayed here but can be referred to in appendix A

Discussion of parameter study of Simcenter SPH

The difference in wetting pattern on each side is possibly due to asymmetry in the contact maintained between the truck and the wading channel. The contact was manually established by the user in this software and hence there could be minor gaps or asymmetries in the placement as the truck wades through the pool resulting in the asymmetric wetting patterns. Another possible reason for the asymmetry is that the y and 3y/2 particle size is so large that it is unable to pass through the small gaps present between the wheel and the road or the wheel and wheel housing to generate the expected symmetric wetting pattern. The instantaneous wetting pattern in this case is able to capture the overall wave pattern but it is unable to capture the splash and spray on the walls. This can be attributed to the way in which the wetting is captured and displayed in Simcenter SPH. In this software, if a particle strikes a particular cell on a solid, the whole cell is displayed as wet and the exact position of the particle strike is lost. If the exact position needs to be identified then the cell size of the meshes would have to be lowered probably to sizes close to the SPH particle sizing used in the simulations.

The parameter study done for the solid-liquid contact angle seems to indicate that it has an influence on the time for which the surface is wet but it does not seem to significantly change the wave pattern or the area

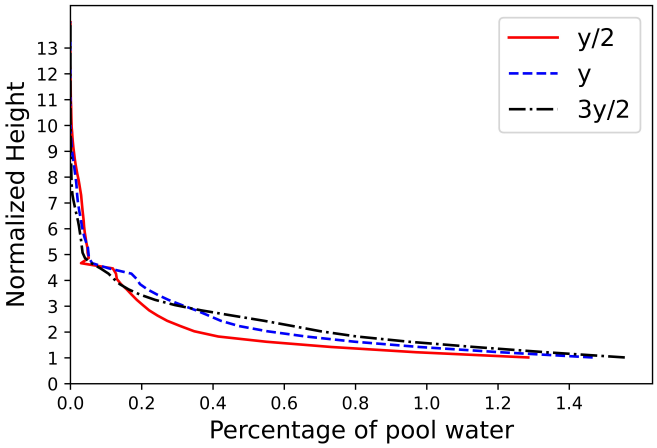

Figure 4.8: *Splash Height Distribution for different Particle Sizes in Simcenter SPH*

wetted by the fluid. The contact angle does not significantly change the run time and hence it could be fine tuned to obtain more realistic surface wetting phenomena that could replicate painted metallic surfaces or rubber tires. It must be noted again that at a different particle size the effect of variation in contact angle might be stronger or weaker.

The parameter study done on the drag model used in Simcenter SPH indicates that the drag model marginally damps the splashes and waves produced by the truck as it wades through the channel. However, the effect is not significant and similar results can be obtained without the presence of the drag model. The active drag model case seems to require a marginally higher number of core hours but since only one simulation was run in the drag active and inactive case with similar settings it could not be concluded whether the drag model adds significantly to the computational cost. The effect of the drag model might also be stronger or weaker at a different particle size and has not been studied here.

4.1.3 LS-DYNA

The results obtained from LS-DYNA for the parameter study have been displayed and discussed in this subsection. The default simulation was run using a particle size of y, a numerical surface adhesion coefficient of β and an active drag model. Each of these parameters were varied independently to understand their influence on the results.

Particle Sizing

The particle sizing was again varied between y/2, y, and 3y/2 in the case of LS-DYNA as well. The average wetting pattern on the truck, the instantaneous wetting of the wading channel walls and the splash height distribution for the three simulations have been analyzed to understand the influence of the particle sizing on the simulation.

Average Wetting - The average wetting of the under body of the trucks as the SPH particle sizing was varied in the LS-DYNA simulations is depicted in figure 4.9. As observed in the images, the wetted surface area increases with a decrease in particle sizing. However, it is interesting to note that the 3y/2 case seems to produce more intense wetting patches than the y case close to the center of the front wheel house. Apart from this, it is interesting to note that in the case of the y/2 particle sizing the wetting patch is red for almost the whole of the wet region.

In the case of the average wetting images of the side surface of the truck shown in figure 4.10, it can be be again seen that the wetted surface area increases with decrease in particle sizing. There is an especially intense wetting patch towards the front of the wheel house in the case of the y/2 simulation.

Instantaneous Wetting - The instantaneous wetting of the wading channel walls is depicted in figure 4.11. All three particle sizing seem to capture the waves generated by the front and rear wheels. However, the size of the waves seem to flatten out a bit towards the larger particle size. In the 3y/2 case, the front and rear waves are difficult to distinguish from the instantaneous wetting images of the walls. It can also be seen that the y/2 case has very jagged edges on top of the wave which could indicate splashes and sprays but the results

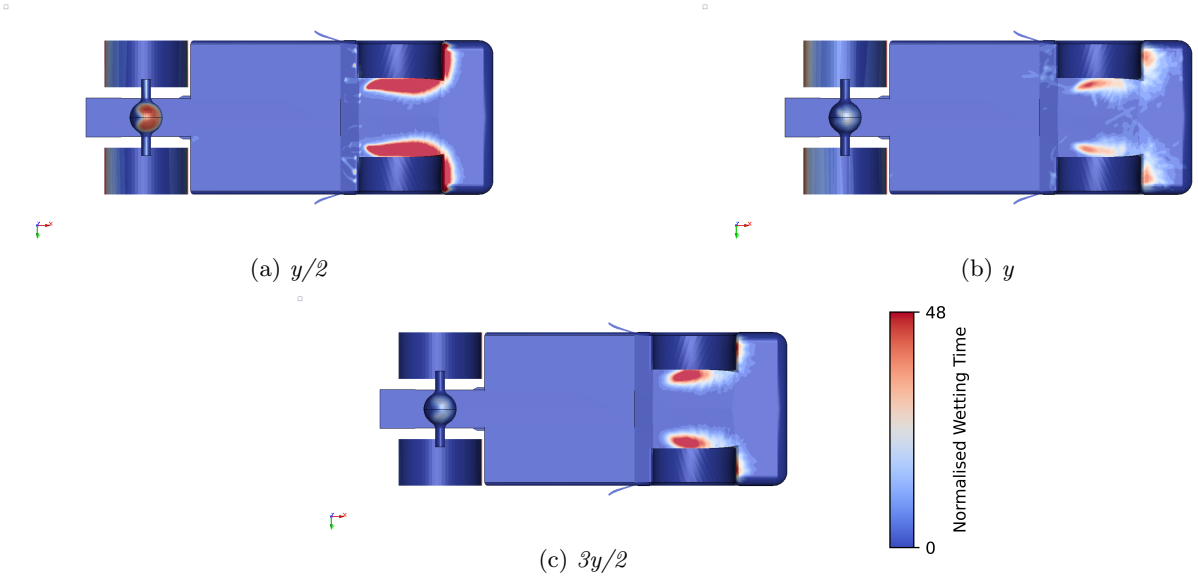

(a) *y/2* (b) *y*

(c) *3y/2*

Figure 4.9: *Average wetting of the bottom surface of the simplified truck as the SPH particle sizing used for LS-DYNA simulations was varied between y/2, y and 3y/2*

don't seem to be able to clearly distinguish between the wave and the splash. These jagged spikes in the wave vanish towards the larger particle size indicating splash and spray are not observed at larger particle sizing.

Splash Height Distribution - The splash height distribution as the particle size was varied in LS-DYNA is shown in figure 4.12. The splash height is highest for particle sizing of y/2 and lowest for particle sizing of y. In this case there does not seem to be a clear trend with the particle sizing. The graphs for y/2 and 3y/2 converge at the lower heights.

Core hours - The normalized core hours along with the normalized number of particles in the simulation is shown in table 4.3 as the particle sizing is varied for the LS-DYNA simulations. Similar to the previous two software, the simulation run time increases exponentially as the particle size decreases with the increase in time proportional to the increase in the number of particles in the simulation. The increase in particles is again approximately equivalent to $(oldparticlesize/newparticlesize)^3$ as mentioned in the Preonlab section.

Particle Sizing	Normalized no of particles	Normalized Core Hours
y/2	7	27
y	0.8	5
3y/2	0.2	2

Table 4.3: Core Hours for LS-DYNA simulations as the particle size is varied

Surface Adhesion Coefficient (Beta)

The surface adhesion coefficient(Beta) in this case was varied between $\beta/10$, β and 10β. As the coefficient was increased the attractive forces between the solid surfaces and the fluid particles increases and the fluid particles is expected to stick to the surfaces for a longer duration. The average wetting pattern of the truck body shows that the area wetted by the fluid increases in both intensity and size with the increase in adhesion coefficient value. There is no significant difference in the instantaneous wetting images of the walls. When it comes to the splash height distribution the $\beta/10$ simulation seems to produce a slightly higher splash height but the β and 10β produce the same graph. When it comes to the core hours used per simulation, the lower adhesion coefficients of $\beta/10$ and β do not have significantly different core hours but it is interesting to note that the largest adhesion coefficient had a significantly lower number of core hours. Since there is no significant difference between the three cases, the results have only been displayed in appendix A.

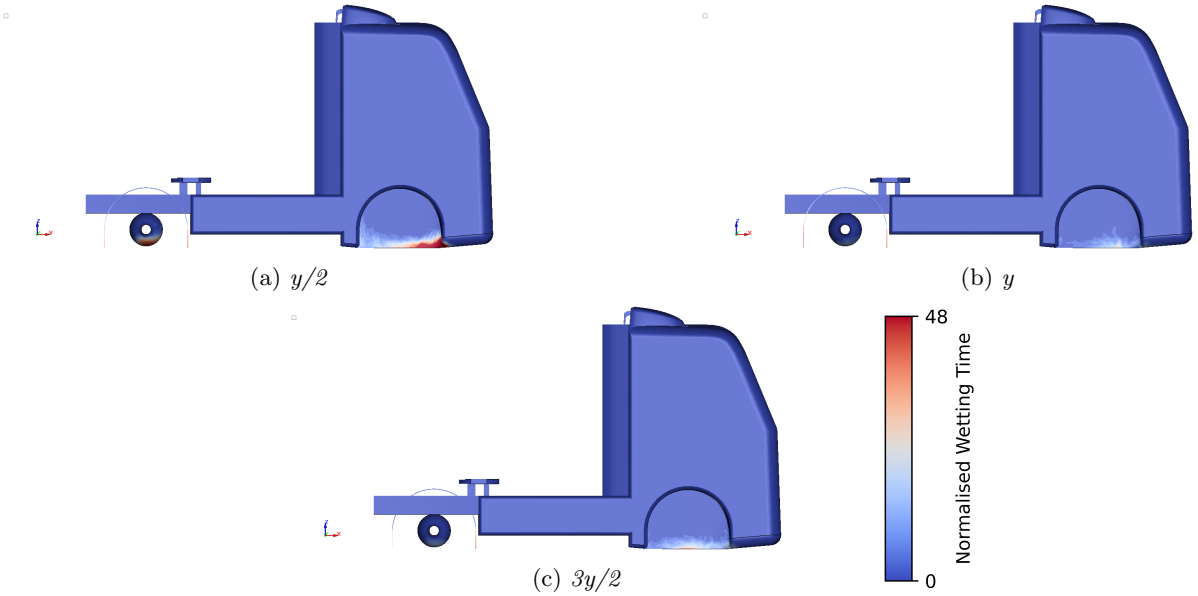

(a) *y/2* (b) *y* (c) *3y/2*

Figure 4.10: *Average wetting of the side surface of the simplified truck as the SPH particle sizing used for LS-DYNA simulations was varied between y/2, y and 3y/2*

Drag Model Usage

The drag model used in the LS-DYNA simulations was turned from active to inactive to see how the results varied. With the drag model active, truck surface wetting pattern is marginally shifted towards the back compared to the drag inactive simulation. The intensity of wetting is also marginally lower in the drag active case. The instantaneous wetting of the walls does not show any significant differences apart from a few extra splash drops in the drag inactive case. The splash height distribution graphs however show some significant differences between the two models with the drag inactive case having larger fluid volumes rising to higher heights. The core hours used for both the simulations were quite close with the drag inactive case having marginally higher number of core hours. The images corresponding to the drag model parameter study have not been shown here since most of them show only minor differences but they can be referenced to in the appendix A.

Discussion about LS-DYNA parameter study

In general, it can be seen from the parameter study on the particle study that the area wetted increases with decrease in particle size in the case of LS-DYNA as well. There is an increase in intensity in the wet patch in the case of the 3y/2 simulation which was noted in the results. The smallest particle sizing of y/2 also show intense wetting in most of the wet patch indicating an even equal split of wetting. The intense red patch could be because the particles have stuck to the surface for a longer duration which might be true in the case of the smaller particle sizing but unlikely in the large particle sizing. The adhesive forces in the larger particle sizing is less likely to counteract the gravitational forces and cause sticking for such long duration. In the large particle sizing it is more likely that the particles struck the same region multiple times during the simulation to cause the intense wetting pattern. However, further simulations with variation in the surface adhesion coefficient would have to be carried out to determine which of these reasons causes the intense red patch. The instantaneous wetting pattern and the splash height distribution seem to show the presence of water at higher heights at the smallest particle size implying the smaller size captures more splash and spray. The splash and spray cannot be clearly seen from the instantaneous wetting image in this case as well. The reason for this is the same as in Simcenter SPH results. A mesh is used in this case as well to capture where the fluid particles strike the solid surface. In case a cell in the mesh is struck by fluid particles then the whole cell is highlighted as wet resulting in very blurred or jagged wetting patterns.

The parameter study also showed that the surface adhesion factor does increase the time for which the surface is wet. However, since the splash height distribution is almost the same for the two larger adhesion factors, it seems like the effect of the adhesion factor on wave and splash generation saturates above β. The

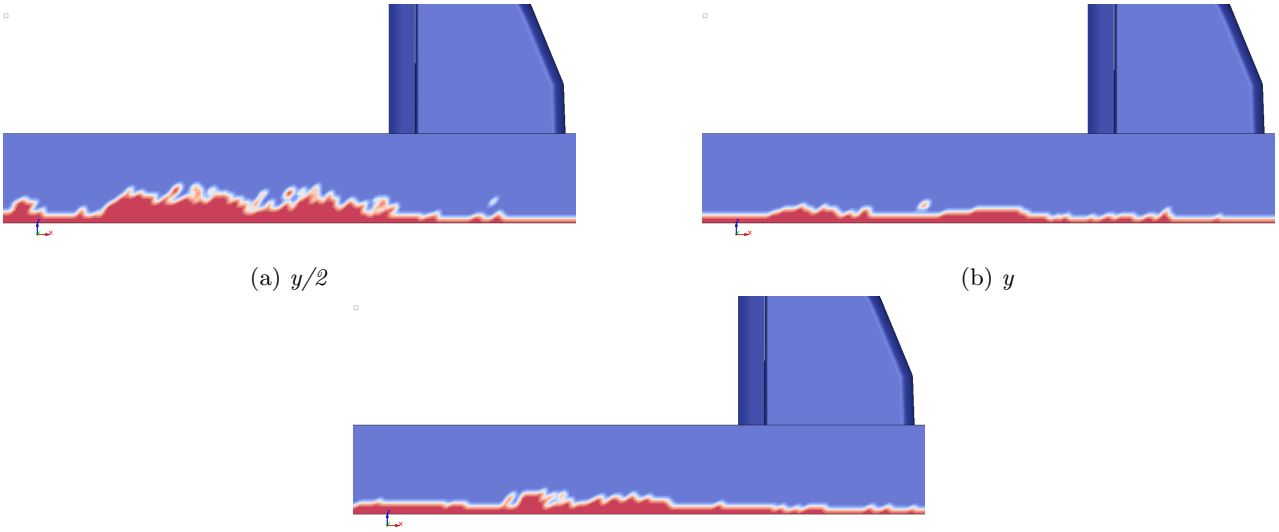

(a) *y/2*

(b) *y*

(c) *3y/2*

Figure 4.11: *Instantaneous wetting of the walls of the wading channel as the SPH particle sizing used for LS-DYNA simulations was varied between y/2, y and 3y/2*

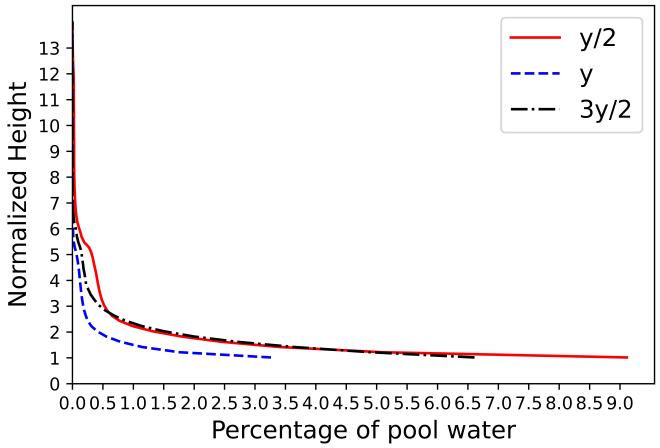

Figure 4.12: *Splash Height Distribution for Different Particle Sizing in LS-DYNA*

core hours indicate that increasing the adhesion factor from β to 10β significantly reduces the amount of core hours need from the simulation. But since all the other factors such as number of particles as well as wetting patterns are quite close, an exact reason for this reduction could not be identified. Further simulations varying the adhesion coefficient would have to be carried to understand the exact effect on the amount of core hours and the reason for the difference. The surface adhesion coefficient in this case could also be fine tuned in the future to closely resemble real world material wetting behaviors. Its effect with variation of particle size is also something that could not be analyzed during this parameter study.

The drag model study indicates that its presence does dampen the fluid particle movement and particles rise to lower heights when the drag model is active. It does not produce any significant difference in the amount of core hours and could hence be used to replicate the effects of the presence of air around the truck.

4.1.4 Comparison between simulations at default settings in the different software

The results from the simulations run at the default settings in each of the software have been shown and discussed in this section.

Average Wetting - In the case of the surface wetting, except for the asymmetry shown in the Simcenter

SPH simulations, all three software show surface wetting on the under body region close to the front wheel house. The LS-DYNA simulation seems to show more wetting towards the front of the wheel house than the the other two simulations. It also shows more spread in the wetting pattern in general compared to the other two software. However, the results produced by Preonlab are more sharper than the results of the other two which have more blurred edges making it hard to locate fine splash and spray wetting patterns.

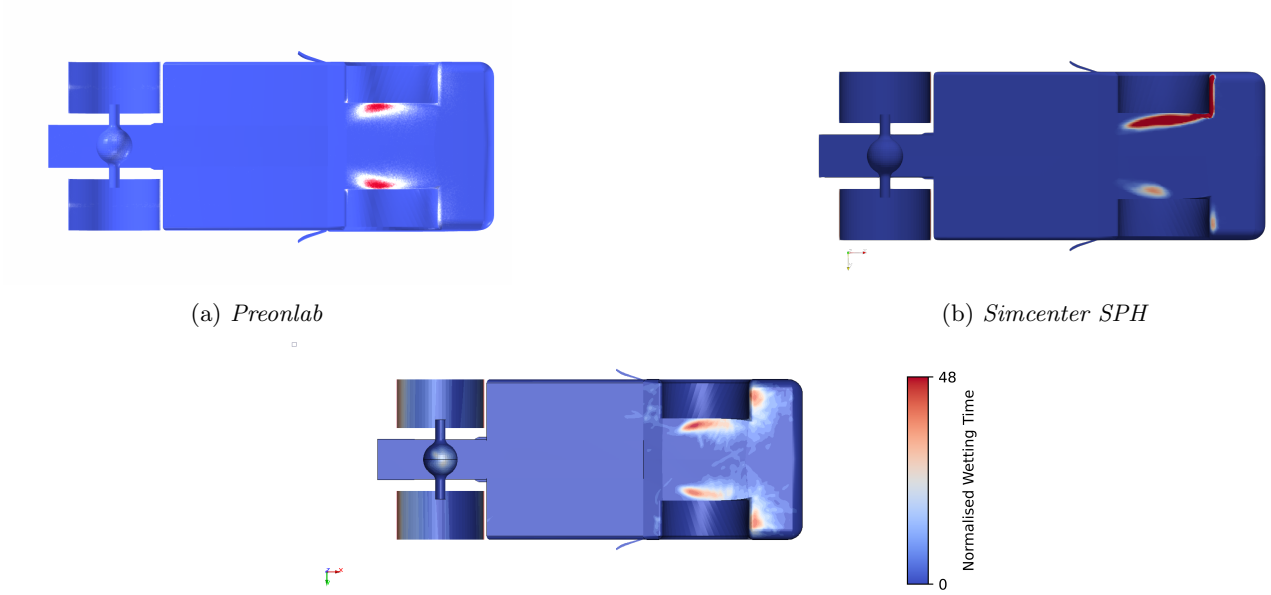

(a) *Preonlab* (b) *Simcenter SPH*

(c) *LS-DYNA*

Figure 4.13: *Average wetting of the bottom surface of the simplified truck in the default settings for all three software*

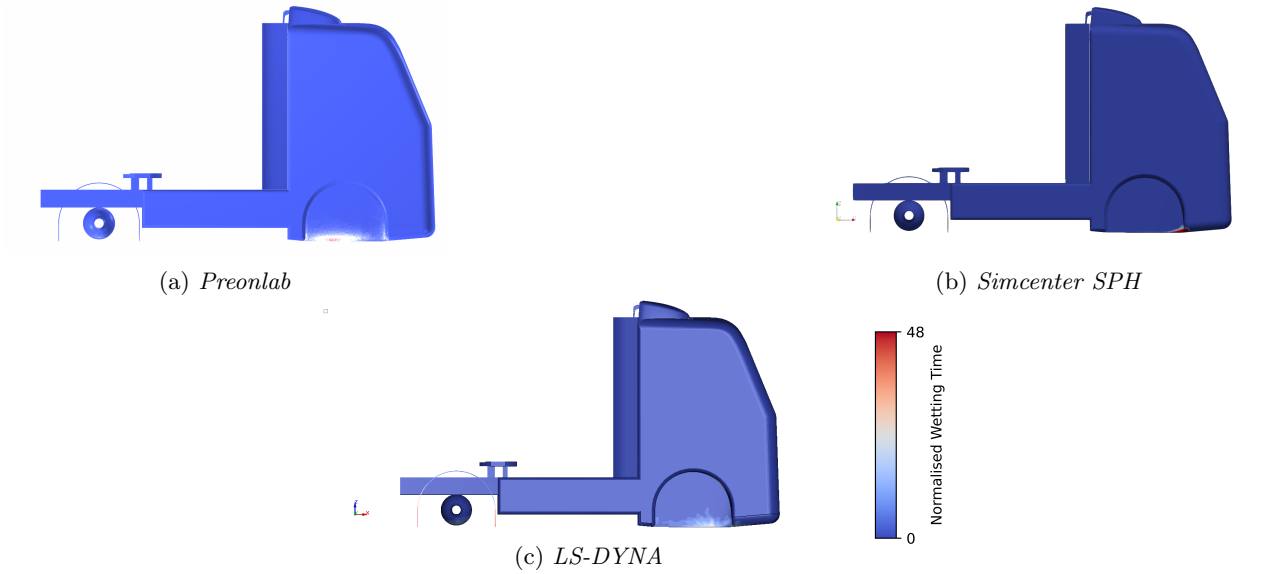

(a) *Preonlab* (b) *Simcenter SPH*

(c) *LS-DYNA*

Figure 4.14: *Average wetting of the side surface of the simplified truck in the default settings for all three software*

In the case of the side surface, the average wetting pattern is concentrated more to the rear of the front wheel house in the case of Preonlab. But in the case of LS-DYNA the wetting pattern is concentrated more to the front of the wheel house. In the case of Simcenter SPH only the front corner of the front wheel house seems

to have been wet in the simulations.

Instantaneous Wetting - In the case of the instantaneous wetting of the side walls as shown in figure 4.15, all three software capture the two waves of water generated by the front and rear wheels. The Preonlab result again captures the splash and spray strikes on the wall clearly. In contrast, Simcenter SPH and LS-DYNA results show wetting patterns on the walls that do not clearly differentiate between the waves and the splashes.

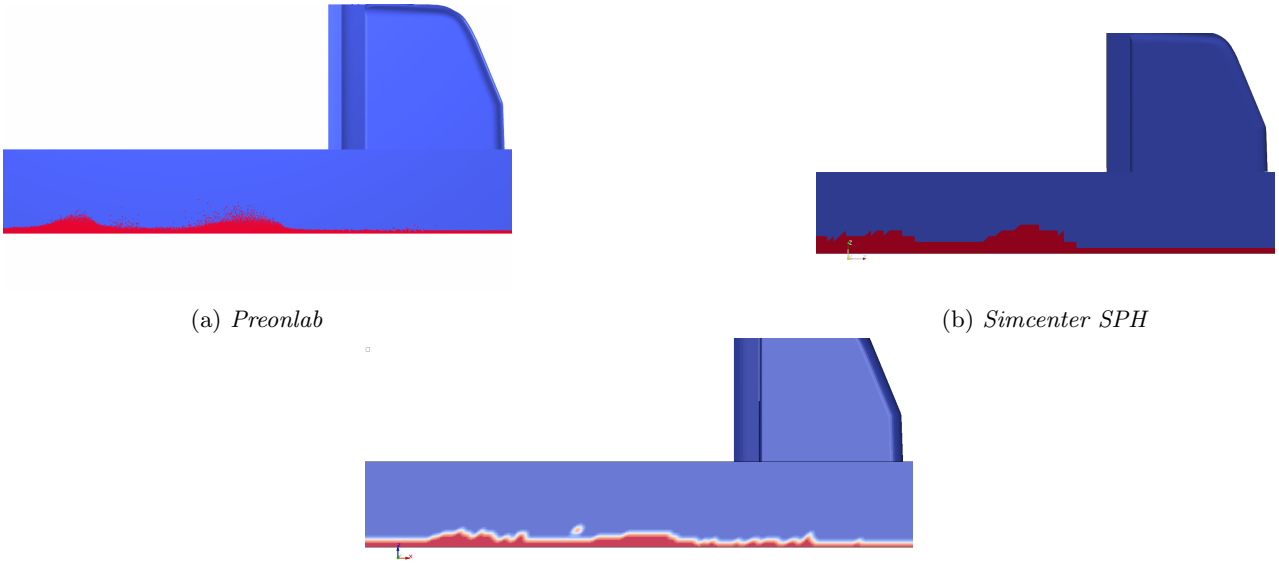

(a) *Preonlab*

(b) *Simcenter SPH*

(c) *LS-DYNA*

Figure 4.15: *Instantaneous wetting of the walls of the wading channel in the default settings for all three software*

Splash Height Distribution - In the case of the splash height distribution, LS-DYNA shows the highest splash height followed closely by Preonlab and then Simcneter SPH. There does not seem to be a major difference in the volume of fluid rising up to the highest heights between the three software. But towards the lower heights especially between 2-4 times the wading channel height, Simcenter SPH seems to show marginally higher volume of water than the other two software. At the lowest heights close to the wading channel pool surface, LS-DYNA shows the maximum volume of water rising from the surface.

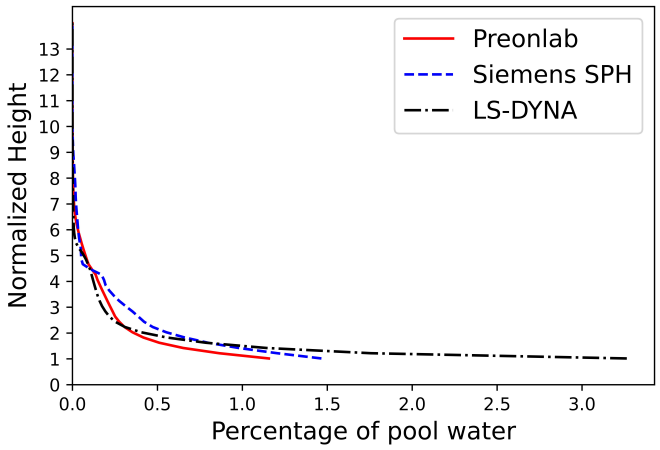

Figure 4.16: *Splash Height Distribution comparison between the software in the defaults settings for all three software*

Core Hours - The table 4.4 shows the normalized core hours used by each simulation simulation at their default settings using particle sizing of y . It can be seen that Preonlab used the least number of core hours followed by LS-DYNA and then finally Simcenter-SPH. The number of particles in the simulation were quite

close in the case of Preonlab and Simcenter SPH but LS-DYNA had significantly lesser number of particles.

Software	Normalized no of particles	Normalized Core Hours
Preonlab	1	1
Simcenter SPH	1	10
LS-DYNA	0.8	5

Table 4.4: Normalized core hours used by each software in the default case with simplified truck model

4.1.5 Discussion about comparison between the results of the defaults simulations in all the three software

In case of the wetting pattern, LS-DYNA seems to depict more wetting between the three software. A possible reason for this could be the way that kinematics was set up in the three software. LS-DYNA allows for prescribed motion of the truck body while also accommodating the contact between the tyres and the wading channel. LS-DYNA might resemble real world physical motion the most since it accounts for contact forces. In contrast Preonlab and Simcenter SPH have more explicit ways of defining kinematics. Preonlab uses a Python script that ensures that the truck moves forward maintaining almost zero gap between the wheel and the wading channel. In Simcenter SPH the gap between the tyre and the the wading channel was manually set to zero by the user at the beginning of the simulation. The positions of the truck at different time steps was provided as a text file to move the truck through the wading channel. These variations in the way kinematics was implemented could contribute to how close the tyre was to the wading channel base and how it generates splashes and sprays.

Another interesting observation was how Preonlab was able to capture the spray and splashes on the surfaces while Simcenter SPH and LS-DYNA have more blurred edges to their wetting results. In Preonlab, the solid surface is sampled with SPH particles as well that are depicted as being wet once they come into contact with the fluid particles resulting in the capture of fine wetting phenomena. While in the case of Simcenter SPH and LS-DYNA, the results are captured on the mesh used to generate the solid surfaces as mentioned in the previous sections. Thus, whole cells of the mesh are recorded as wet resulting in the average wetting as well as the instantaneous wetting getting smudged out. Hence, while Preonlab result capture depends on the SPH particle sizing used in the simulations, the other two software's results depend on SPH particle sizing as well as the mesh cell sizing used for the solid geometries.

4.2 Detailed Truck Simulations

The results from the simulations run using the detailed truck model will be presented in this section and compared with images obtained from the tests conducted at the HPG wading channel. The truck in the simulation was run at two speeds namely v_1 and v_2 with v_2 being faster than v_1. The simulations were run with the default setting for particle sizing, surface tension parameters and with the drag model active. As mentioned in the methodology, these were approximately the same speeds that were used to drive the truck at the HPG wading channel but since the truck was manually driven there could have been variations in the speed during the test that have not been taken into consideration while comparing the results. The images captured from the test are each compared with corresponding views from the software simulations to analyse how closely they are able to capture the physical phenomena observed in the tests. A rendered image as well as a particle height map have been generated in each software for the purpose of these comparisons. The rendered images captures the general shape of the waves and splashes however some of the finer details might get lost in the rendering as it smoothens out the particles to generate fluid surfaces. The particle height map on the other hand is an image of the fluid as SPH particles with colouring given to them based on their height from the wading channel base. This often gives a better idea of the quantity of fluid present at various heights and positions than rendered images. All the images were captured towards the end of the simulation so that the truck was far enough into the wading channel to avoid the influences from the entry slope of the wading channel.

4.2.1 Center View

The center view of the truck from the front as it was driving through the wading channel at speed v_1 has been depicted here in figure 4.17. The splash generated by the front wheels is clearly visible in this view. It can be seen that there is an asymmetry in the splash generated on each side of the truck. The presence of the front

Figure 4.17: *Center view of truck at speed v_1 during the test*

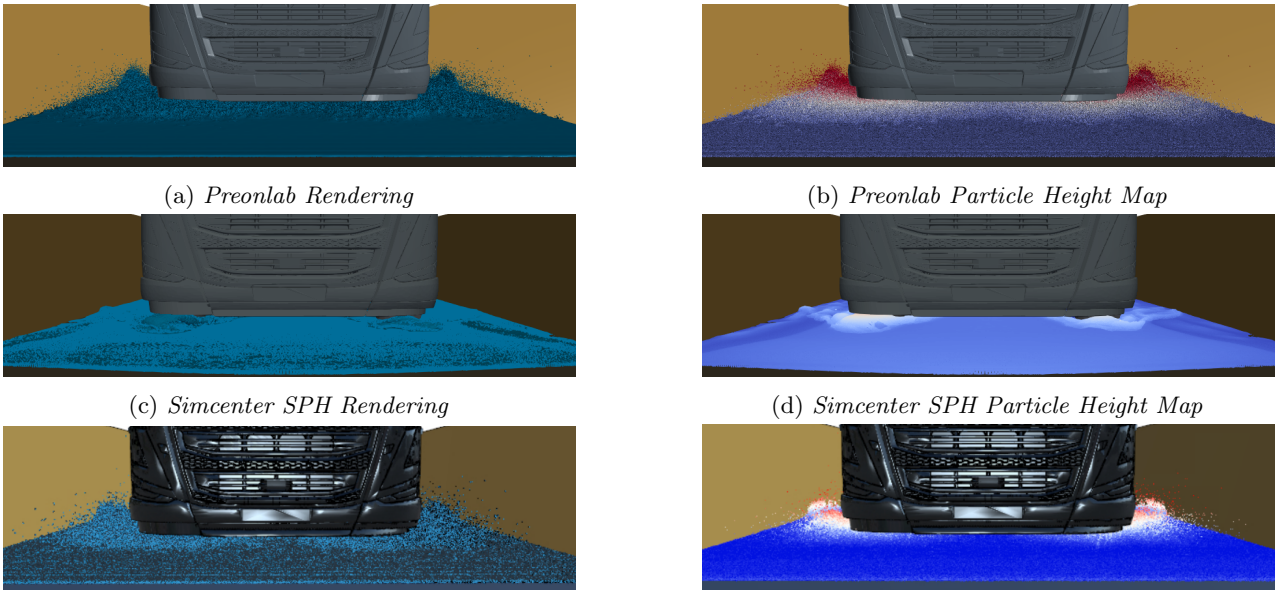

(a) *Preonlab Rendering*

(b) *Preonlab Particle Height Map*

(c) *Simcenter SPH Rendering*

(d) *Simcenter SPH Particle Height Map*

(e) *LS-DYNA Rendering*

(f) *LS-DYNA Particle Height Map*

Figure 4.18: *The center views obtained from the simulations while moving the truck at speed v_1 are shown here*

spoiler on the driver side and its absence on the passenger side is what causes the difference in splash shape. The exact same geometry has been used in the simulations to see if they were capable of capturing such effects from differences in the geometry of the truck. The center view images from the software at the same speed are shown in figure 4.18. It can be seen from the images that Preonlab and LS-DYNA simulations depict splash phenomena quite clearly both in the rendering and the height maps. Simcenter SPH only seems to show the larger waves generated by the wheels. The Simcenter SPH results however seem to show an asymmetry in the waves generated on each side which is not noticeable in the Preonlab or LS-DYNA simulations. Preonlab seems to show marginally higher splash than LS-DYNA but neither seem to generate splashes with the same intensity as seen in the HPG test image. The center view for the second speed of v_2 is shown in figure 4.19. It can be seen that the splash generated is now much higher since the speed of the truck was higher. The simulations results shown in figure 4.20 also seem to show the same trend with the splash generated by all three being considerably higher than the simulations at speed v_1. In this case as well, Simcenter SPH results only seem to capture the larger wave and splash sheet but not the spray generated further sideways. The Preonlab and LS-DYNA capture more of the splash and spray but not to the intensity seen in the test image. The height distribution of the splash seems to be comparable now between Preonlab and LS-DYNA. Again, Simcenter SPH is the only result that clearly shows the asymmetry in the splash pattern on either side of the truck while the Preonlab and LS-DYNA results do not show significant differences between the two sides of the truck.

Figure 4.19: *Center view of truck at speed v_2 during the test*

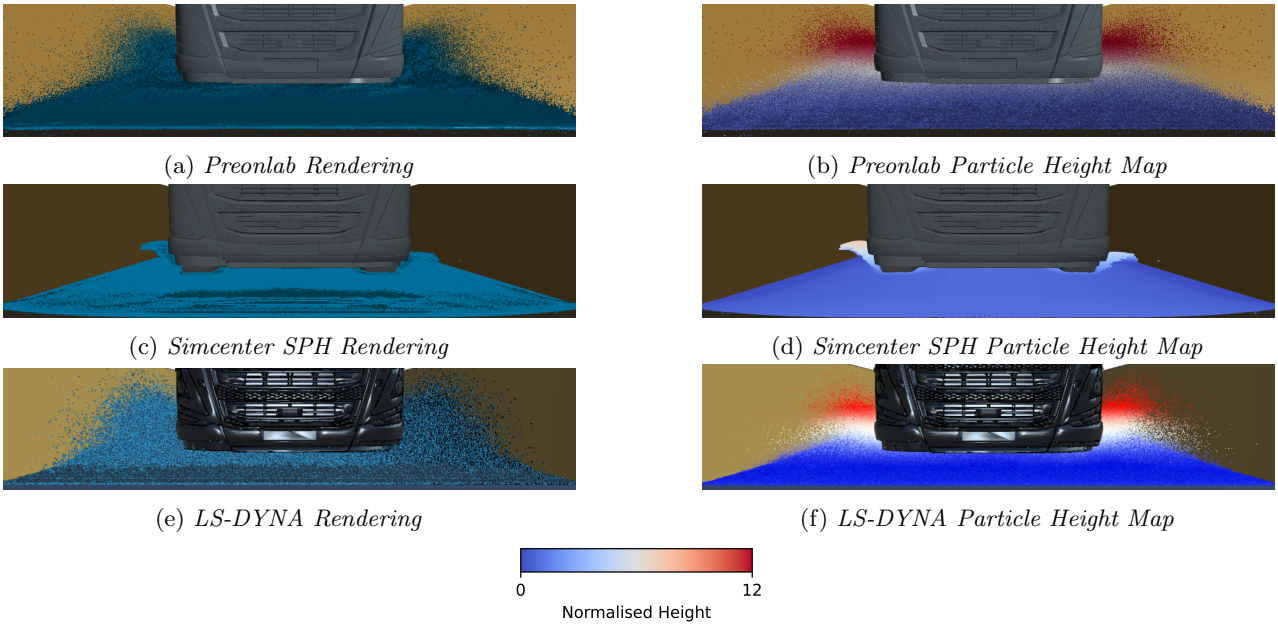

(a) *Preonlab Rendering* (b) *Preonlab Particle Height Map*

(c) *Simcenter SPH Rendering* (d) *Simcenter SPH Particle Height Map*

(e) *LS-DYNA Rendering* (f) *LS-DYNA Particle Height Map*

Figure 4.20: *The center views obtained from the simulations while moving the truck at speed v_2 are shown here*

4.2.2 Front View

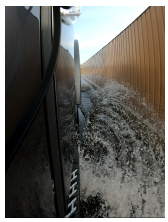

Figure 4.21: *Front view of truck at speed v_1 during the test*

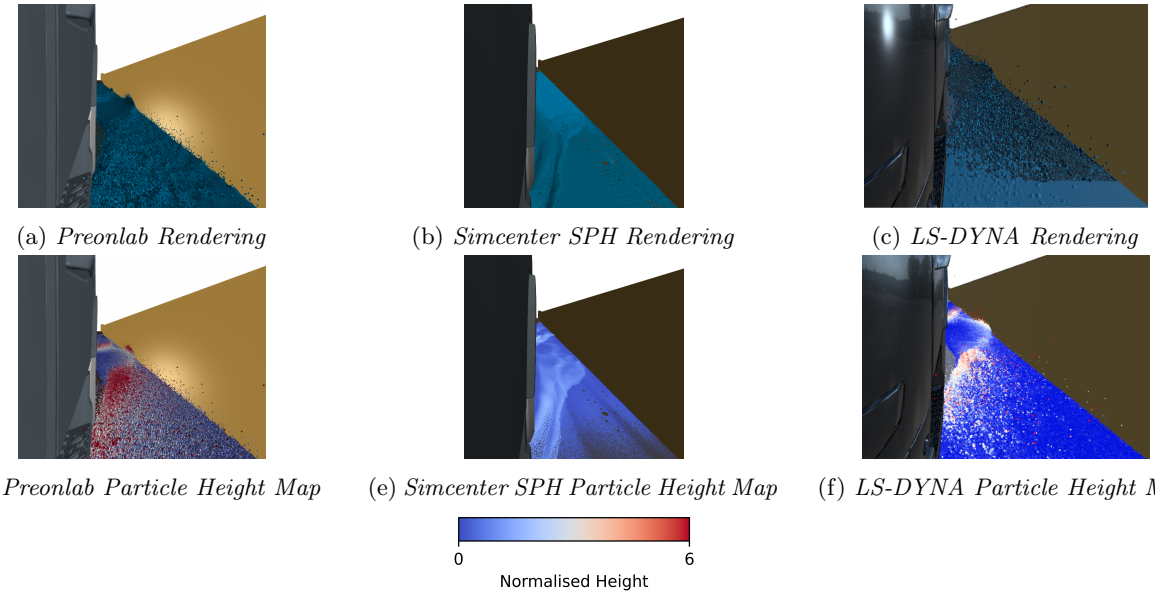

(a) *Preonlab Rendering* (b) *Simcenter SPH Rendering* (c) *LS-DYNA Rendering*

(d) *Preonlab Particle Height Map* (e) *Simcenter SPH Particle Height Map* (f) *LS-DYNA Particle Height Map*

Figure 4.22: *The front views obtained from the simulations while moving the truck at speed v_1 are shown here*

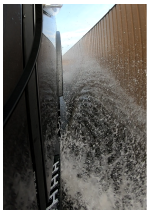

Figure 4.23: *Front view of truck at speed v_2 during the test*

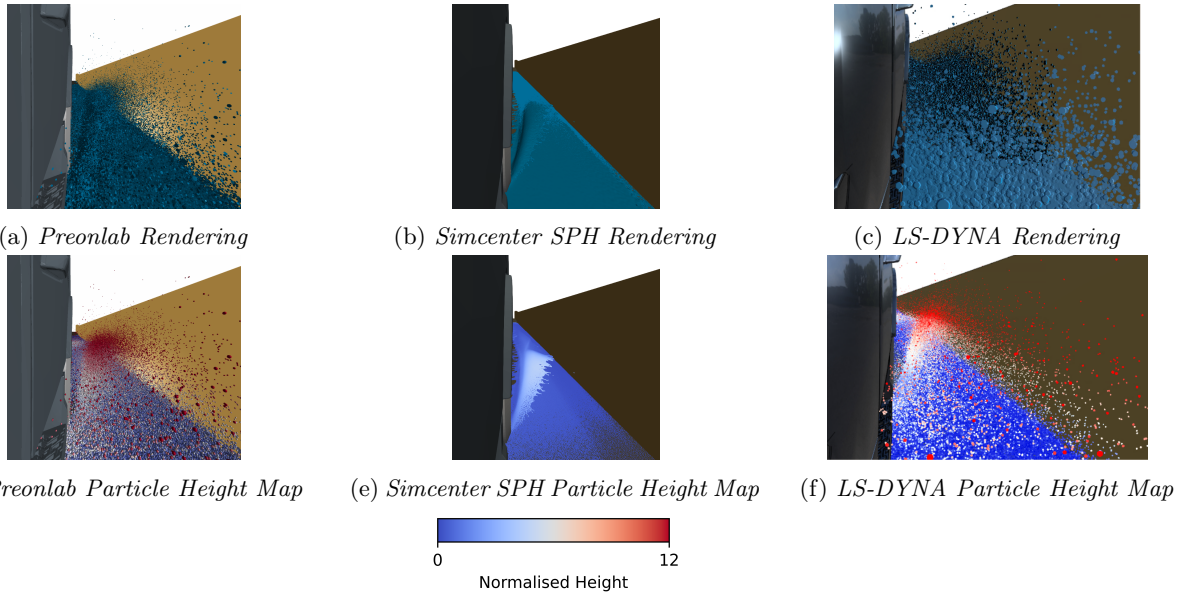

(a) *Preonlab Rendering* (b) *Simcenter SPH Rendering* (c) *LS-DYNA Rendering*

(d) *Preonlab Particle Height Map* (e) *Simcenter SPH Particle Height Map* (f) *LS-DYNA Particle Height Map*

Figure 4.24: *The front views obtained from the simulations while moving the truck at speed v_2 are shown here*

The front view of the splash generated by the driver side front wheel is depicted in figure 4.21. The features of the side wave and splash are more clearly visible in this view. It can be seen that large drops of water are ejected sideways in a projectile motion as the truck drives through the water. There is a clearing generated behind the front wheel that is bounded by a wave of water that extends back until it hits the wading channel walls and rebounds into the wading channel. The same view has been captured in all three software and displayed in figure 4.22. All three software depict the wave generated by the front wheel that extends towards the rear of the truck before it hits the wall and rebounds. Preonlab and LS-DYNA show the clearing behind the wheel clearly with the sideways wave being more clearer as well. Although both Preonlab and LS-DYNA show the splash, Preonlab appears to have more particles in the splash than the LS-DYNA results.

The front view at the speed v_2 is displayed in figure 4.23. The higher splash generated at v_2 along with the clearing behind the wheel is visible in the image. However, the wave extending from the front wheel towards the rear is partially hidden by the splash. The simulation images depict the higher splash clearly with Preonlab having the highest particle density in the splash followed closely by LS-DYNA. Simcenter SPH does not show any splash at the higher heights and only shows a sheet of water splashing up from the surface with the details of the splash lost in both the rendering and the particle height map.

4.2.3 Top View

The top view of the splash generated by the front wheel at speed v_1 has been depicted in figure 4.25. While the height of the splash was clearly captured in the front view, the spread of the splash is more clearly visible in this view. The wake behind the wheel, the shape of the wave extending behind the wheel and the forward splash generated by the wheel are clearly seen here. As seen from the previous views, the simulations are able to capture the large scale wave patterns clearly. The clearing behind the wheel is only captured by Preonlab and LS-DYNA while Simcenter SPH seems to allow for some fluid to pass under the wheel. The forward splash is not clearly visible in any of the software. There are some red spots in front of the wheel in the height maps from Preonlab and LS-DYNA indicating that the front splash is occurring in these software. However, the

quantity of fluid shooting forward is again much less than expected from the images.

The top view of the front wheel splash at the higher speed v_2 is shown in figure 4.27. The shape of the splash is quite similar to that seen in v_1 speed except that the fluid appears to be projected out with a faster speed than in the v_1 speed case. The images from the simulation at speed v_2 are shown in figure 4.28. In this case, the forward splash is better captured both in Preonlab and LS-DYNA. More particles can be seen shooting ahead of the tyre but still the fluid volume in the splash appears to be less than expected from the images. Simcenter SPH shows a higher and wider splash but not the sideways spread.

Figure 4.25: *Top view of truck at speed v_1 during the test*

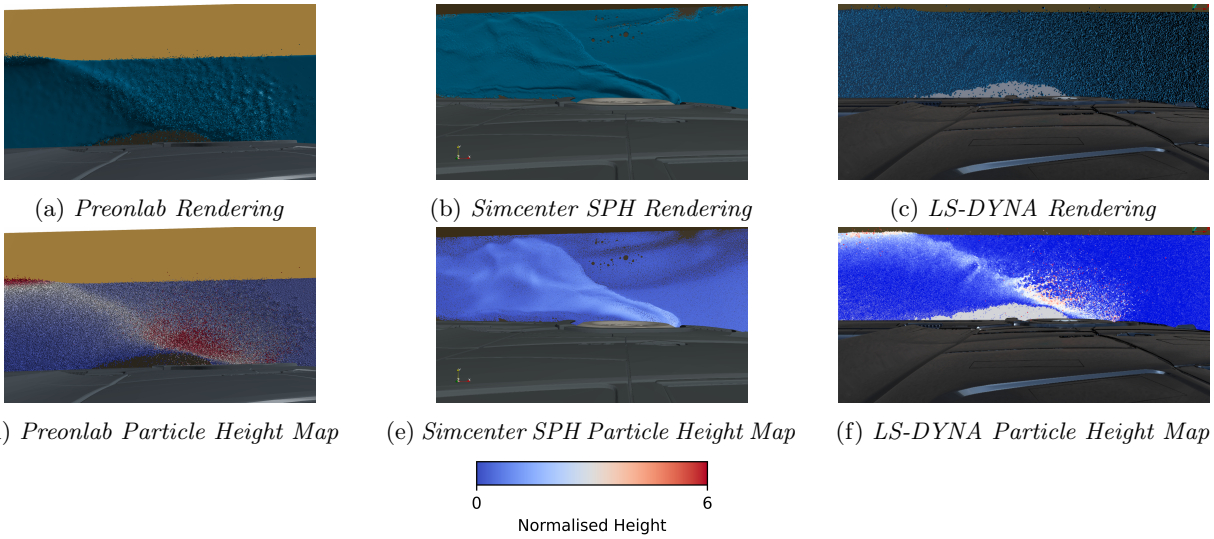

(a) *Preonlab Rendering* (b) *Simcenter SPH Rendering* (c) *LS-DYNA Rendering*

(d) *Preonlab Particle Height Map* (e) *Simcenter SPH Particle Height Map* (f) *LS-DYNA Particle Height Map*

Figure 4.26: *The top views obtained from the simulations while moving the truck at speed v_1 are shown here*

Figure 4.27: *Top view of truck at speed v_2 during the test*

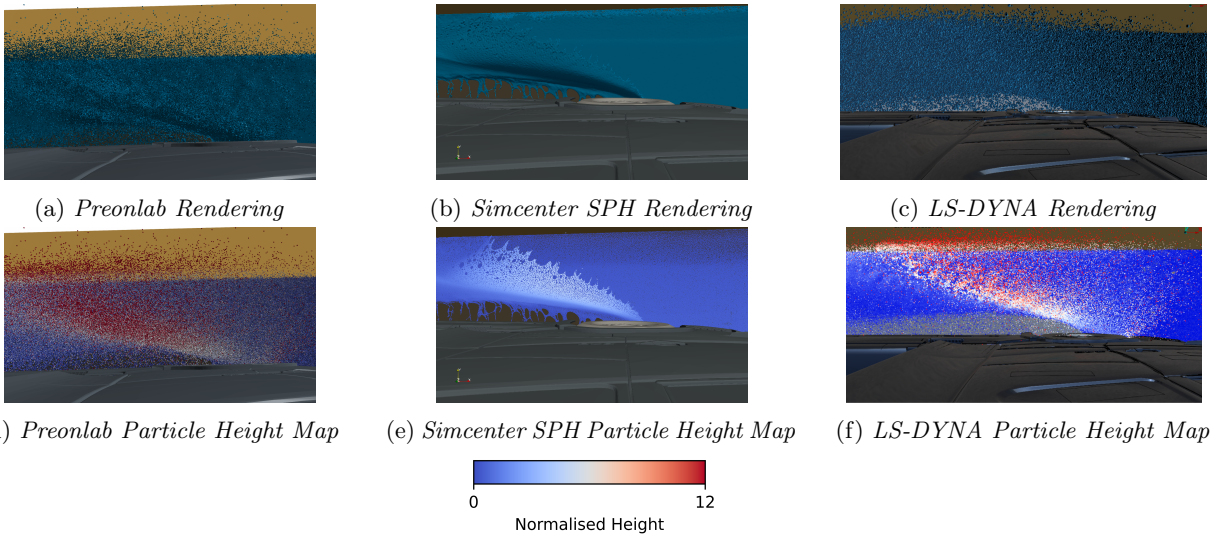

(a) *Preonlab Rendering* (b) *Simcenter SPH Rendering* (c) *LS-DYNA Rendering*

(d) *Preonlab Particle Height Map* (e) *Simcenter SPH Particle Height Map* (f) *LS-DYNA Particle Height Map*

Figure 4.28: *The top views obtained from the simulations while moving the truck at speed v_2 are shown here*

4.2.4 Back View

The back view of the truck at speed v_1 is depicted in figure 4.29. The general wake pattern behind the truck can be observed in this image. There are two wakes generated, one by each of the rear wheels on each side of the truck. There is also a foamy wake running through the middle of the channel starting from the rear of the truck. This seems to be generated by the side splashes created by the wheels meeting in the center of the wading channel and then moving out behind the truck. The corresponding images from the simulations are displayed in figure 4.32. All three software capture the general wake pattern but it does not appear so clearly in the case of Simcenter SPH as compared to the other two software. The Preonlab and LS-DYNA simulation also seem to show the splash around the rear wheels quite well.

Figure 4.29: *Back view of truck at speed v_1 during the test*

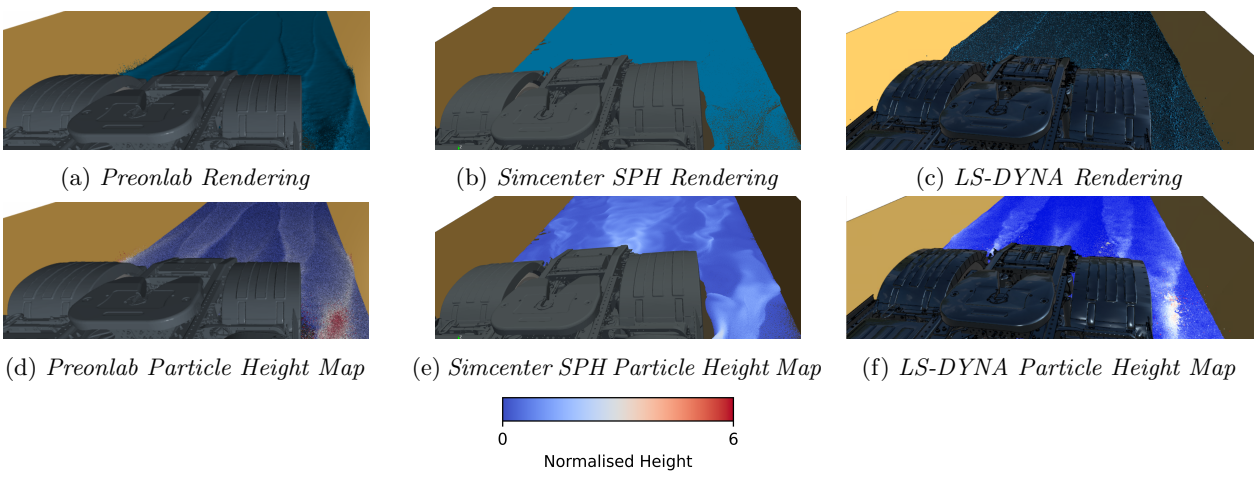

(a) *Preonlab Rendering* (b) *Simcenter SPH Rendering* (c) *LS-DYNA Rendering*

(d) *Preonlab Particle Height Map* (e) *Simcenter SPH Particle Height Map* (f) *LS-DYNA Particle Height Map*

Figure 4.30: *The back views obtained from the simulations while moving the truck at speed v_1 are shown here*

Figure 4.31: *Back view of truck at speed v_2 during the test*

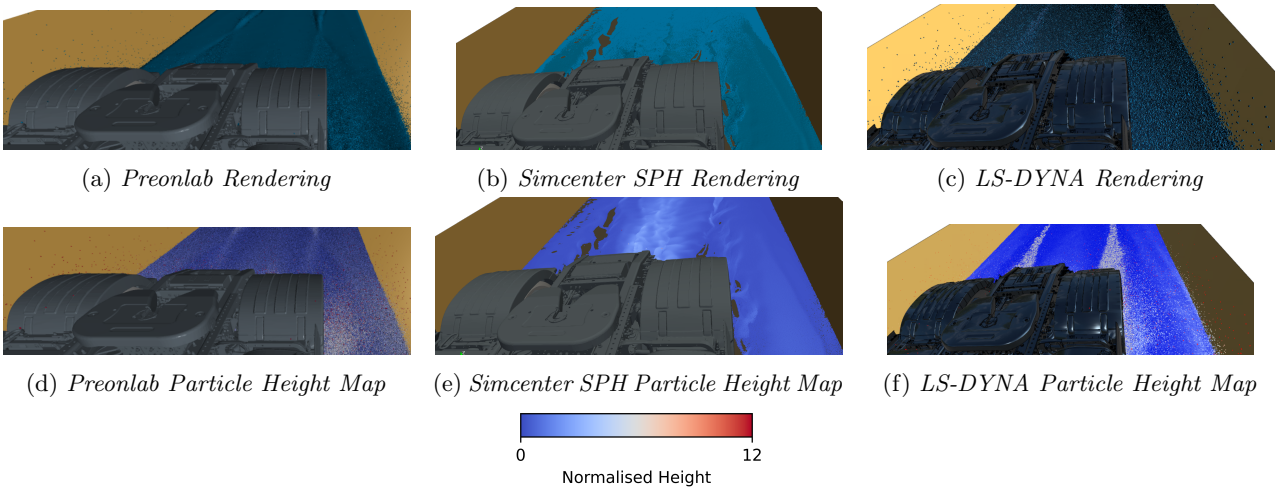

(a) *Preonlab Rendering* (b) *Simcenter SPH Rendering* (c) *LS-DYNA Rendering*

(d) *Preonlab Particle Height Map* (e) *Simcenter SPH Particle Height Map* (f) *LS-DYNA Particle Height Map*

Figure 4.32: *The back views obtained from the simulations while moving the truck at speed v_1 are shown here*

The back view at speed v_2 is depicted in figure 4.31. The wake is more chaotic in this case compared to speed v_1 with more churning and foaming behind the wheels.The corresponding results from the software are depicted in figure 4.32. Although the general shapes of the wake are captured by the software, none of them show the chaotic behavior seen in the image. Both the particle height maps as well as the rendered images show very smooth transitions. The Simcenter SPH image in this case is the one that shows some sort of rolling pattern behind the truck.

4.2.5 Average Wetting of Instep

The driver side instep was photographed after the truck was run through the wading channel at both speeds. The image corresponding to the v_1 run is depicted in figure 4.37. Water drops can be seen to cover the bottom as well as the side surfaces of the instep. The average wetting pattern of the instep was generated from the simulations as shown in figure 4.34 to compare with these images. Preonlab and LS-DYNA depict wetting of the bottom as well as side surfaces of the instep while Simcenter SPH only shows wetting below the surface of the instep. Although the exact locations of the splash is different the general pattern is captured in both Preonlab and LS-DYNA.

Figure 4.33: *Image of the driver side instep of the truck after driving through the wading channel at speed v_1 during the test*

The image of the driver side instep after driving through the wading channel at v_2 speed is shown in figure 4.39. The number of droplets and wetted surface is marginally higher in this case compared to v_1 case. The corresponding average wetting images shown in figure 4.36 depict this trend of increased wetting in the case of Preonlab and LS-DYNA with Simcenter SPH showing no wetting in this case as well. The intensity of wetting

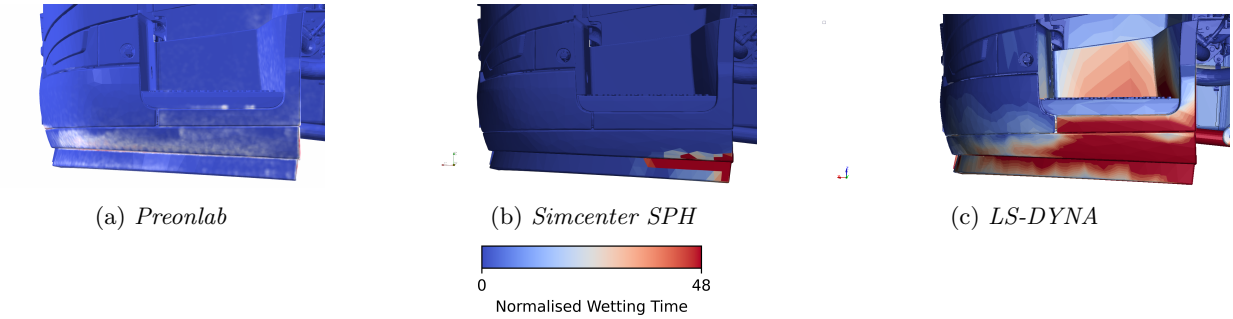

(a) *Preonlab* (b) *Simcenter SPH* (c) *LS-DYNA*

Figure 4.34: *Average wetting of the driver side instep of the truck at the speed v_1 for all three software*

has gone up along with the area wetted in the case of Preonlab and LS-DYNA.

Figure 4.35: *Image of the driver side instep of the truck after driving through the wading channel at speed v_2 during the test*

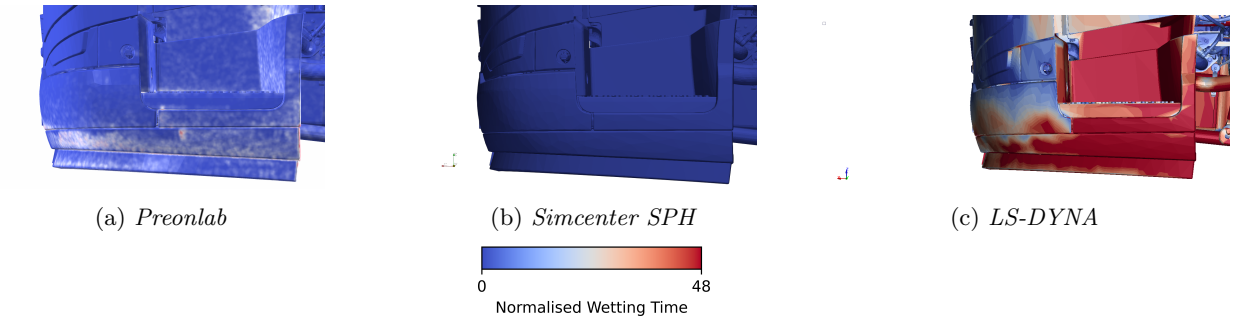

(a) *Preonlab* (b) *Simcenter SPH* (c) *LS-DYNA*

Figure 4.36: *Average wetting of the driver side instep of the truck at the speed v_2 for all three software*

4.2.6 Average Wetting of Side Skirt

The images of the side skirt after driving through the wading channel are depicted in this section. The first figure 4.37 shows the wetting after the test at v_1 speed. There are drops of water present from the bottom of the side skirt all the way to the top. There are drops also present on the outer surface of the front wheel fender. The corresponding average wetting images from the simulations are shown in 4.40 . The Preonlab and Simcenter SPH simulations show no wetting of the side skirt or fender at this speed. The LS-DYNA simulation shows some wetting of the fender and the bottom of the side skirt.

The side skirt image from the test done at speed v_2 is shown in figure 4.39. There are water droplets present again from the bottom to the top of the side skirt as well as the front wheel fender with the only difference being that there are a larger number of drops compared to the image from the v_1 case. The simulation results for this case are shown in figure 4.40. In this case, in addition to LS-DYNA, Preonlab results also show wetting of the side skirt. In the case of Preonlab, there are only faint wetting patterns towards the bottom of the side skirt with the top mostly dry. The LS-DYNA result show more intense wetting of the bottom region with faint wet patches even at the top. The Simcenter SPH results in this case are again completely dry.

Figure 4.37: *Image of the driver side side skirt of the truck after driving through the wading channel at speed v_1 during the test*

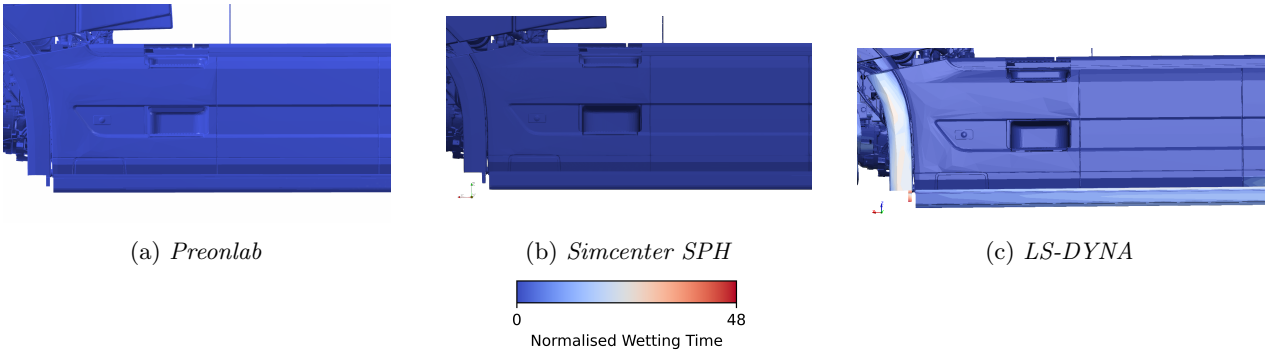

(a) *Preonlab* (b) *Simcenter SPH* (c) *LS-DYNA*

Figure 4.38: *Average wetting of the driver side side skirt of the truck at the speed v_2 for all three software*

Figure 4.39: *Image of the driver side side skirt of the truck after driving through the wading channel at speed v_1 during the test*

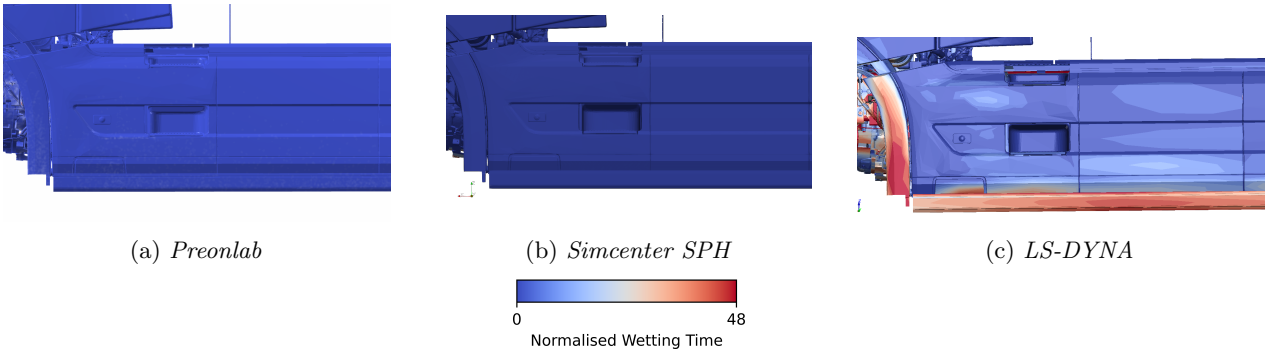

(a) *Preonlab* (b) *Simcenter SPH* (c) *LS-DYNA*

Figure 4.40: *Average wetting of the driver side side skirt of the truck at the speed v_2 for all three software*

4.2.7 Discussion about detailed truck simulations

In general it could be seen that all the Simcenter SPH results showed only the bigger wave patterns and not the splash phenomena expected from the test. As in the case of the parameter study, this could again be attributed to the manual placement of the truck geometry on the wading channel by the user at the beginning of the simulation. This could lead to gaps and asymmetries in the contact between the tyre and the wading channel base later as the simulation is running allowing for fluid particles to pass under the wheels.

In the center view images, it was observed that the asymmetry in the splash pattern is noticeable in the Simcenter SPH results which can be attributed to the asymmetry in the truck geometry in the front. The other two software do not show such asymmetry in the center view of the splash because the splash generated covers the general wave pattern from the front. The splashes themselves might not be showing the expected asymmetry in these two software since the number of particles in the splash is too low in density to clearly display this difference.

The front and top views of the front wheel splash show a larger number of particles in the splashes captured in Preonlab compared to LS-DYNA. This seems to indicate that Preonlab can capture the splash phenomena better than LS-DYNA at the default particle sizing of y. Both software show the general splash trends with respect to particles being projected in similar directions as seen in the test results but with lower amount of fluid than expected. A lower particle sizing might generate more splash as observed from the parameter study resulting in better visualization of the splash structure.

The back view images at the higher speed show that none of the software are capable of accurately capturing the turbulence phenomena required to depict the churned up behavior in the wake left behind by the truck. The Simcenter SPH simulation with its explicit solver is the one that comes closest in this case in capturing the turbulent behavior. However, it might be prudent to map the particle velocities in this case to see whether their directions indicate vortices. These details might be missing in a height map or rendered image.

LS-DYNA and Preonlab show good capability of capturing the wetting of the instep, with LS-DYNA showing more wetting of this region of the truck. Although, the intensity of wetting is insufficient to say which of the two are closer to the phenomena seen from the test. However, when it comes to the side skirt, LS-DYNA is able to capture the wetting better than Preonlab upon comparison with the image taken during the test. But, the extent of wetting seen in both cases are seen to be lesser than the test image. This could be because the driver side of the truck was closer to the wading channel wall in the test which resulted in more splash to bounce off the walls, thereby increasing the wetting on the side of the truck. It should also be noted here that the wetting pattern shown by LS-DYNA is smudged out by the mesh used to represent the solid geometry. Hence, wetting of the whole region shown in the images need not have occurred during the simulation.

4.3 Discussion about software user friendliness

The discussion about user friendliness of each software is based on the amount of pre-processing needed to get the simulation running and the challenges that were faced when post-processing the results from the simulation. This section is subdivided on the basis of each software and details pertaining to the corresponding software are presented here. The starting point for all software were from ANSA to create the geometry setup presented in the methodology chapter. Particular attention was paid to ensure the accurate positioning of the truck on the road surface of the wading channel. A common geometric part split of the truck was imported into each software to evaluate wetting pattern in the case of the simplified truck for the parameter study and the wetting pattern on the side skirt as well as instep of the detailed truck.

4.3.1 Preonlab

Pre-processing work needed in Preonlab was straightforward from geometry import to simulation runs for both simplified and detailed truck. With the detailed truck, the rotational speeds had to be recalculated due to different wheel diameters used in the front and rear axles and input to the python script. But otherwise no changes were needed to be made for the switch from the simplified truck to detailed truck simulations. No issues were encountered when the simulations for both the simplified and detailed truck were run on the cluster. The Preonlab GUI was sufficient for all pre- and post-processing. Wetting sensors were employed to capture the average and instantaneous wetting of the surfaces of the truck and the walls of the wading channel. Splash height distribution was generated using volume sensors. Volume sensors were periodically placed to

comprehensively capture the entire splash height. From this setup the fluid volume at different heights in the wading channel was captured into a Comma-Separated Values (CSV) file and plotted using a Python script.

4.3.2 Simcenter SPH

Simcenter SPH GUI was sufficient to carry out all pre-processing. Although, the geometry setup for simplified truck was straightforward, the detailed truck geometry had to be split into multiple smaller files. This needed to be done since all imported geometry were stored in a temporary folder located in home directory that had a memory restriction smaller than the size of the detailed truck geometry. Further, the kinematics and trajectory of the truck were explicitly calculated using a text file. However, the later versions of Simcenter SPH have been reported to control the trajectory using an implicit method. Licensing issues hindered the access to this version of the software for this thesis. Simulation runs part of parameter study could not be distributed beyond a certain number of cores else it resulted in a crash. Subsequently, with the detailed truck simulations the number of nodes used for the simulation had to be further reduced and the distribution had to be fine tuned. This is possibly due to the larger size of the geometry files andor complexity of the geometry. It resulted in longer simulation time due to sub-optimal usage of the computing resources. Further investigations were not carried since it was beyond the scope of this thesis.

Postprocessing was carried out using Paraview. The output file generated were in the .xmf format. Information about wetting i.e, instantaneous and average wetting were available as part of the default setting in Simcenter SPH. The splash height distribution was captured using flow rate sensors. Like in Preonlab, these sensors were periodically placed to capture the splashed fluid volume in different heights of the wading channel. These were stored in a CSV file and were plotted using a Python script.

4.3.3 LS-DYNA

Preprocessing in LS-DYNA required knowledge of LS-Prepost and ANSA. ANSA facilitated easier creation of rigid joints for motion of the truck, altering parameters of the surface mesh and automatic offsetting of node numbers that were common to the truck and wading channel geometry. Though these functionalities could have been added using LS-Prepost, ANSA does provide assistance to setup different keycards, making it more user friendly. However, some of the functionalities like **Boundary_Prescribed_Motion*, **Load_Body_Z* were lost when the .k file was reopened using LS-Prepost. These were included again using LS-Prepost. LS-Prepost was used to include the SPH functions in to the simulation model.

Most simulations that were part of the parameter study could be run quickly by altering the relevant parameters as mentioned in methodology. The simulation run using y/2 particle sizing frequently ran into dynamic memory allocation issues. Due to smaller particle sizing more of particles were generated which overloaded the memory allocation that was used for the default simulations of the parameter study. With some trial and error the correct value of memory allocation needed to get the simulation running was found. The transition from the simplified truck to detailed truck simulations were not straightforward. The finer mesh used in the detailed truck had an influence on some of the SPH functions and the **Contact* keycard. These parameters had to be re-tuned through trial and error.

The results were stored in a number of output files termed as d3plots. Within these d3plots included information of all particles at the corresponding timestep. META and LS-Prepost were used as post-processing tools to extract the required information from the d3plots. The average and instantaneous wetting pattern were extracted using only LS-Prepost. All renderings and particle height maps were generated using META. The particle positions used for the splash height distribution graphs were extracted using a Python script which could was run in META. META does provide many capabilities that can be customized but would require some prior experience using this tool.

5 Conclusions and Future Work

In this thesis theoretical background about different particle-based approaches for modeling multiphase systems was studied. Particular attention was paid to SPH regarding the assumptions, formulation of different terms used in the governing equations. Two popular methods of enforcing incompressibility and the surface tensions models were highlighted in great detail. Comparative studies of SPH with VOF and MPS were presented as well. Accurate modelling of water in the three software was obtained using the recommendations provided by the software suppliers.

The algorithm used in LS-DYNA and Preonlab was based on the IISPH model, while Simcenter SPH was based on Riemann-SPH, a weakly compressible model. The surface tension model used in all three software was based on the PF model presented in the theory section. However, the exact method of implementation in each software differed and were not disclosed.

A computational model of a truck wading through a pool of water was created and the behavior of each software was evaluated using a parameter study. Additionally, a similar setup with a detailed truck was used to replicate the experimental test carried out at HPG. From these simulations, the software were evaluated for the following:

Accuracy of Physics

Comparison of the results from the detailed truck simulations at two different speeds that aimed to replicate the experiment(s) showed that all three software could capture the large scale phenomena such as waves. The general direction of splash and spray observed in LS-DYNA and Preonlab were closer to the images captured during the test than Simcenter SPH. The intensity of such splash and spray phenomena could be increased with smaller particle sizing. The resolution of splash droplets captured seem to be dependent on the particle sizing as seen from the increase in splash and spray in the parameter study on decreasing particle sizing. The kinematics in Preonlab and Simcenter SPH were explicitly programmed using a Python script and a text file respectively, to control the contact of the truck with the surface of the wading channel and the motion of the truck through the wading channel. While in LS-DYNA, the kinematics was incorporated implicitly using prescribed motion assigned to different parts of the truck, gravity loading and friction. LS-DYNA thus allows for the inclusion of multi-physics which is not implicitly supported by the other two software. When it comes to the results from the software, the wetting pattern was noted to have an influence from the resolution of mesh used since the results are dependent on the particle-mesh interpolation techniques in the case of LS-DYNA and Simcenter SPH. Preonlab seems to show more accurate result display in these cases as it seems capable of tracking exact fluid particle strike locations.

Computational Cost

The computational cost has been evaluated between the three software by using same amount of computational resources and were compared using the core hours consumed to run a similar simulation setup. From parameter study, it could be inferred that core hours increased exponentially with decrease in particle sizing in all three software. The overall trend seen was that Preonlab consumed least amount of computational resources followed by LS-DYNA and then Simcenter SPH. It must however be noted that with further understanding of the MPP and time stepping parameters in each software, the simulations could be set up to run faster.

Ease of Usage

Preonlab and Simcenter SPH were straightforward to use in terms of the time needed to go from geometry import to simulation run. Since LS-DYNA was more of a multi-physics tool the learning curve was steeper in order to gain a good understanding of the functions that were incorporated into the model as well as the workflow which was fairly more complex compared to the other two. Simcenter SPH had issues with usage of computational resources beyond a certain threshold and the maximum number of cores that could successfully complete the simulation had to be determined thorugh trial and error in the case of the detailed truck simulations. Certain functions used in LS-DYNA were sensitive to the mesh resolution used when going from simplified to detailed truck model. In contrast Preonlab required no corrections when going from the simplified truck model to the detailed truck model making it the easiest software when changing truck models. Post processing for Simcenter SPH and LS-DYNA were carried out using specialized post-processing tools Paraview and META respectively. While post-processing could be carried out within the Preonlab GUI. In general, Preonlab had the least amount of issues while working with the simulations.

5.1 Future Work

As part of the parameter study it was noticed that the splash and spray phenomena seem to increase in all software with decrease in particle size. However the accuracy of these splash and spray phenomena could not be verified during this thesis work. Hence a possible avenue for future exploration would be to compare the splashes generated by simulations run at lower particle sizing against experimental tests. A correlation could be developed between SPH particle sizing and the spray phenomena clarifying which particle sizing can resolve what droplet sizes. The SPH particle sizing for future simulations could be easily made using this correlation study as a reference without having to test multiple sizes.

The parameter study done in this thesis focused on changing the individual parameters but it could be interesting to inspect how strong of a dependency drag force, surface tension parameters and particle sizing have on each other. It would be especially interesting to see how strong of an influence these factors have if the particle sizing is reduced. It is possible that a change in drag force might produce a sharper effect on a smaller SPH particles. The same could also be true in the case of surface tension but further study is required before it can be concluded.

Another aspect that was not explored during the thesis was fine tuning of surface tension parameters. A study could be done to adjust the surface tension parameters along with the particle sizing such that the simulations are able to replicate the wetting phenomena seen on real life truck building materials such as metals, glasses, tyre rubber etc. These surface tension parameters could perhaps be verified using experimental tests recording the contact angle between water and such surfaces. Another aspect that could be explored as an extension of the parameter study would be to include a realistic air flow field generated in another software into the SPH simulations along with the drag model present in these software to see if the air flow field produced a more accurate simulations result.

All the simulations in this thesis were run using slick tyres with no treads. In the future, SPH simulations could be run on treaded tyres to see if they capture phenomena such as tread pickup and capillary adhesion. These simulations could be verified against experiments of independent tyres spun through pools of water.

SPH as a viable tool for modeling snow accumulation could not be studied during this thesis due to time constraints. It could be another project worthy of investigation in the futures. Apart from this the scope of SPH in simulating exterior water management(EWM) in the case of trucks could also be explored.

Bibliography

[1] G. Volvo. Volvo Active Driver Assist. *https://www.volvotrucks.ca/en-ca/our-difference/safety/active-driver-assist/* (2022).

[2] A. P. Gaylard, K. Kirwan, and D. A. Lockerby. Surface contamination of cars: A review. *Proceedings of the Institution of Mechanical Engineers, Part D: Journal of Automobile Engineering* **231**.9 (2017), pp. 1160–1176.

[3] A. M. Wallace et al. Combining automotive radar and LiDAR for surface detection in adverse conditions. *IET Radar, Sonar & Navigation* **15**.4 (2021), 359–369.

[4] G. Volvo. Volvo Trucks Media Library. *https://images.volvotrucks.com/detailpage/42865* (2022).

[5] A. P. Gaylard et al. Insights into Rear Surface Contamination Using Simulation of Road Spray and Aerodynamics. *SAE International Journal of Passenger Cars - Mechanical Systems* **7**.2 (2014), pp. 673–681.

[6] A. Gaylard et al. "The Simulation of Brake Dust Deposition". Oct. 2010, pp. 271–287.

[7] M. Liu and G. Liu. Smoothed Particle Hydrodynamics (SPH): an Overview and Recent Developments. *Archives of Computational Methods in Engineering* **17** (2010), 25–76.

[8] J. Idoffsson. "Wading – Evaluation of SPH-based simulations versus traditional Finite Volume CFD." MA thesis. 2019.

[9] H.-G. Lyu et al. A Review of SPH Techniques for Hydrodynamic Simulations of Ocean Energy Devices. *Energies* **15** (2022).

[10] D. H. Weir, J. Strange, and R. K. Heffley. "Reduction of adverse aerodynamic effects of large trucks, Volume I. Technical report". 1978.

[11] Lagrangian vs. Eulerian: An Analysis of Two Solution Methods for Free-Surface Flows and Fluid Solid Interaction Problems. *Fluids* **6** (2021).

[12] A. Shakibaeinia and Y.-C. Jin. MPS mesh-free particle method for multiphase flows. *Computer Methods in Applied Mechanics and Engineering* **229-232** (2012), 13–26.

[13] S. Sasic. Multiphase flows, Lec 4. *University Lecture* (2021).

[14] S. Natsui et al. Stable mesh-free moving particle semi-implicit method for direct analysis of gas–liquid two-phase flow. *Chemical Engineering Science* **111** (2014), 286–298.

[15] L. Fu and Y.-c. Jin. Simulating gas–liquid multiphase flow using meshless Lagrangian method. *International Journal for Numerical Methods in Fluids* **76** (2014).

[16] Preon Solver Theory, Surface tension. *Version 5.1, Fifty2 Technology GmbH* (2022).

[17] SPH-flow 21.11.0 Documentation. *Siemens Digital Industries Software* (2022).

[18] A. Kabanovs et al. Modelling the Effect of Spray Breakup, Coalescence, and Evaporation on Vehicle Surface Contamination Dynamics. *SAE International Journal of Passenger Cars - Mechanical Systems* **11** (2018), 463.

[19] K. T. and C. s. Approaches to Vehicle Soiling Progress in Vehicle Aerodynamics. *Numerical methods Renningen Expert-Verlag IV 111 123 2006* ().

[20] J. K. Dukowicz. A particle-fluid numerical model for liquid sprays. *Journal of Computational Physics* **35**.2 (1980), 229–253.

[21] S. Sasic. Multiphase flows, Lec 6. *University Lecture* (2021).

[22] T. Hagemeier, M. Hartmann, and D. Thévenin. Practice of vehicle soiling investigations: A review. *International Journal of Multiphase Flow* **37** (2011), 860–875.

[23] S. Raymond, B. Jones, and J. Williams. A strategy to couple the material point method (MPM) and smoothed particle hydrodynamics (SPH) computational techniques. *Computational Particle Mechanics* **5** (Dec. 2016).

[24] K. Abe, K. Soga, and S. Bandara. Material Point Method for Coupled Hydromechanical Problems. *Journal of Geotechnical and Geoenvironmental Engineering* **140**.3 (2014).

[25] V. Lemiale, J. Nairn, and A. Hurmane. Material Point Method Simulation of Equal Channel Angular Pressing Involving Large Plastic Strain and Contact Through Sharp Corners. *Computer Modeling in Engineering & Sciences* **70** (2010), 41–66.

[26] D. Sulsky et al. Using the material-point method to model sea ice dynamics. *J. Geophys. Res* **112** (Feb. 2007).

[27] A. Stomakhin et al. A material point method for snow simulation. *ACM Transactions on Graphics (TOG)* **32** (2013), 1–10.

[28] D. Z. Zhang et al. Material point method applied to multiphase flows. *Journal of Computational Physics* **227** (2008), 3159–3173.
[29] S. Koshizuka and Y. Oka. Moving-particle semi-implicit method for fragmentation of incompressible fluid. *Nuclear Science Engineering* **123** (1996), 421–434.
[30] S. Tokura. Comparison of Particle Methods: SPH and MPS. 13^{th} *International LS-DYNA Users Conference* (2007).
[31] J. J. Monaghan. Smoothed Particle Hydrodynamics. *Annual Review of Astronomy and Astrophysics* **30** (1992), 543–574.
[32] R. Gingold and J. Monaghan. Kernel estimates as a basis for general particle methods in hydrodynamics. *Journal of Computational Physics* **46**.3 (1982), 429–453.
[33] X. Y. Hu and N. A. Adams. Angular-momentum conservative smoothed particle dynamics for incompressible viscous flows. *Physics of Fluids* **18**.10 (2006), 101702.
[34] J. Swegle, D. Hicks, and S. Attaway. Smoothed Particle Hydrodynamics Stability Analysis. *Journal of Computational Physics* **116**.1 (1995), 123–134.
[35] J. Monaghan. SPH without a Tensile Instability. *Journal of Computational Physics* **159**.2 (2000), 290–311.
[36] M. Macklin and M. Müller. Position Based Fluids. *ACM Trans. Graph.* **32**.4 (2013).
[37] G. Akinci et al. Parallel Surface Reconstruction for Particle-Based Fluids. *Computer Graphics Forum* **31**.6 (2012), 1797–1809.
[38] H. Schechter and R. Bridson. Ghost SPH for Animating Water. *ACM Trans. Graph.* **31**.4 (2012).
[39] J. P. Morris, P. J. Fox, and Y. Zhu. Modeling Low Reynolds Number Incompressible Flows Using SPH. *Journal of Computational Physics* **136**.1 (1997), 214–226.
[40] B Lautrup. *Physics of Continuous Matter: Exotic and Everyday Phenomena in the Macroscopic World (2nd ed.)*. CRC Press, 2011.
[41] G. Akinci and M. Teschner. Versatile surface tension and adhesion for SPH fluids. *ACM Trans. Graph* (2013).
[42] E. Arai et al. Comparison of surface tension generation methods in smoothed particle hydrodynamics for dynamic systems. *Computers and Fluids* **203** (2020).
[43] K. Szewc et al. A Study on Application of Smoothed Particle Hydrodynamics to Multi-Phase Flows. *International Journal of Nonlinear Sciences and Numerical Simulation* **13** (2012), 383–395.
[44] A. M. Tartakovsky and P. Meakin. Pore scale modeling of immiscible and miscible fluid flows using smoothed particle hydrodynamics. *Advances in Water Resources* **29** (2006), 1464–1478.
[45] J. J. Monaghan. Smoothed particle hydrodynamics. *Reports on Progress in Physics* **68**.8 (2005), 1703–1759.
[46] E. Lee et al. Comparisons of Weakly Compressible and Truly Incompressible Algorithms for the SPH Mesh Free Particle Method. *Journal of Computational Physics* **227** (2008), 8417–8436.
[47] J. Monaghan and R. Gingold. Shock simulation by the particle method SPH. *Journal of Computational Physics* **52**.2 (1983), 374 –389.
[48] M. Antuono et al. Free-surface flows solved by means of SPH schemes with numerical diffusive terms. *COMPUTER PHYSICS COMMUNICATIONS* **181**.3 (2010), 532 –549.
[49] M. S. et al. delta-SPH model for simulating violent impact flows. (2011).
[50] E. Yreux. Implicit SPH in LS-DYNA for Automotive Water Wading Simulations. 12^{th} *European LS-DYNA Conference 2019, Koblenz, Germany* (2019).
[51] M. Ihmsen et al. Implicit Incompressible SPH. *IEEE Transactions on Visualization and Computer Graphics, Visualization and Computer Graphics, IEEE Transactions on, IEEE Trans. Visual. Comput. Graphics* **20** (2014), 426 –435.
[52] Advanced Tutorial (v5.1), Vehicle Water Wading. *Version 5.1, Fifty2 Technology GmbH* (2021).
[53] Wading/River crossing, Step by step tutorial for SPH-flow Designer. *Siemens Digital Industries Software* (2021).
[54] LS-DYNA Keyword User's Manual. *Livemore Software Technology(LST), An Ansys Company* (2021).

A Appendix A

A.1 Parameter Study

A.1.1 Preonlab

Solid-Liquid Adhesion Factors

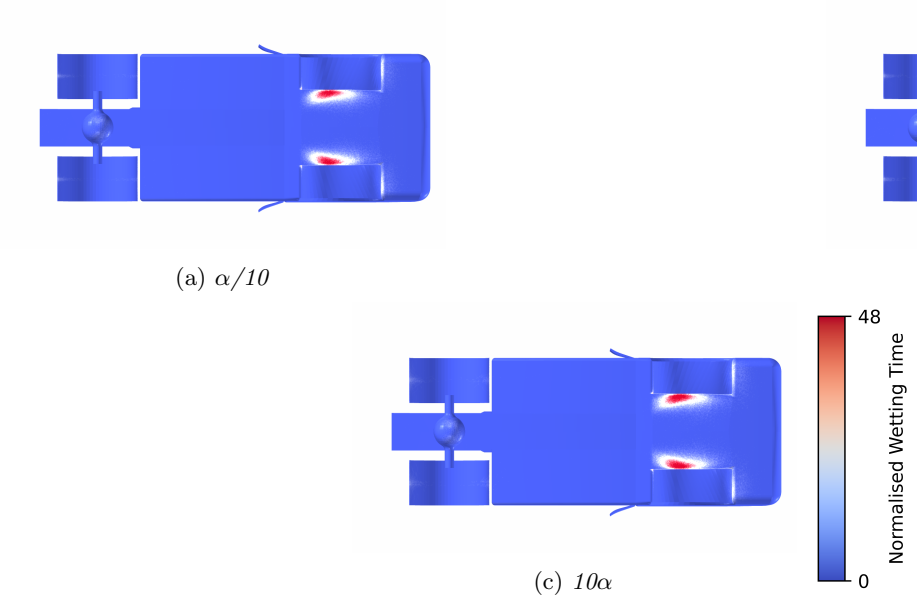

(a) $\alpha/10$ (b) α

(c) 10α

Figure A.1: *Average wetting of the bottom surface of the simplified truck as the solid-liquid adhesion factor used for the Preonlab simulations was varied between $\alpha/10$, α and 10α*

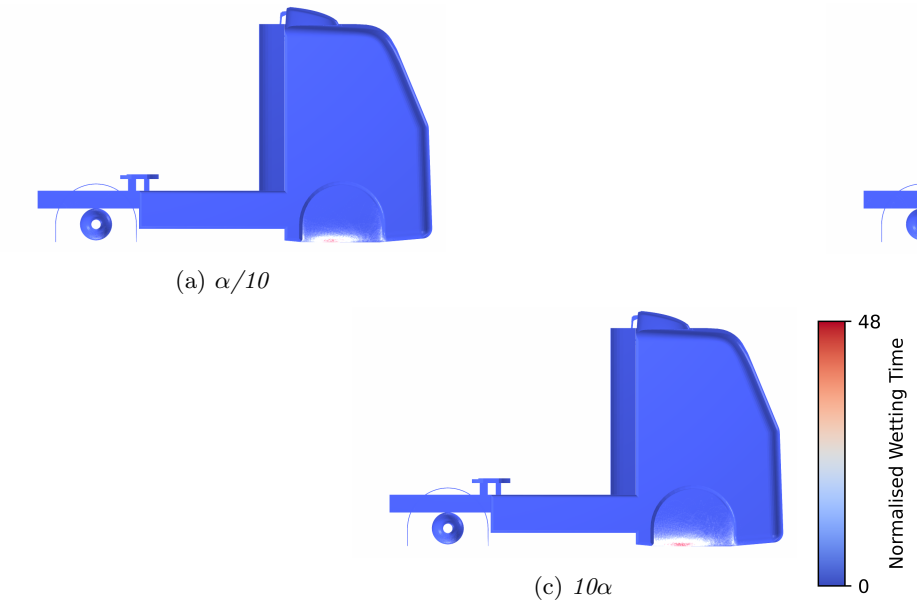

(a) $\alpha/10$ (b) α

(c) 10α

Figure A.2: *Average wetting of the side surface of the simplified truck as the solid-liquid adhesion factor used for the Preonlab simulations was varied between $\alpha/10$, α and 10α*

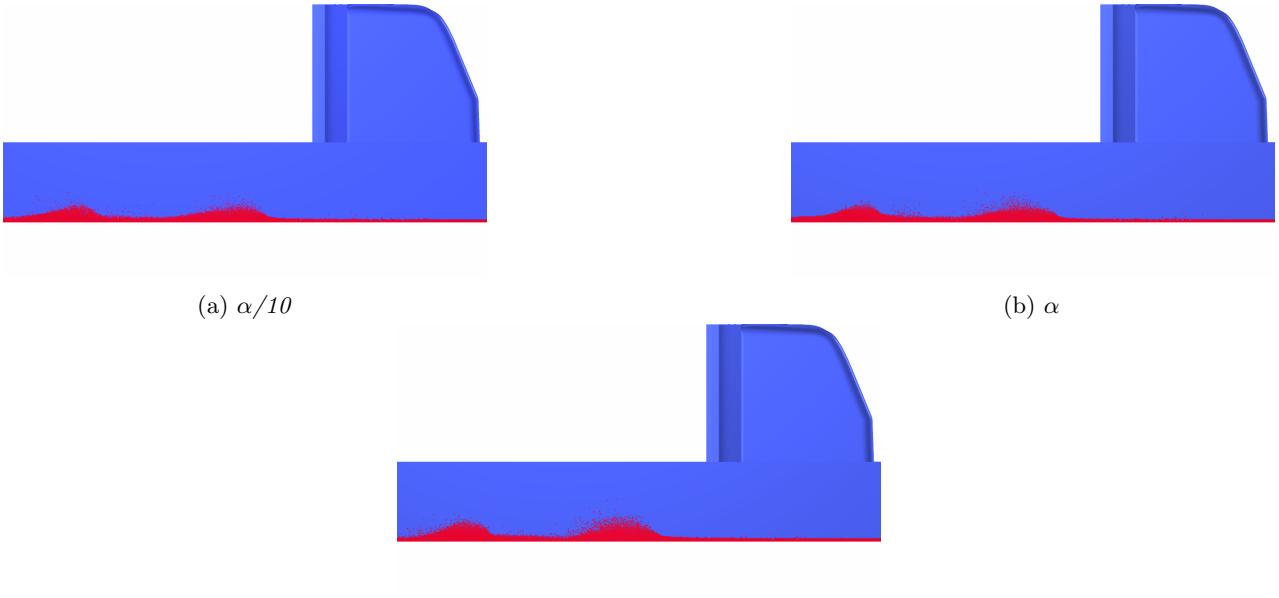

(a) $\alpha/10$

(b) α

(c) 10α

Figure A.3: *Instantaneous wetting of the walls of the wading channel as the solid-liquid adhesion factor used for the Preonlab simulations was varied between $\alpha/10$, α and 10α*

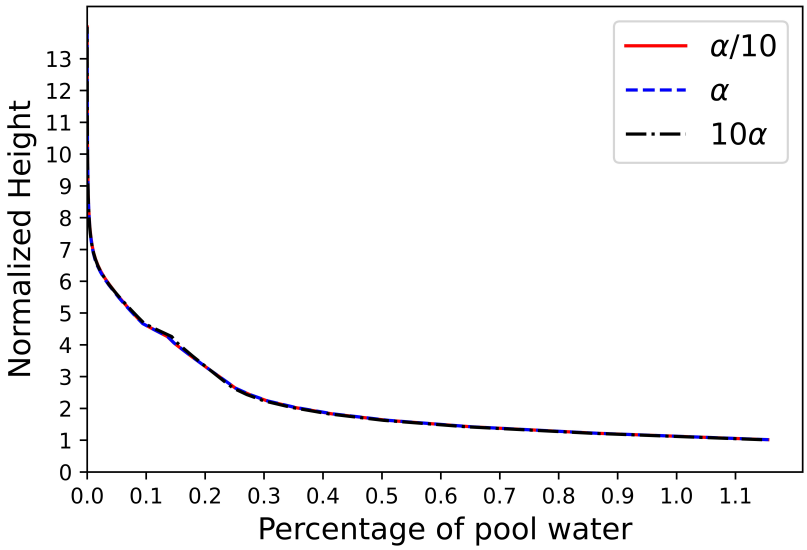

Figure A.4: *Splash Height Distribution for different Solid-Liquid Adhesion Factor in Preonlab simulations*

Solid-Liquid Adhesion Factor	Normalized no of particles	Normalized Core Hours
$\alpha/10$	1	1.001
α	1	1
100α	1	0.99

Table A.1: Normalised Core Hours for Preonlab simulations as the solid-liquid adhesion factor is varied

Drag Model Usage

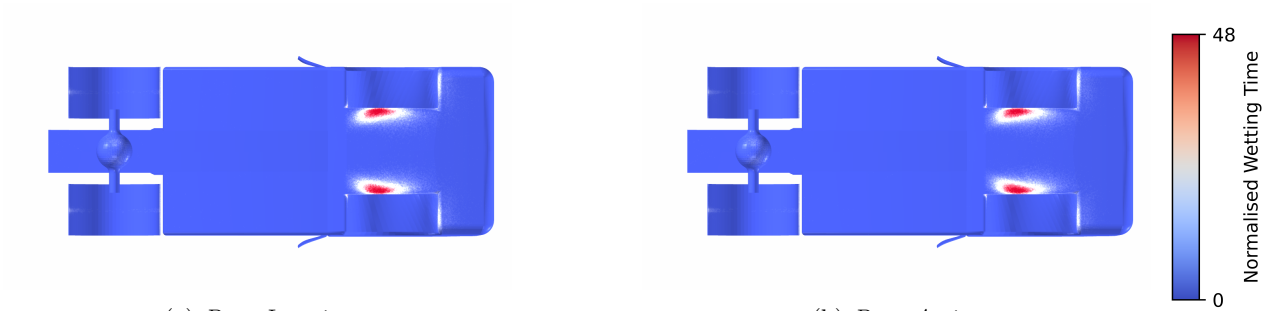

(a) *Drag Inactive* (b) *Drag Active*

Figure A.5: *Average wetting of the bottom surface of the simplified truck as the air drag model is turned from inactive to active for the Preonlab simulations*

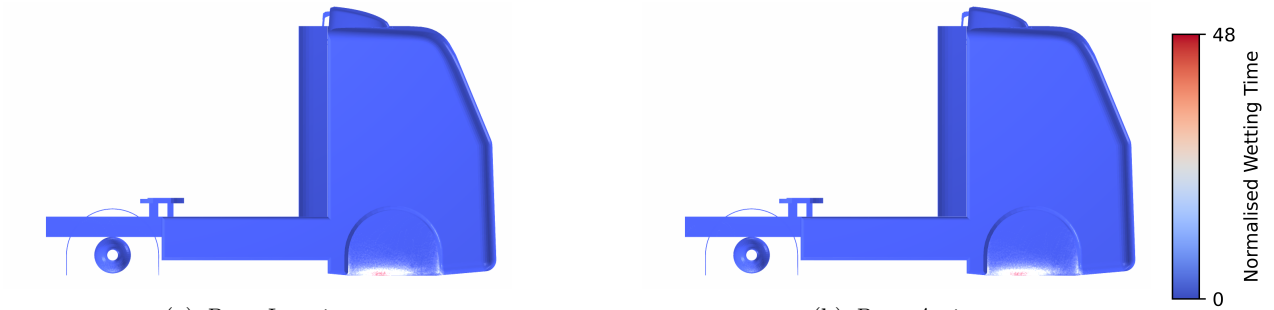

(a) *Drag Inactive* (b) *Drag Active*

Figure A.6: *Average wetting of the side surface of the simplified truck as the air drag model is turned from inactive to active for the Preonlab simulations*

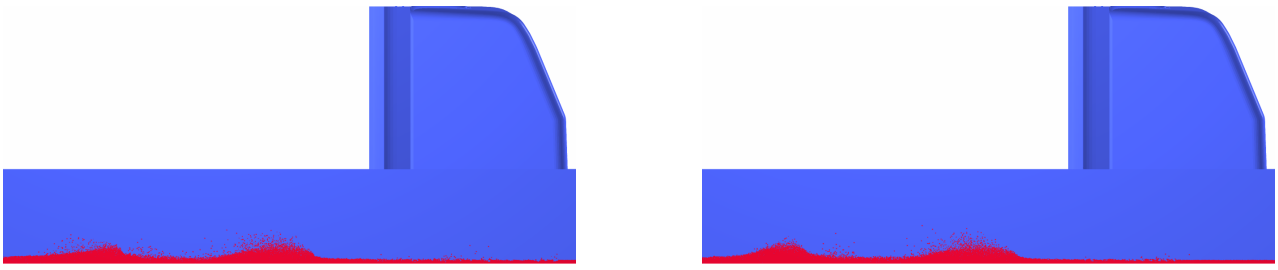

(a) *Drag Inactive* (b) *Drag Active*

Figure A.7: *Instantaneous wetting of the walls of the wading channel as the air drag model is turned from inactive to active for the Preonlab simulations*

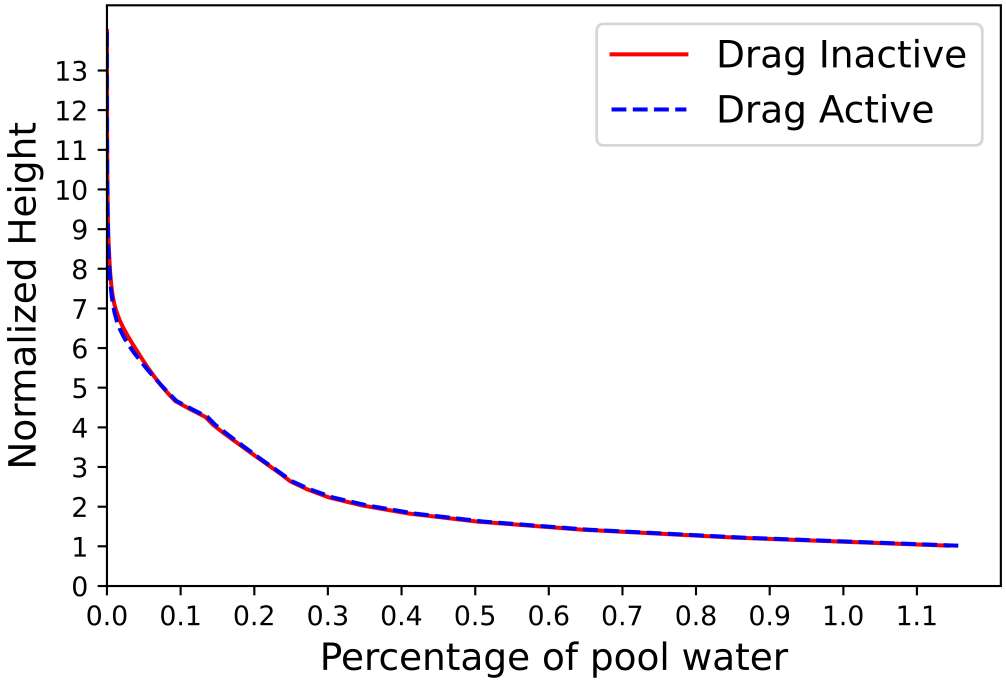

Figure A.8: *Splash Height Distribution variation with usage of Drag model in Preonlab simulations*

Drag Model	Normalized no of particles	Normalized Core Hours
Inactive	1	1.01
Active	1	1

Table A.2: Normalised Core Hours for Preonlab simulations with the inclusion and exclusion of the drag model

A.1.2 Simcenter SPH

Solid-Liquid Contact Angle

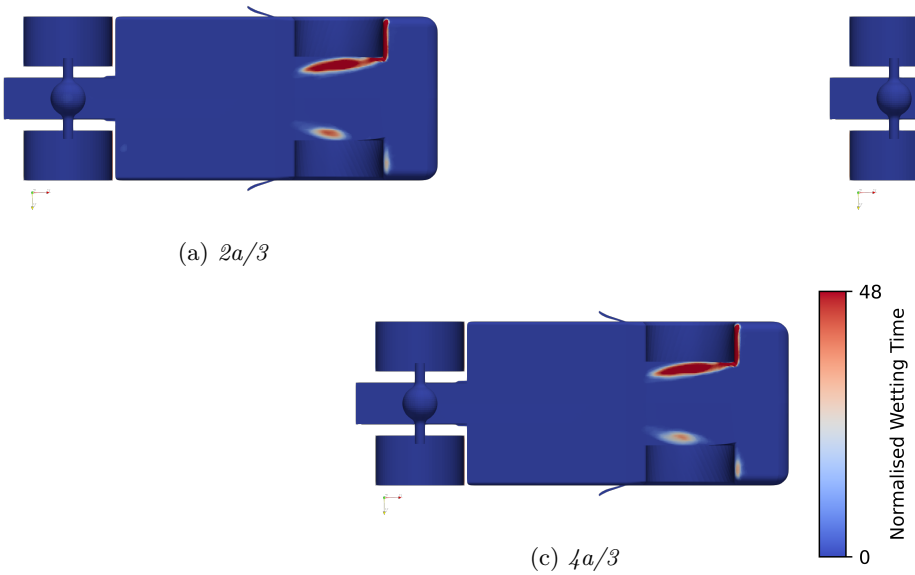

(a) *2a/3* (b) *a*

(c) *4a/3*

Figure A.9: *Average wetting of the bottom surface of the simplified truck as the contact angle between the solid and liquid phases used for the Simcenter SPH simulations was varied between 2a/3 , a and 4a/3*

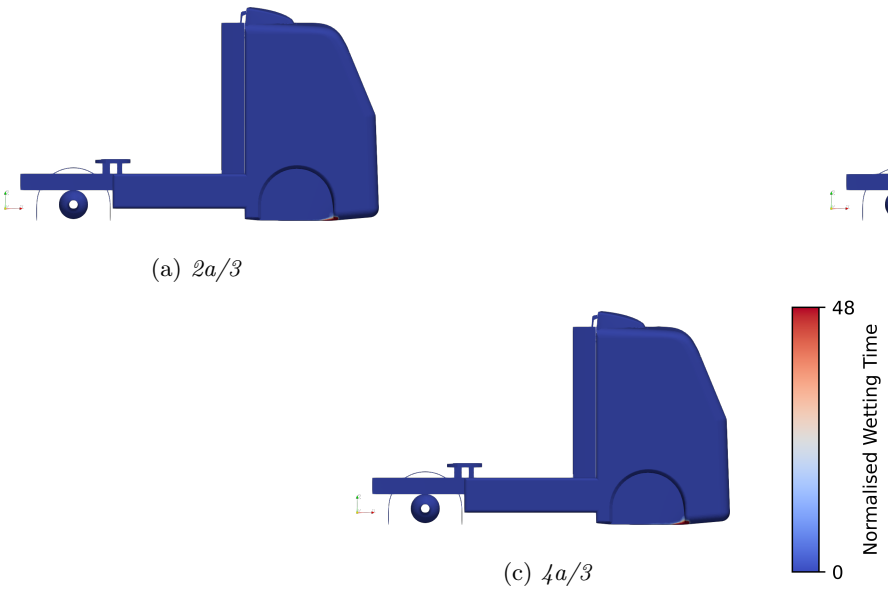

(a) *2a/3* (b) *a*

(c) *4a/3*

Figure A.10: *Average wetting of the side surface of the simplified truck as the contact angle between the solid and liquid phases used for the Simcenter SPH simulations was varied between 2a/3 , a and 4a/3*

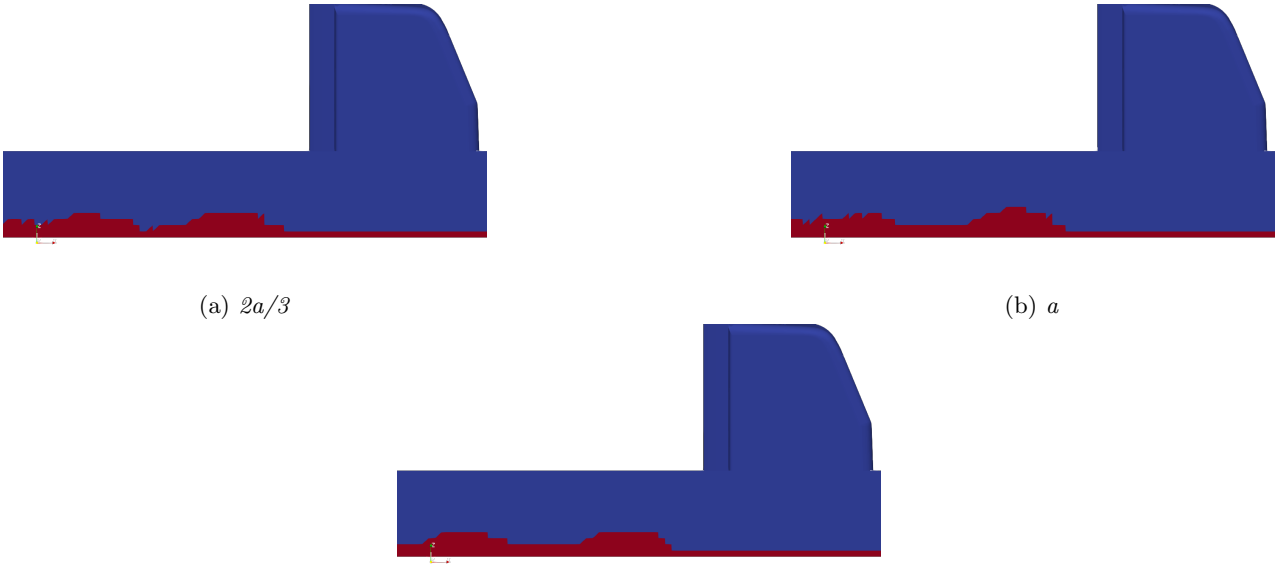

(a) *2a/3*

(b) *a*

(c) *4a/3*

Figure A.11: *Instantaneous wetting of the walls of the wading channel as the contact angle between the solid and liquid phases used for the Simcenter SPH simulations was varied between 2a/3 , a and 4a/3*

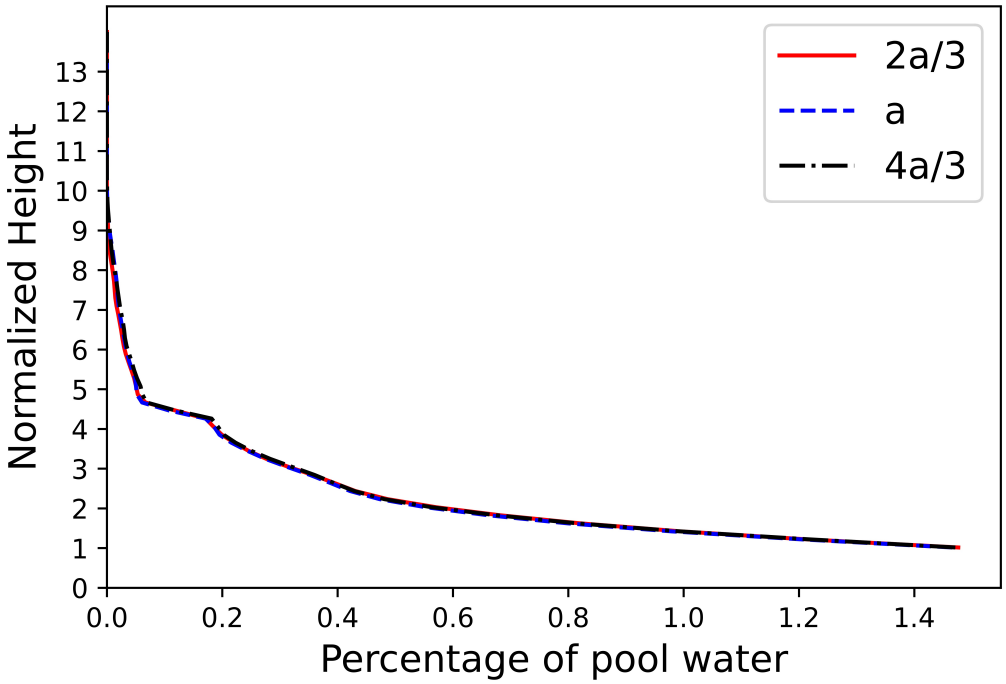

Figure A.12: *Splash Height Distribution for different Solid-Liquid Contact angles in Simcenter SPH*

Solid-Liquid Contact Angle	Normalized no of particles	Normalized Core Hours
2a/3	1	9.5
a	1	9.6
4a/3	1	9.5

Table A.3: Normalised Core Hours for Simcenter SPH simulations as the solid-liquid contact angle is varied

Drag Model Usage

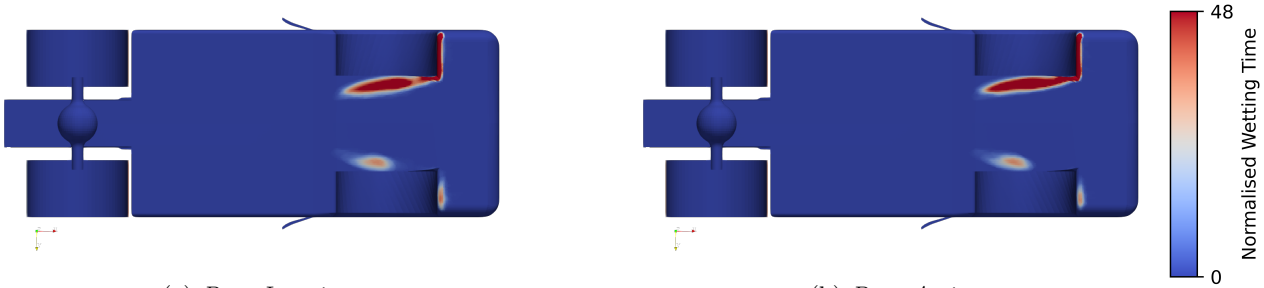

(a) *Drag Inactive* (b) *Drag Active*

Figure A.13: *Average wetting of the bottom surface of the simplified truck as the air drag model is turned from inactive to active for the Simcenter SPH simulations*

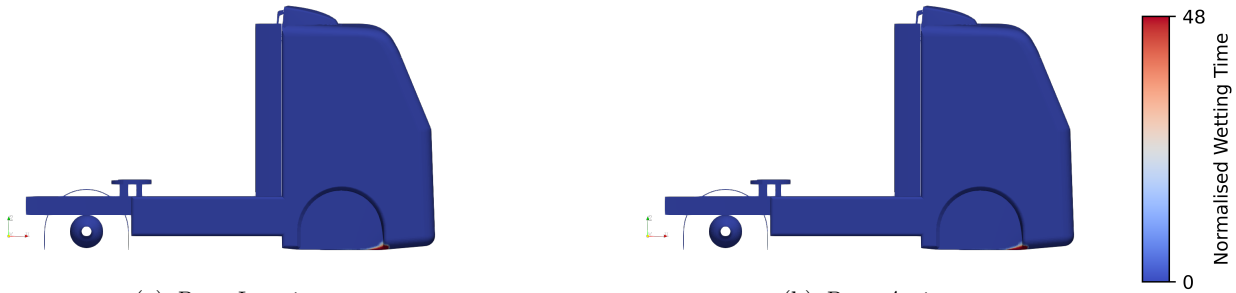

(a) *Drag Inactive* (b) *Drag Active*

Figure A.14: *Average wetting of the side surface of the simplified truck as the air drag model is turned from inactive to active for the Simcenter SPH simulations*

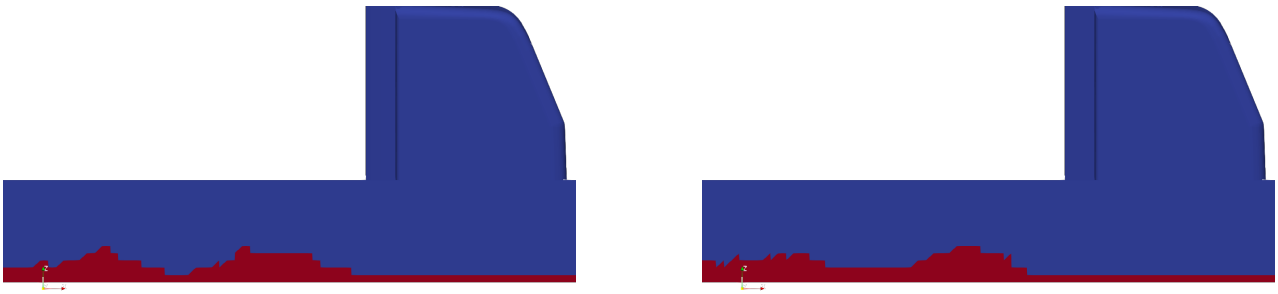

(a) *Drag Inactive* (b) *Drag Active*

Figure A.15: *Instantaneous wetting of the walls of the wading channel as the air drag model is turned from inactive to active for the Simcenter SPH simulations*

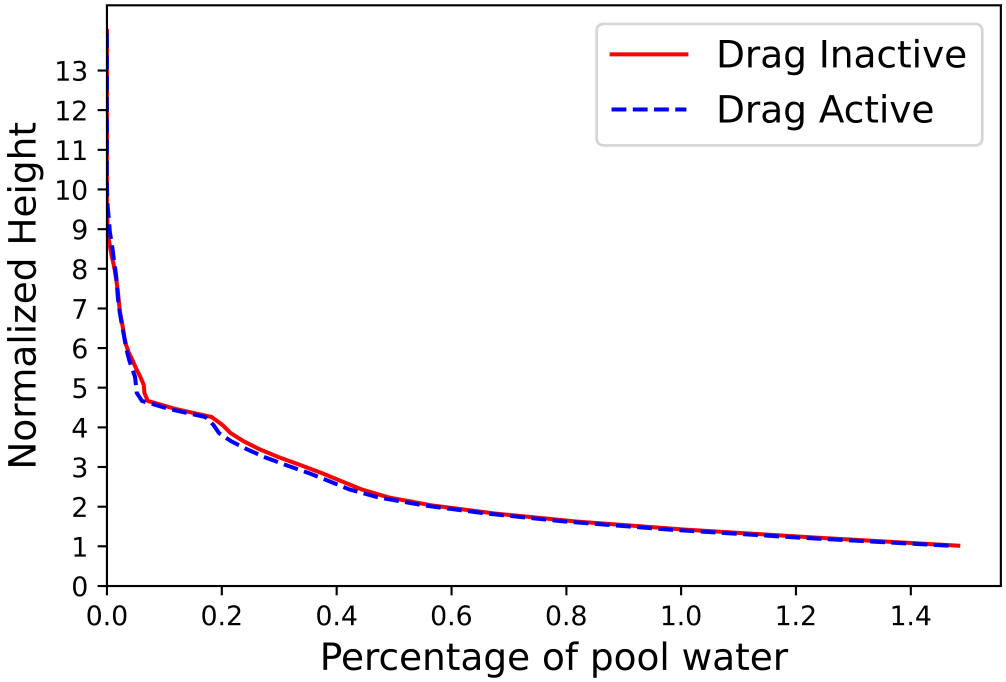

Figure A.16: *Splash Height Distribution variation with usage of Drag model in Simcenter SPH*

Drag Model	Normalized no of particles	Normalized Core Hours
Inactive	1	9.5
Active	1	9.6

Table A.4: Normalised Core Hours for Simcenter SPH simulations as the drag model is changed from inactive to active

A.1.3 LS-DYNA

Surface Adhesion Coefficient (Beta)

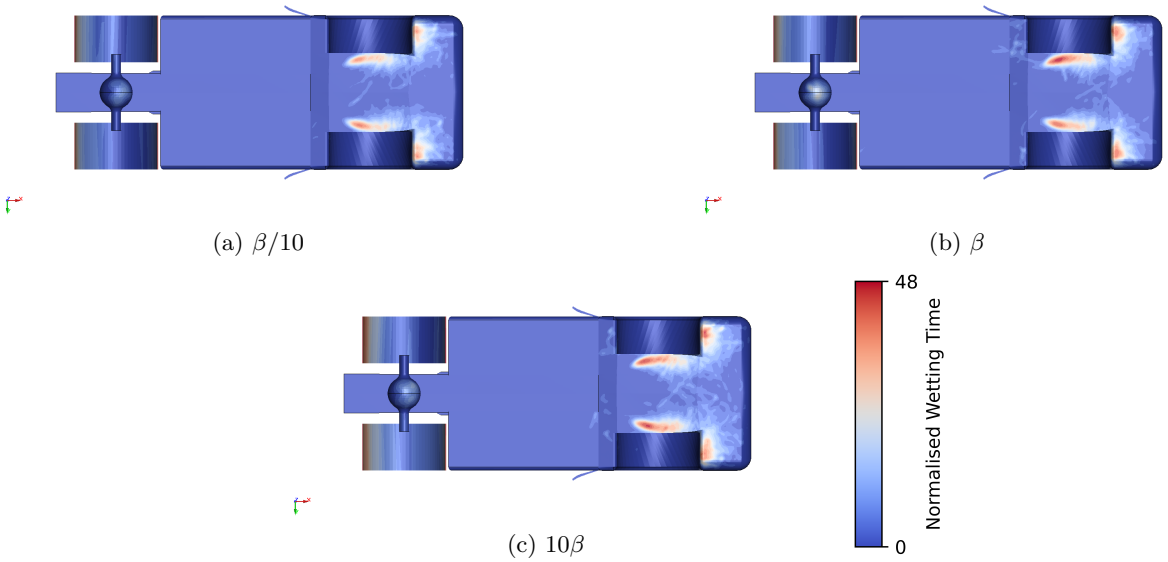

(a) $\beta/10$ (b) β

(c) 10β

Figure A.17: *Average wetting of the bottom surface of the simplified truck as the adhesion factor beta used for LS-DYNA simulations was varied between* $\beta/10$, β *and* 10β

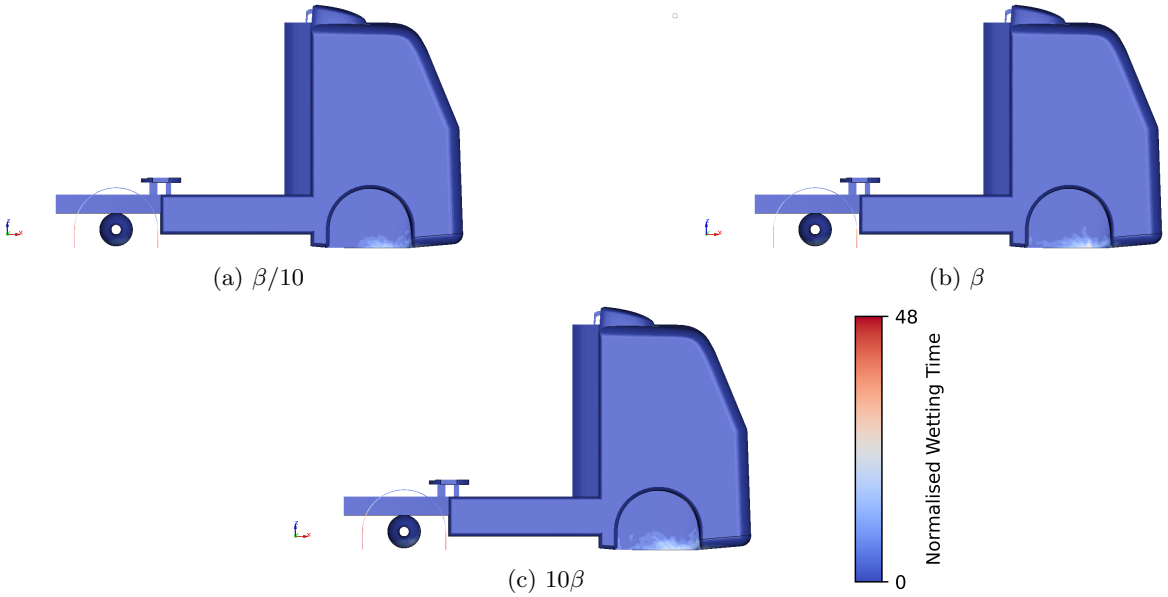

(a) $\beta/10$ (b) β

(c) 10β

Figure A.18: *Average wetting of the side surface of the simplified truck as the surface adhesion coefficient used for LS-DYNA simulations was varied between* $\beta/10$, β *and* 10β

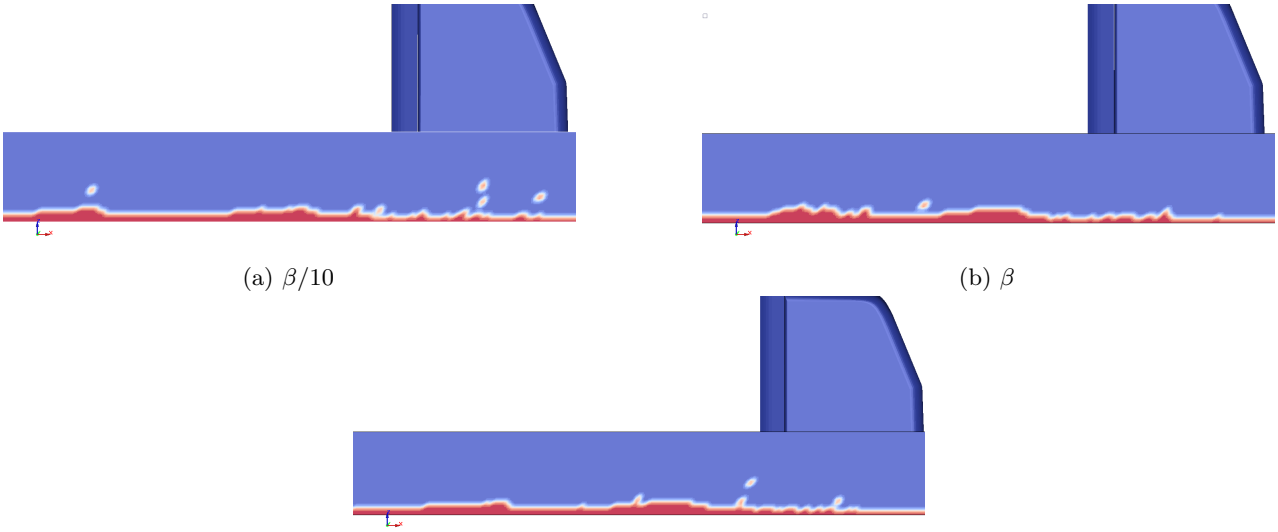

(a) $\beta/10$

(b) β

(c) 10β

Figure A.19: *Instantaneous wetting of the walls of the wading channel as the surface adhesion coefficient used for LS-DYNA simulations was varied between* $\beta/10$, β *and* 10β

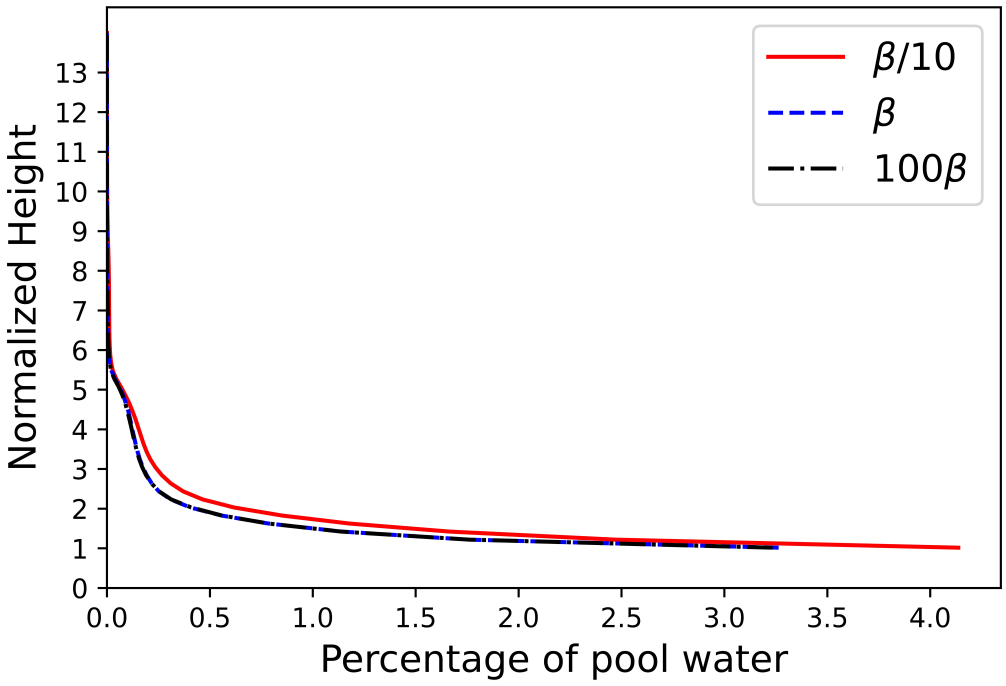

Figure A.20: *Splash Height Distribution for Beta Values in Surface Tension model*

Surface Adhesion Factor(Beta)	Normalized no of particles	Normalized Core Hours
beta/10	0.8	4.6
beta	0.8	4.7
10beta	0.8	3.1

Table A.5: Normalised Core Hours for Simcenter SPH simulations as the surface adhesion coefficient is varied

Drag Model Usage

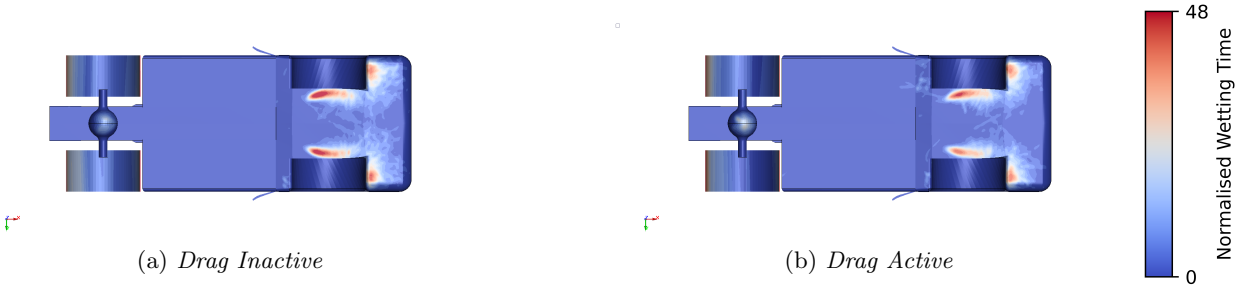

(a) *Drag Inactive* (b) *Drag Active*

Figure A.21: *Average wetting of the bottom surface of the simplified truck as the air drag model is turned from inactive to active for the LS-DYNA simulations*

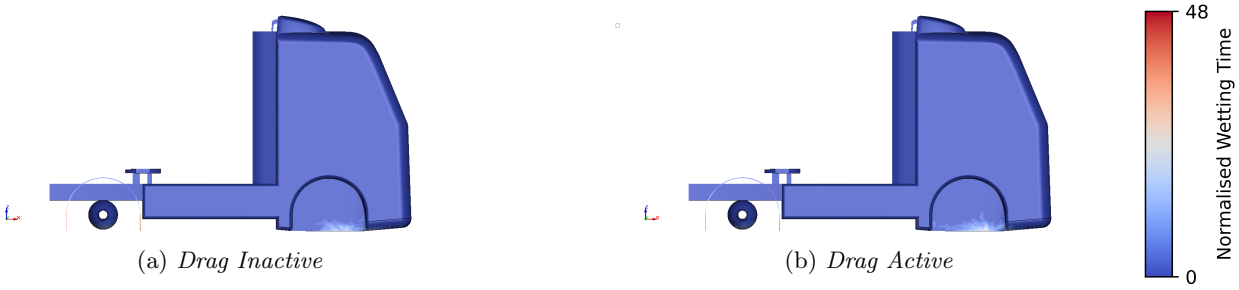

(a) *Drag Inactive* (b) *Drag Active*

Figure A.22: *Average wetting of the side surface of the simplified truck as the air drag model is turned from inactive to active for the LS-DYNA simulations*

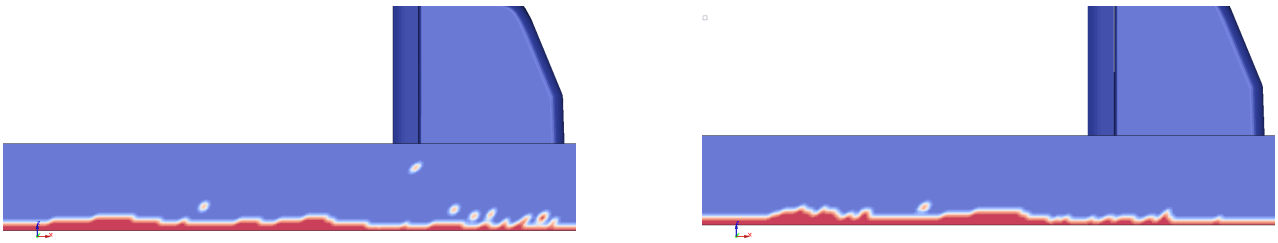

(a) *Drag Inactive* (b) *Drag Active*

Figure A.23: *Instantaneous wetting of the walls of the wading channel as the air drag model is turned from inactive to active for the LS-DYNA simulations*

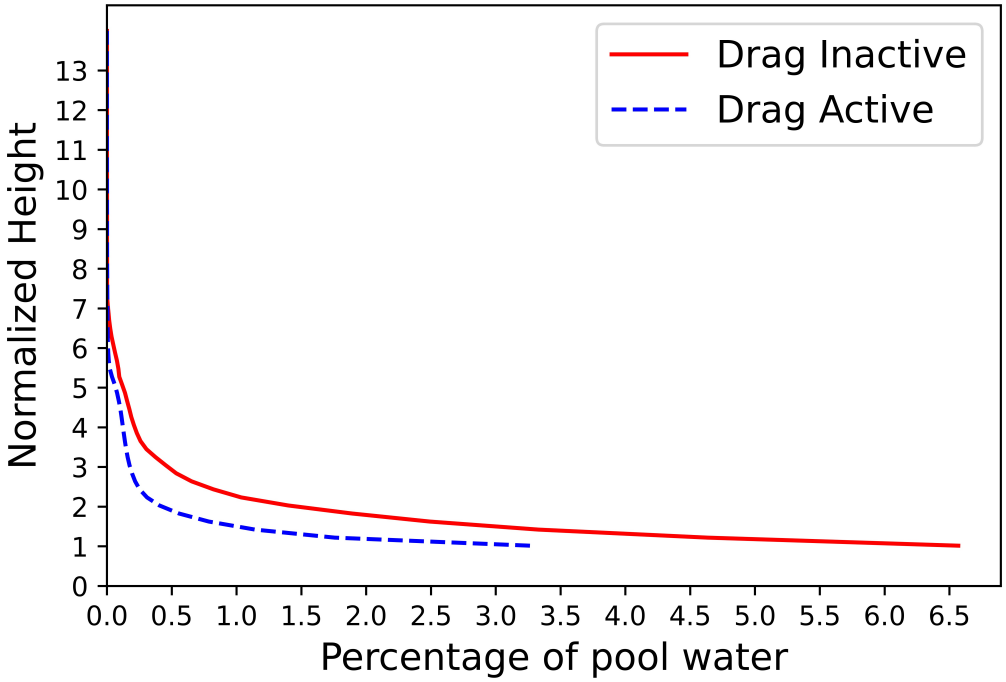

Figure A.24: *Splash Height Distribution variation with usage of Drag model*

Drag Model	Normalized no of particles	Normalized Core Hours
Inactive	0.8	4.8
Active	0.8	4.7

Table A.6: Normalised Core Hours for Simcenter SPH simulations as the drag model is changed from active to inactive

DEPARTMENT OF MECHANICS AND MARITIME SCIENCES
CHALMERS UNIVERSITY OF TECHNOLOGY
Gothenburg, Sweden 2022
www.chalmers.se

CHALMERS
UNIVERSITY OF TECHNOLOGY